THE AUSTENITE → FERRITE TRANSFORMATION IN TUNGSTEN STEELS AND SOME OTHER TERNARY STEELS

By

SUNIL KISHORE SAHAY

Darwin College, Cambridge

A dissertation submitted for the degree of
Doctor of Philosophy
at the University of Cambridge, September 1986

PREFACE

This dissertation is submitted for the degree of Doctor of Philosophy in the University of Cambridge. The research described was performed during the period from October 1983 to September 1986 in the Department of Metallurgy and Materials Science, University of Cambridge.

Except where acknowledgment and reference to previous work has been made, this work is, to my best knowledge, original and has been carried out without collaboration. Neither this dissertation, nor any one substantially similar to it has been or is being submitted for a degree, diploma or other qualification at any other University. This dissertation consists of less than 60,000 words. The research was carried out under the supervision of Prof. R.W.K. Honeycombe R.F.S. (1983-84) and Dr. H.K.D.H. Bhadeshia (1984-86).

Sunil Kishore Sahay

Sunil Kishore Sahay

September 1986

ACKNOWLEDGEMENTS

I would like to express my sincere gratitude to Professor R.W.K. Honeycombe (1983-84) and Professor D. Hull (1984-86) for laboratory facilities and for their encouragement and advice throughout the course of this work. I am also grateful to my friends and colleagues in the Department of Metallurgy and Materials Science, in particular, J.L. Steiner, G. Hillier, D. Burry, Y. Sato, R. Paulo, B. Soylü, J.R. Yang, M. Strangwood, A. Sugden and S. Atamert.

Acknowledgement is also made to the Assistant staff of the laboratory, in particular, J. Leader, for his aid in alloy preparation and B. Barber for photography.

I greatly acknowledge my wife Anjali for her moral support in all possible ways during the entire period of my research. I also express my gratitude to my parents for their constant encouragement in the time of need. My son Abhisek needs special appreciation.

The research has been financially supported through Cambridge Commonwealth Trust Award, ORS and an award from Darwin College.

Thanks is also due to Miss Lesley Parks for her careful typing.

CONTENTS

PREFACE .. .. (i)

ACKNOWLEDGEMENTS .. .. (ii)

ABSTRACT .. .. (iii)

CHAPTER I : General Introduction .. .. 1 - 2

CHAPTER II : Literature Review .. .. 3 - 14

2.1 Introduction 3

2.2 The $\gamma \rightarrow \alpha$ reaction 4

2.3 Interphase precipitation 8

CHAPTER III : Experimental Techniques .. .. 15 - 23

3.1 Alloy preparation and Fabrication 15

3.2 Nickel Electroplating 15

3.3 Heat-Treatment 16

3.4 Optical-Microscopy 18

3.5 Transmission Electron Microscopy 20

3.6 Isothermal Dilatometry 21

3.7 Microanalysis on SEM 22

CHAPTER IV : The Austenite → Ferrite transformation in Fe-5.5W-2.03Si-0.37C (wt%) and Fe-5.8W-0.4C (wt%) alloy .. .. 25 - 75

4.1 Introduction 25

4.2 Experimental Results on Fe-5.5W-2.03Si-0.37C (wt%) alloy 26

4.3 Discussion 31

4.4 Experimental Results on Fe-5.8W-0.4C (wt%) alloy 35

4.5 Discussion 37

4.6 Conclusions 39

CHAPTER V : The Austenite → Ferrite transformation in Fe-5W-0.23C (wt%) .. .. 76 - 106

5.1 Introduction 76

5.2 Experimental Results on Fe-5W-0.23C (wt%) alloy 79

5.3 The effects of small addition of titanium (0.14%) on transformations in Fe-5.9W-0.21C (wt%) alloy 82

5.4 Discussion 83

5.5 Conclusions 85

CHAPTER VI : The $\gamma \rightarrow \alpha$ transformation in Fe-5W-2.3Si-0.15C (wt%) alloy .. .. 107 - 131

6.1 Introduction 107

6.2 Experimental Results 108

6.3 Discussion 110

6.4 Conclusions 112

CHAPTER VII : The influence of carbide precipitation on nucleation of allotriomorphic ferrite in Fe-5.8W-0.5C (wt%) alloy .. .. 132 - 141

7.1 Introduction 132

7.2 Experimental Procedure 133

7.3 Results and Discussion 134

CHAPTER VIII : The study of growth kinetics in Fe-2.99Cr-0.11C (wt%) .. .. 142 - 190

8.1 Introduction 142

8.2 Local equilibrium at the γ/α interface .. 142

8.3 Para-equilibrium 148

8.4 Calculation of parabolic growth rate using para-equilibrium model 151

8.5 Experimental Results 152

8.6 Discussion 154

8.7 Conclusions 163

CHAPTER IX : The study of Growth Kinetics in Fe-3.28Ni-0.11C (wt%) alloy .. .. 191 - 208

9.1 Introduction 191

9.2 Experimental Results 191

9.3 Discussion 193

9.4 Conclusions 196

CHAPTER X : Conclusions and suggestions for future work .. 209 - 212

10.1 Conclusions 209

10.2 Suggestions for future work 212

Appendix I : Calculations used for constructing TTT diagrams 213

Appendix II : A review on thermodynamics of diffusional decomposition of austenite .. .. 216 - 221

Appendix III : Nucleus Composition .. .. 222 - 226

References : . .. . 227 - 242

ABSTRACT

The present work is concerned with "The Austenite→Ferrite transformation in tungsten steels and some other ternary steels". Emphasis is given to the understanding of the fundamental factors influencing nucleation and growth phenomena during the diffusional decomposition of austenite. Precipitation at the advancing γ/α interface (i.e. interphase precipitation) has also been studied.

It is found that the $\gamma \rightarrow \alpha$ transformation proceeds by the nucleation of α i.e. allotriomorphic ferrite) at the prior-austenite grain boundaries, followed by its growth. Hence the kinetics of the $\gamma \rightarrow \alpha$ transformation depend on the ease with which the α is nucleated at the austenite grain-boundaries as well as its ability to grow. In order to enhance hardenability, it is essential to impede both the nucleation of ferrite and its subsequent growth.

Using a Fe-W-C alloy, an attempt has been made to suppress the grain boundary nucleation of α by first partially covering these boundaries with copious precipitation of tungsten carbide. The presence of such precipitation at the prior austenite grain-boundaries was found to lead to a drastic drop in the nucleation rate of α, at low undercoolings in spite of the fact that carbide formation removes carbon from solid solution. However, at high undercoolings, the reverse phenomenon was observed. It is concluded that at low undercoolings, nucleation kinetics depend more on the number of available active sites; the prior formation of tungsten carbides reduces the number of sites and hence causes a drop in nucleation frequency. On the other hand, at high undercoolings, driving force dominates the nucleation kinetics (i.e. since carbon is precipitated at the prior austenite grain-boundaries as carbide, it causes an overall increase in the driving force for transformation) and so leads to an increased nucleation rate. The growth kinetics of allotriomorphic ferrite (α) in Fe-C-X alloys (where X is Cr or Ni) have been studied. Parabolic rate constants for thickening kinetics of α have been determined as a function of isothermal transformation temperature and compared with calculated values based on a para-equilibrium model for one-dimensional growth. A good agreement was noticed for a Ni-containing steel. But in the case of a Cr-steel, the agreement was rather poor. The sources of discrepancies were examined in the light of available experimental observations. It was concluded that factors such as presence of planar facets, pinning of the γ/α interface by

carbides, solute drag-like effect and stereological effects are responsible for the discrepancies in our results.

Another part of the research is concerned with the study of interphase-precipitation during the $\gamma \rightarrow \alpha$ transformation. Interphase-precipitation has been studied in Fe-Si-W-C alloys and compared with alloys of similar composition but without silicon. It was observed that silicon has strong tendency to induce interphase-precipitation at high temperatures. High proportions of low energy facets (i.e. semi-coherent interface) containing ledges of variable height were noticed in silicon-containing steels transformed at high temperatures (i.e. low undercoolings). It is suggested that silicon tends to favour the development of low energy facets which move by ledge mechanism. At the same time silicon is believed to decrease the solid-solubility of carbides in ferrite. These factors probably combine to enhance interphase precipitation.

Finally, the effect of a small addition of titanium on the $\gamma \rightarrow \alpha$ transformation in Fe-5W-0.23C(wt.%) alloy has been investigated. Like Nb, titanium showed a tendency to retard $\gamma \rightarrow \alpha$ transformation. Titanium forms carbides both at the prior austenite grain-boundaries and within the grains. Formation of TiC at the austenite grain-boundaries impedes nucleation while the growth is hindered by the pinning action of TiC which are present within the austenite grains.

CHAPTER I

General Introduction

The austenite (γ) → ferrite (α) transformation in alloy steels is a topic of vital concern to metallurgists. Considerable attention has been given in recent years to elucidate the mechanisms which govern the nucleation and growth of the α during the diffusional decomposition of the austenite.

The present dissertation is an attempt to understand and explore the various aspects of the diffusional decomposition of the austenite. Attention has been focused on both the nucleation and growth processes and on the role of carbide particles in influencing these aspects.

The project initially started with work on four alloy systems and was extended to include other systems. Tungsten was selected as the main substitutional alloying element. It forms coarse tungsten carbides which can easily be detected using optical microscopy. Two of the four initial alloys also contained silicon. Silicon was added to suppress the pearlite reaction. Silicon is also believed to decrease the solid-solubility of carbides in ferrite. This aspect may be utilized to enhance interphase-precipitation during the transformation. In addition, it extends the α phase-field. So the temperature range for the study of interphase-precipitation can be expanded. In one of the tungsten steels (Fe-5.9W-0.21C (wt%)), a small amount of titanium (0.14% wt) was also added to examine its effect on the transformation kinetics. For studies of growth kinetics, Fe-C-X (where X is Cr or Ni) systems were selected. Nickel was selected primarily because it does not form its own carbide. So the effects of carbide precipitation on growth kinetics could in principle be eliminated, allowing an appropriate test for the theory for growth. In another alloy Cr was added. The addition of Cr helps us to understand any deviation of the experimental results from growth theory due to carbide precipitation or other effects such as solute-drag.

The dissertation has been set out as follows:

Chapter II is mainly devoted to the experimental techniques. Techniques such as alloy preparation and fabrication, heat-treatment, nickel plating, optical microscopy, transmission electron microscopy, scanning electron microscopy Quantimet and dilatometry are briefly discussed. Chapter III reviews the current understanding in the area of diffusional decomposition of austenite. It contains a literature review on the morphological

development of α and carbide precipitation during the transformation. Chapter IV highlights the microstructural features which develop during the γ → α transformation in a Fe-5.5W-2.03Si-0.37C (wt%) alloy. An alloy with similar composition but without silicon has also been studied to compare transformation characteristics. Many differences are reported between Fe-W-Si-C and Fe-W-C alloys and explanations are offered for these variations. Chapter V deals with the γ → α transformation in Fe-5W-0.23C (wt%). Special attention has been paid to the mechanism of the carbide precipitation, which occurred during the latter stages of growth. The effects of small addition of titanium on the kinetics of the γ → α transformation in this particular alloy have been examined. Chapter VI is concerned with the γ → α transformation in Fe-5W-2.3Si-0.15C (wt%) alloy. The nature of carbide precipitation has been observed and discussed in detail. The effects of carbide pre-precipitation on the kinetics of the γ → α transformation are reported in Chapter VII. An attempt has been made to establish the fact that the pre-precipitation of carbides at the austenite grain-boundaries can be employed to retard the γ → α transformation at low supersaturation. Studies on growth kinetics of α in a Fe-3.05Cr-0.11C (wt%) also are reported in the Chapter VIII. Similarly Chapter IX is concerned with growth kinetics of α in a Fe-3.28Ni-0.11 C (wt%) alloy. Finally, conclusions and suggestions for future work are presented in Chapter X.

CHAPTER II

LITERATURE REVIEW

2.1 INTRODUCTION

Study of the Austenite→Ferrite transformation in alloy steels is important partly because of the technological importance of the transformation and also because of the rich variety of structures and related properties accessible through variations in heat treatment. This transformation can be utilized as a direct route for strengthening alloy steels by fine dispersions of alloy carbides. These dispersions occur by repeated nucleation of carbides at the γ/α interface during the transformation and the reaction is therefore termed "interphase precipitation". Microstructures developed by interphase-precipitation are sensitive to both transformation temperature and alloy composition. Microstructurally, this mode of precipitation appears in planar, curved and irregular dispersions of alloy carbides. Planar or banded structures predominate when the interface is semi-coherent in the majority of cases. (Semi-coherent interfaces are regarded as low energy facets which move by a ledge mechanism. The band spacing depends upon the ledge height and may vary in the range of 5 to 50nm. Temperature and composition are the two main variables which decide the band spacing. Interphase precipitation is not only confined to low energy facets but it can also occur on the mobile high energy incoherent interfaces, leading to curved and irregular dispersion of alloy carbides. A bowing mechanism operates to form irregular dispersions of alloy carbides while quasi-ledge mechanism is responsible for curved dispersion of alloy carbides. The bowing mechanism predominates when the precipitate spacing is more than the minimum critical value, whereas a quasi-ledge mechanism operates when it is less than the critical value.

Though the mechanism of interphase precipitation has undergone considerable development in the recent past, many difficulties still persist, particularly with respect to the mechanism responsible for banded alloy carbide dispersions in isothermally transformed steels. Several recent reviews explore the ledge mechanism but none of them fully explain the factors that govern the ledge mechanism.

2.2 The $\gamma \rightarrow \alpha$ reaction

Depending upon the alloy composition and transformation temperature, austenite can decompose into proeutectoid ferrite, proeutectoid cementite, pearlite and bainite. Among those reactions, the proeutectoid ferrite reaction is the most important one. This is the first transformation product to occur over wide ranges of temperature and composition in most steels produced in large quantities. The kinetics of this reaction directly determine the hardenability of these steels and play a major role in establishing the mechanical properties. The proeutectoid ferrite reaction is also simplest from the viewpoint of ascertaining the effects of alloying elements upon the fundamental quantities determining the kinetics of a diffusional transformation, namely the rates of nucleation and the rates of growth.

The morphologies of proeutectoid ferrite can be complex and strongly temperature-dependent. The effects of alloying elements on the morphologies of ferrite have been deemed to be of least importance[1], although the kinetics are greatly altered by the presence of alloying elements. However, no correlation has ever been reported in literature concerning the effects of alloying elements on the morphologies of ferrite but the intuitive feeling is that it follows the general trends of Dube's morphological classification. This classification was further extended in detail by Aaronson.[2,3] Dube observed that the various shapes which ferrite crystals develop in plain carbon steels as the γ/α transformation temperature is lowered, can be classified into a few distinctive and well-defined morphologies. The following are the components of the Dube system in its present form:

1. Grain boundary allotriomorphs (Figure 1.1a): Crystals which nucleate at grain-boundaries in the matrix phase and grow preferentially and more or less smoothly along these boundaries. The morphology of a grain-boundary allotriomorphs does not reflect its internal crystallographic symmetry. These allotriomorphs start nucleating at the highest temperatures, i.e. just below Ae_3, and during the growth stage have a semi-coherent interface with one abutting austenite grain and an incoherent interface with the other adjacent abutting grain. As the transformation temperature is lowered, these crystals develop facets on at least one side but often on both sides of the boundary.

2. Widmanstätten side plate (Figure 1.1b): These plates nucleate at the γ-boundary but grow along well-defined matrix planes. They grow either directly from the boundaries (Primary side plates) or grow on pre-existing ferrite allotriomorphs (Secondary side plates).

3. Widmanstätten sawteeth (Figure 1.1c): They develop from the austenitic grain-boundaries and possess a triangular cross section in the plane of polish. Primary sawteeth grow directly from the matrix grain-boundaries whereas the secondary sawteeth develop from grain-boundary allotriomorphs.

4. Idiomorphs are equiaxed in shape and usually prefer to form within the interior of austenite grains (Figure 1.1d), but occasional evidence of grain-boundary idiomorphs has also been reported in literature.[4,5]

5. Intragranular Widmanstätten plates: These plates form within the grain and are similar to those growing from grain-boundaries (Figure 1.1e).

6. Massive structure: Such structure develops due to impingement of crystals of other morphologies (Figure 1.1f).

Although similar comprehensive reviews have never been reported concerning alloy steels, it is quite probable that this generalisation with some modifications may be applicable to these complex alloy systems.

Grain-boundary allotriomorphs are the dominant morphology which develops over wide ranges of composition and temperature in plain carbon steels. Nucleation of allotriomorphs takes place at high angle grain boundaries. Toney and Aaronson[4] using Fe-Si alloy, Hawbolt and Brown[6] and Clark[7] in Al-Ag alloy came to similar conclusions after examining the nature of the grain-boundaries at which allotriomorphs first nucleate. It is believed[8] that the formation of allotriomorphs takes place by the formation of a coherent plate-shaped nucleus at a high angle grain-boundary (Figure 1.2a). Grain-boundaries are more energetically favourable sites for the nucleation of allotriomorphs compared with interior of the grains, especially at the highest transformation temperatures where the driving force is rather low. The surface energy barrier to nucleation is minimized by elimination of grain-boundary area by precipitate matrix interface. Moreover, a coherent plate-shaped nucleus may be expected

whenever the precipitate and the matrix differ in volume and represent a compromise in the minimization of strain and surface energies.[9] Growth of the particle normal to the habit plane occurs due to enhanced diffusion along the grain-boundary (Figure 1.2a). The combination of transformation and growth along the boundary results in a loss of the strict precipitate habit and thus an allotriomorph with a disordered boundary is thought to develop from the initial nucleus. An alternate mechanism[10] for the development of allotriomorphs is shown in Figure 1.2b. Here the grain-boundary is believed to reorientate itself parallel to the habit plane of the nucleus. The driving force for this reorientation is the minimization of the interfacial energy of the particle. Again diffusion along the grain-boundary is invoked to produce non-crystallographic growth and subsequent loss of good matching between the precipitate and the matrix lattice.

With increasing supersaturation, secondary side plates develop from only one side of a grain-boundary allotriomorph. Widmanstätten plates are refined (i.e. length to width ratio increases) and growth occurs from both sides of allotriomorphs as the transformation temperature is lowered further. The source for the generation of secondary side-plates is believed to be the presence of protuberences which develop due to differences in the rates of migration of the interphase-boundaries. A second school of thought concerning the nucleation of secondary side-plates is due to Townsend and Kirkaldy[10] who postulated that ferrites nucleate at austenite grain-boundaries on $\{111\}_\gamma$ planes tangent to the boundaries (Figure 1.3a). A rational orientation relationship (K-S orientation relationship[11]) is proposed with respect to the grain in which nucleation occurs. This results in one low energy interface, the other being generally irrational. As the precipitate grows in dimensions, it loses its coherency (Figure 1.3b) and develops perturbation on the γ/α interfaces (Figure 1.3c) due to anisotropic surface tension. Widmanstätten plates ultimately develop due to anisotropic growth rate of the γ/α interface (Figures 1.3d,e).

Primary side-plates develop directly from the small-angle austenite grain-boundary[12] or near coincidence site boundaries. Plate-shaped nucleus is considered to form at or near dislocations in the boundary in order to minimize the effect of volume strain energy accompanying the transformation. The coherent regions between dislocations do not provide diffusion short circuit. The interfacial energy nor the mobility is available to convert the nucleus into

allotriomorphs. The broad faces of the nucleus thus remain immobile and the crystallographic shape is maintained during growth.

Plate-shaped nuclei grow through the action of the point effect of diffusion at the edge of growing plate, the concentration gradient about the edges are much steeper than the broad faces of the plates.[13] The crystallographic relationships which determine the orientation and habit plane of the nucleus are considered to be unimportant during the growth.[8] The shape and the habit plane of the nucleus are simply reproduced by the geometry of the diffusion of solute toward or away from the nucleus. However, a point effect alone cannot account for the evolution of side-plates almost invariably parallel to only one of four habit planes from such a crystal. It is speculated[8] that the anisotropic nature of the strain fields of the dislocations in the boundary produces an unequal distortion of the four $\{111\}_\gamma$ habit planes. As a result of this the atomic configuration on one of these equivalent habit planes is thought to best match with that of the precipitate, with a reduction of the surface energy for nucleation. This preferential reduction in interfacial energy is thought to result in the observed unique precipitate habit.

Nabarro attempted to analyse in detail the influence of volume strain energy on precipitate morphology in a series of excellent reviews.[14,15,16] According to his analysis, the plate-shaped morphology results from minimization of volume strain energy accompanying a transformation. However, the crystallographic nature of the plate morphology in transformations in which the lattice structures of the matrix and precipitate are different does not appear to be so explicable on this basis. The crystallography of the broad faces of Widmanstätten plates points strongly to interfacial energy and structure, rather than strain energy as the fundamental factors in the formation of plates. C.S. Smith[17] proposed a general theory of morphology in terms of interfacial structures and their migration characteristics. According to his hypothesis, the ferrite nuclei would have one coherent or semi-coherent interface with the austenite and thus normally a random or incoherent interface with the adjacent austenite grain. The normal orientation relationship between austenite and ferrite is represented by the Kurdjumov-Sachs relationship which applies to Widmanstätten ferrite and indeed probably in many cases to ferrite with an equiaxed appearance; viz

partially transformed specimens of a vanadium steel to show that precipitates formed in sheets parallel to the γ/α interface. They also made a detailed crystallographic analysis associated with these carbide formations. They observed that VC obeyed a Baker-Nutting[29] orientation relationship with the ferrite:

$$\{100\}_{\alpha} // \{100\}_{VC}$$

$$\langle 011\rangle_{\alpha} // \langle 010\rangle_{VC}$$

Since VC is crystallographically related to the ferrite, they came to the conclusion that these carbides nucleated at the γ/α interface and grew in the ferrite. They also noticed that only one variant of this orientation relationship was found within any precipitate colony. This was attributed to the restricting effects of the phase boundary on the precipitation reaction, forcing the precipitate to adopt the habit plane close to that of the boundary. This common mode of precipitation has been observed in many isothermally transformed alloy steels containing Ti[30], Mo[31], Nb[32], Cr[33], Cu[34], Au[35], etc. and termed as "interphase precipitation".

While there is general agreement that the sheets of precipitate form on the interphase interface, the exact mechanism for the movement of this interface during the precipitation reaction remained unexplained until 1974.[36] Heikkinen [38,39] proposed that an interface bowing mechanism may operate (Figure 1.4) in V-steel. The alloy carbide (VC) initially exerts a pinning action on the interface but as it grows the austenite ahead of the interface is depleted of carbon and thereby reduces the stability of the austenite. Under these circumstances, the interface would easily bow between precipitate particles. Having crossed the precipitate, it will straighten due to the surface tension and the process would continue. However, this mechanism could explain the observation of curved sheets of interphase precipitation but cannot be applied to explain the formation of planar arrays of interphase precipitation. Campbell and Honeycombe[36] proposed a ledge mechanism responsible for planar arrays precipitated in chromium steels. Frequent observations[37,35,36] of ledges on planar interfaces, strongly implies that these interfaces are of the partially coherent type which are related by a Kurdjumov-Sachs orientation relationship and displaced by the migration of ledges. The planar array of

precipitates nucleates at regular intervals on low energy interfaces and not on the energetically more favourable ledges during transformation. This is because the high mobility of the ledge prohibits nucleation and this has been confirmed by Aaronson et al.[23]

Curved as well as irregular dispersions of alloy carbides have sometimes been observed in association with planar arrays of precipitates. Those two types of carbide dispersion are associated with mobile incoherent γ/α interfaces Figure 1.5 is a schematic diagram illustrating the essential features of the bowing mechanism[40] which operate when the spacing between the precipitate is greater than the critical value. The critical value of precipitate spacing can be obtained using the relationship

$$a_{cri} = \frac{2\delta V}{\Delta G}$$

where a_{cri} = ½ spacing of precipitates along the row

ΔG = the free energy change per mole of γ transformed

V = the molar volume of austenite

δ = the surface energy/unit area

When the precipitate spacing is below this critical value, a quasi-ledge mechanism operates[41] to form curved arrays of precipitates (Figure 1.6).

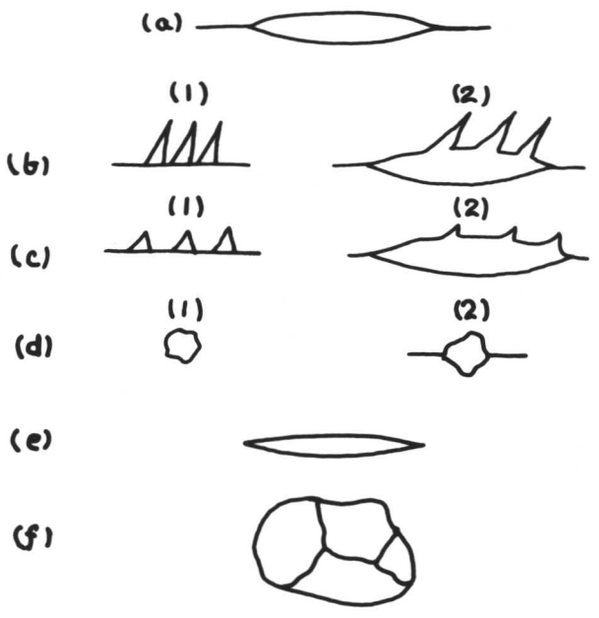

Fig. 1.1: (a) Grain-boundary allotriomorph

(b) Widmanstätten side plate

(c) Widmanstätten sawteeth

(d) Idiomorphs

(e) Intragranular Widmanstätten plates

(f) Massive structure

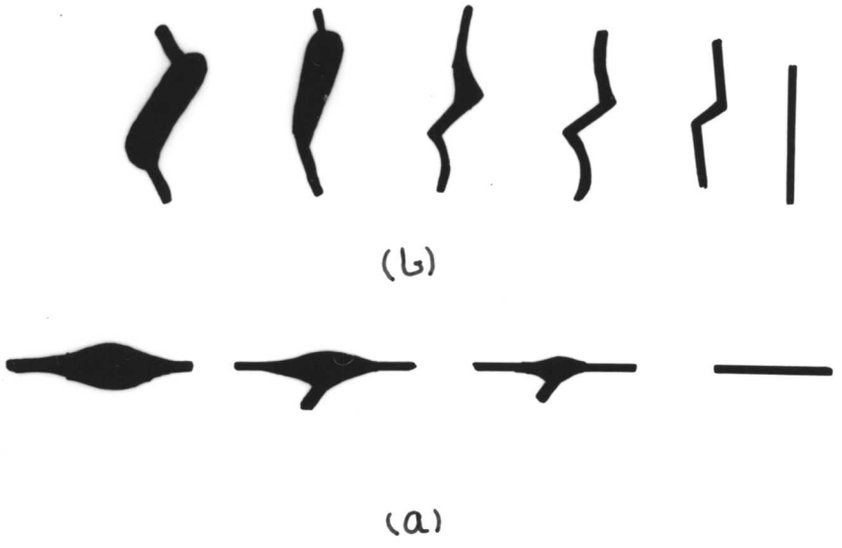

Fig. 1.2: Formation of grain-boundary allotriomorphs

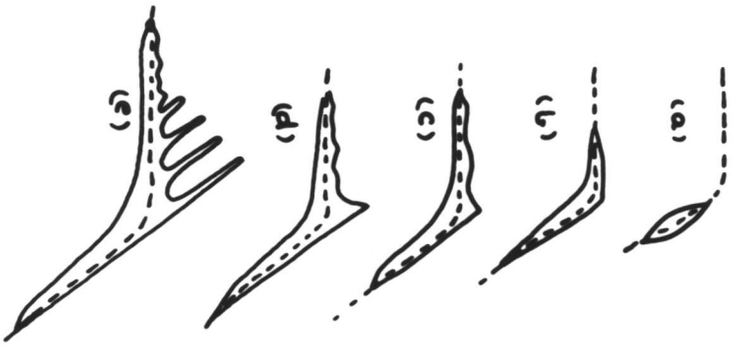

Fig. 1.3: Profile for developing Widmanstätten ferrite

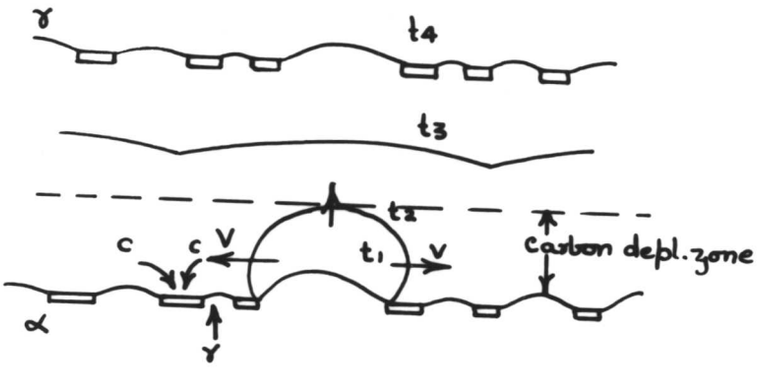

Fig : schematic model for the mechanism of interphase precipitation, proposed by Heikkinen

Fig. 1.4: Schematic model for the mechanism of interphase precipitation, proposed by Heikkinen.[38,39]

Where C = Carbon atom

V = Solute atom (i.e. vanadium)

t_i = Surface tension/area

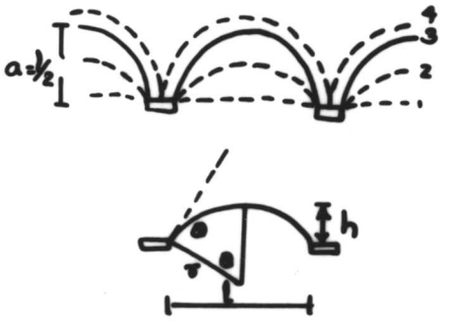

Fig: Schematic diagram of geometry of model used to calculate free energy balance associated with migration of interphase boundary by bowing mechanism.

Fig. 1.5: Schematic diagram of geometry of model used to calculate free-energy balance associated with migration of interphase boundary by bowing mechanism.[40]

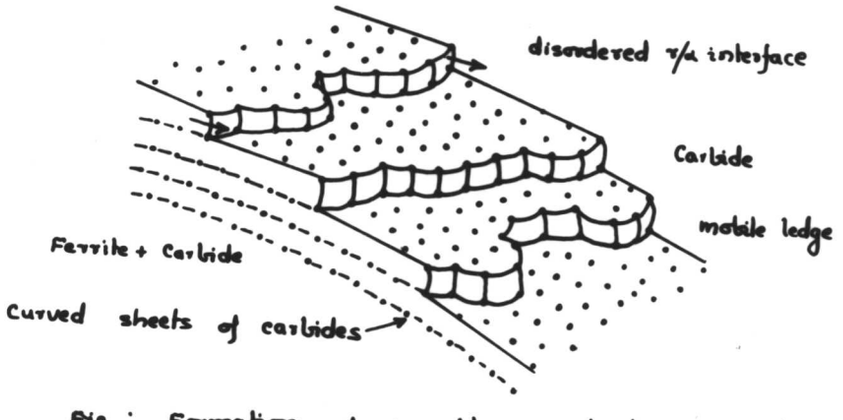

Fig: Formation of non planar sheets of precipitate by a "quasi-ledge" mechanism

Fig. 1.6: Schematic diagram showing quasi-ledge mechanism.[41]

In the third and final step of heat-treatment, the austenitized specimens were subjected to isothermal transformation in the temperature range of 850° to 700°C, followed by water quenching. The time of transformation varied from 0 to 500 minutes. After austenitizing, the silica tube was smashed and the specimen was immediately introduced in the fluidised bed furnace for isothermal transformation. It was felt essential to break the silica tubing before the commencement of isothermal transformation and to bring the specimen to transformation temperature as quickly as possible. The fluidising effect was produced by introducing air through the bottom of the bed. The flow rate of the air in the outer chamber was maintained at 250 cm^3/sec while in the inner chamber it was 84 cm^3/sec. An uniform temperature was maintained in the fluidised bed under these flow conditions. Al_2O_3 powder was used as fluidising medium for the outer chamber while Zr_2O_3 powder was used in the inner chamber. The temperature variation in all cases was maintained within the limit of ±2°C. Hand gloves and tongs were used while handling the specimens during heat-treatment.

The heat-treatment given to Fe-C-X alloys for optical metallograpy consisted of two stages. During the first stage, the specimens were austenitized at 1250°C for one hour and fifteen minutes. The long holding time at high austenitizing temperature was selected to ensure that the grain-boundaries are essentially perpendicular to the intended plane of polish. The specimens were in the form of small strips having a thickness of 5 mm. Prior to heat-treatment, more specimens were encapsulated in silica tubing containing argon gas at a partial pressure of 120 mm Hg.

In the second stage of heat-treatment, the austenitized specimens were subjected to isothermal transformation in the fluidized bed, followed by quenching in iced-brine solutions. The temperature of isothermal transformation varied from 750 to 600°C depending upon the type of alloy used. Similarly the time of transformation varied in the range 0 to 180 minutes or even higher in some cases. The silica-tube containing the specimen was broken quickly before introducing it into the fluidised bed for isothermal treatment.

The heat-treatment given to each alloy for TEM examination followed the same steps as mentioned above except that the austenitizing temperature was reduced to 900°C for 15 minutes. The low austenitizing temperature was selected to obtain a smaller grain size. The smaller grain size helps in locating the grain boundaries more easily during transmission electron microscopy.

3.4 Optical Microscopy

For optical metallography the heat-treated specimens were mounted on non-conducting bakelite and prepared by standard techniques. Care was taken during initial grinding to remove sufficient material to avoid any error caused by nucleation of the transformation product at the free surface.

After final polishing, the specimen was thoroughly cleaned and washed in methanol. 2% nital was used as an etchant in each case. Photography was carried out using an Olympus microscope.

A Quantimet 720 image analysing computer was used to determine the percentage of transformation in each specimen. The Quantimet 720 is attached with a Reichart optical microscope/epidiascope and Videcon/plumbicon television scanner which transfers the image analogue to a computer system. The image is composed of up to 705x896 picture points or pixels and discriminates between phases on a "grey level" basis. The areal fraction of a phase detected by means of grey level is D/N, where D is the number of detected picture points and N is the number of picture points in the "live frame". The machine scans the image with 720 lines at the rate of 7560 lines/sec which is much less than ordinary television camera scanners (i.e. 15650 lines/sec). This scan speed gives a better signal to noise ratio with improved resolution. Additionally, these scans are digitally controlled so that every pixel is of equal length and precisely positioned. The scanners used are plumbicon and videcon. The sensitivity variation of these scanners never exceeds more than 6% over half-million points. This sensitivity variation can be further reduced by "shade correction" by viewing a blank field for 30 seconds. The electrical noise levels are very low; it departs from the true value by one-and-half percent for 500 pixels. The noise variation can further be reduced by a factor of four by taking at least 16 scans of each field. The resolution of the Quantimet is limited by its ability to generate enough contrast from small features. The modulus transfer function $\{M(\lambda)\}$ which is a ratio of the output modulus to the input modulus exhibits a clear loss of resolution on very small feature. However, the videcon seems better than the plumbicon for very small features, and that is why in the present investigation the videcon scanner was preferred over plumbicon. Moreover, the videcon scanner has a constant low noise level than the plumbicon. The noise level in the plumbicon scanner increases as the light levels decrease down, and becomes troublesome. The dark

current or leakage of the Videcon system is higher and becomes troublesome at low light levels. The gamma value which refers to the ability of the electron/photon conversion process varies from 0.3 to 1 for Videcon and 0.9 - 1 for Plumbicon. This is adjusted by varying the illumination and light-sensitivity. In order to achieve high sensitivity at low light levels and to distinguish features of closely similar light intensity, it is essential to precisely adjust the resolution, shading, noise, absolute light sensitivity, dark current and gamma-value. However, at reasonable light levels, the Plumbicon can distinguish two features which differ slightly in their brightness. The Videcon on the other hand can distinguish features which slightly differ in their darkness. But if the features have high contrast, then both scanners will work efficiently. In general, Videcon has a broader dynamic range and should be preferred at distinguishing many different grey levels, while the Plumbicon is better at distinguishing pale features in a narrow contrast range, i.e. the microstructures showing high contrast levels should not be used on Plumbicon. To improve accuracy and stability, the signal from the scanner is passed to the control processor where an internally generated graticule is superimposed on the image for both measurement and calibration. There is also a provision to avoid the edge error by correctly setting the guard region.

The guard region is an area between the two limiting frames. The outer frame is called the live frame. The use of single frame may result in edge error when features are intercepted by frame and are sampled more than once in successive measurements. When the guard region is set correctly to a size which is larger than the largest features measured, the edge error vanishes.

Each feature of the image has an anti-coincidence point associated with it; the anti-coincidence point is a terminating point at the end of each feature (which also identifies a memory containing information about the feature). If the guard region is larger than the largest feature, then the feature which intersects the blank frame has an ACP inside the live frame. Consequently, if ACP lies in the live frame then all the feature must lie in the blank frame and will be correctly detected. Hence, all size and edge errors vanish.

The magnification of the imaging system is usually adjusted so that the smallest particle to be sized has an image at least one pixel in size. However, this is not always possible, because the largest particle may then cut down the size of the live frame to an unacceptably small level, since the size of the live frame equals 896 x 705.

The errors associated with point counting (i.e. D/N) can be assessed on a statistical basis. The relative error which is also called the coefficient of variance is given by σ_{v_f}/V_f where σ_{v_f} is the standard deviation and V_f is the volume fraction of the α-phase. The square of the relative error is known as the proportional variance (i.e.$(\sigma_{v_f}/V_\alpha)^2$) Hilliard and Cahn[2] derived an expression to determine the total proportional variance associated with a real analysis as follows:

$$(\sigma_{v_f}/V_f)^2 = \frac{1}{N_\alpha} \cdot \left| 1 + (\sigma_\alpha/a_\alpha)^2 \right|$$

where D = Number of the detected points/area.

N = Total number of points/area.

N_α = Number of α-phase particles measured.

σ_α = Standard deviation of the area of individual α-phase particles.

a_α = Mean area of the individual α-phase particle.

The above equation denotes that the proportional variance depends on the number of α-phase particles with respect to the size of the area examined and the variation in the size of the α-phase particles within the area examined.

However, in case of two-dimensional random point counting (i.e. D/N), the above expression has been modified to obtain the proportional variance. i.e. for point counting, the proportional variance is given by

$$(\sigma_{v_f}/V_f)^2 = \frac{1}{N_\alpha} \cdot \left| 1 + (\sigma_\alpha/a_\alpha)^2 \right| + \frac{1}{P_\alpha}(1-V_f)$$

where P_α = The number of intersections of the grid (i.e. number of detected picture points) falling in the α-phase.

3.5 Transmission Electron Microscopy

A Philips EM400 TEM was used for the examination of thin foils. A single tilt specimen stage was generally used but some times double tilt was used to obtain diffraction pattern from carbide by controlled tilting. The foils were examined at 120 kV. A magnetic correction was employed to improve resolution and to obtain a sharp image.

1.5 Preparation of thin foil: Discs of 0.25 mm thickness were cut from 3.2 mm diameter rod with the help of an oil-cooled carborundum slitting wheel. The discs were then thinned down to 0.05 mm by abrasion on wet 600 grade silicon

carbide paper. This thinning of the specimen was considered essential to reduce its magnetic mass, thereby minimizing magnetic aberrations in the electron microscope. The discs were jet polished with a "Twin Jet Electropolisher" (Fisschione). 5% perchloric acid plus 25% glycerol in ethanol was used as electrolyte. Optimum polishing conditions varied between alloys and heat-treatments but good results were obtained at an applied voltage between 40 to 50V and at a temperature of $15^{o}C$. After electropolishing, the thin foils were carefully cleaned in methanol and then dried. The foils were immediately examined after jet polishing to minimize the possibility of oxidation and contamination.

3.6 Isothermal Dilatometry

Isothermal transformation studies were done on a high speed dilatometer, namely "Dilatronic III" manufactured by Theta Industries Inc. of Post Washington, New York. Specimens having length of 20 mm and a diameter of 3.2 mm with internal diameter of 1.5 mm were used in this present study of isothermal transformation by Theta dilatometer. This particular dimension was selected to achieve rapid quenching. This hollow rod-shaped specimen was placed inside the silica tube (25 mm long and 4 mm diameter). It was then supported between two hollow silica-push rods and surrounded by radio-frequency induction coil. Radio-frequency induction coil is used to heat the specimen to the desired temperature at a controlled rate. Rapid quenching was achieved by flushing helium gas through the specimen. A vacuum of the order of 10^{-4} torr was created in the heating chamber before starting the experiment to protect the specimen from oxidation and decarburizing. The change in length of the specimen was transmitted to the transducer via a push rod and magnified to 100X 100 times. Both the change in length and temperature were monitored on a chart recorder which moved with a pre-set speed. Using the computer program developed by Yang and Bhadeshia,[3] the instantaneous change in length as a function of time at each isothermal temperature was recorded on a computer disc. These data were then transferred to the mainframe computer. Using the "Camplot" program on main frame, it became easy to plot the curve between the relative length change versus time. While recording the data on the computer disc, a correction was applied for the magnification. An automatic temperature control device was used to quench the specimen from its solution treatment temperature ($1200^{0}C$) to

the pre-set transformation temperature. By carefully setting the valve trigger, it was possible to avoid temperature overshoot by cutting off the quench gas at a pre-set temperature above the isothermal transformation temperature.

3.7 Microanalysis on a SEM

The scanning electron microscope with microanalysis facilities serves as a powerful technique to characterise the microstructural features of the specimen. The area to be examined is irradiated with a finely focused electron beam, which may be static or may sweep in a raster across the surface of the specimen. When the electron beam hits the surface, it emits radiation such as secondary electrons, backscattered electrons, Auger electrons, characteristic X-rays and photons of various energies. These radiations serve as signals to examine many characteristics of the samples (e.g. composition, surface topography etc.). For microanalysis on a SEM, the primary radiation of interest are the characteristic X-rays, emitted as a result of the electron bombardment. These characteristic X-rays are analysed to give both qualitative and quantitative compositional information from regions of a specimen as small as a few micrometers in diameter. Moreover, the detailed microcompositional information can be directly correlated with optical metallography.

For microanalysis, one needs to measure the energy and intensity distribution of the X-ray signal generated by a focused electron beam and to convert these data into a useful form for qualitative and quantitative analysis. This can be achieved in two ways:

(a) Wavelength-Dispersive Spectrometer (WDS)

In this method, a small portion of the X-ray signal generated from the specimen passes out of the electron optical and impinges on an analysing crystal. The incoming X-rays are diffracted by the analysing crystals provided the Bragg law is satisfied (i.e. $n\lambda = 2d \sin \phi$.)

The diffracted X-rays are detected by a proportional counter and then they are amplified, converted to a standard pulse size by a single-channel analyser (SCA) and finally, counted with a scaler or displayed as a rate meter output on a strip chart recorder. Standard tables are used to identify the element from crystal spectrometer readings.

(b) Energy-Dispersive X-ray Spectrometer (EDS)

In this method, the X-ray signal from the samples passes through a thin beryllium window into a cooled lithium-drifted silicon detector. The incoming X-rays are absorbed by the detectors which in turn ejects photo-electrons. These photo-electrons give up most of their energy to the formation of electron-hole pairs. The electron-hole pairs are swept away by the applied bias to form a charge pulse by a charge-sensitive pre-amplifier. The signal is finally passed to a multi-channel analyser (MCA) after amplified by main amplifier. MCA sorts out the pulses by voltage. The contents of the MCA memory are transmitted to a computer for further processing such as peak identification or quantification.

All the microanalysis experiments have been done on the ISI scanning electron microscope. This is capable of doing both quantitative and qualitative microanalysis of the specimen. It works on the principle of EDS. There is a suite of programs available which permits the calibration and routine quantitative electron microprobe analysis of polished bulk specimen to be carried out. One such set of programs is ZAF-4/FLS. This program is stored on a diskette and operates on 1K spectra using 10, 20 or 40 eV/channel calibration. It can handle all radiations within the selected range. All overlapping peaks including K, L or M series are deconvolved using standard profiles. In cases where both K and L or L and M lines from one element exist within the spectron, both are deconvolved but only one is used in the ZAF correction procedure.

For quantitative analysis of the specimens using the program ZAF-4/FLS, the relative X-ray intensity ratio between the elements of interest in the specimen (I_{sp}) and the same elements in the standard (I_{st}) are measured. Both specimen and the standard (i.e. cobalt and copper) are examined under identical experimental conditions. The measured intensity ratio is commonly called K_i. The K_i value is then further corrected to take into account the effects such as (1) atomic-number effect expressed by the factor Z_i (2) absorption of X-rays within the specimen, A_i, (3) fluorescence effects F_i. The weight fractions of the element (C_i) of interest is obtained by using the relation

$$C_i = Z_i A_i F_i K_i$$

Table 1.1

Alloy Composition

wt% W	wt% C	wt% Si	wt% Ti	wt% Fe
5.5	0.37	2.03	0.0	Balance
5.8	0.4	0.0	0.0	Balance
5.0	0.15	2.3	0.0	Balance
5.0	0.23	0.0	0.0	Balance
5.8	0.5	0.0	0.0	Balance
5.9	0.21	0.0	0.14	Balance

Table 1.2

Alloy Composition

wt% Cr	wt% Ni	wt% C	Fe
3.05	0.0	0.11	Balance
0.0	3.28	0.11	Balance

CHAPTER IV

The Austenite→Ferrite transformation in Fe-5.5W-2.03Si-0.37C (wt%) and Fe-5.8W-0.4C(wt.%) alloys

4.1 INTRODUCTION

This chapter is concerned with the study of the $\gamma \rightarrow \alpha$ transformation in tungsten steels of composition Fe-5.5W-2.03Si-0.37C (wt.%) and Fe-5.8W-0.4C(wt.%). This transformation has been utilised for the fundamental investigation of interphase precipitation in many alloy steels. In recent years, it has become increasingly clear that interface precipitation represents the common mode of precipitation of alloy carbide in steels containing carbide formers like V, Ti, Nb, Cr, Mo, etc. Non-carbide forming elements such as Cu and Au have also precipitated by the interphase precipitation mechanism. In this structure, the ferrite contains closely spaced parallel bands or sheets of fine alloy carbide precipitates. The sheet spacing is sensitive to temperature and composition, and varies in the range of 5 to 50 nm. The planar array of precipitates nucleates at regular intervals on low energy interfaces during the transformation and hence delineates the path of the γ/α interface. These low energy interfaces are displaced by the migration of ledges which are taken to have a "disordered" structure. In all studies to date, the precipitation has been found to be limited to the low energy interface facets in preference to the ledges. According to classical nucleation theory, the ledges should be the favoured sites for nucleation to occur relative to the low energy facets. The most convincing and yet very powerful argument in support of this interesting reversal of nucleation behaviour is given by Honeycombe in his excellent review[1] on "Transformation from Austenite in Alloy Steels". These ledges move during transformation and hence provide the least opportunity for nucleation to occur there. Consequently nucleation takes place on the low energy, less mobile interfaces. This hypothesis was further confirmed by Aaronson et al.[2] Their theory indicates that carbide nuclei will be overrun before their development is complete when they attempt to form at the ledges. A meagre and

scant observation was presented concerning precipitation on the disordered ledges in Fe-10%Cr-0.2C (w.t%) alloy.[3] In highly alloyed steels, they believe that the mobility of ledges is reduced and at the same time the solute concentration at the interface is increased. Both conditions favour the formation of precipitates on the ledges. Once the precipitation has occurred, the ledges will be pinned. The sequence of events following this pinning would presumably require the passage of subsequent ledges to overtake and unpin the ledge containing the precipitate.

Interphase precipitation is not only confined to low energy immobile interfaces which grow by the ledge mechanism leaving behind a planar array of discrete particles but also extended to high energy mobile interfaces which ultimately result in curved as well as irregular dispersions of particles due to their inherent growth characteristics. A bowing mechanism operates to form an irregular dispersion of particles when the precipitate spacing is greater than the minimum critical value whereas a quasi-ledge mechanism is believed to operate when their spacing is less than the critical value.[4,5]

The present work is undertaken with a view to exploring some of the elusive phenomena of interphase precipitation which still persist and remain unsolved and hence to provide more viable explanations so that mechanism of interphase precipitation can stand on a much more rigorous quantitative footing.

4.2 Experimental Results on Fe-5.5W-2.03Si-0.37C (wt.%) alloy

4.2.1 Isothermal Transformation at 850°C

Isothermal transformation at 850°C for 5 minutes showed about 10 volume % transformation. The resultant microstructure showed that the nucleation of α-ferrite has occurred predominantly at the austenite grain-boundaries and grew in a blocky manner to form what are known as grain boundary allotriomorphs (Fig. 4.1). Close optical examination of the γ/α interface indicated the presence of both smoothly curved, presumably incoherent, as well as facetted, semi-coherent interfaces. However, the proportion of facetted semi-coherent interface was much more than the curved one. It was also observed that the γ/α interfaces in the majority of the cases were pinned by carbides. Pinning by carbide has occurred in two different ways. Firstly, interphase precipitation

has occurred at the γ/α interface and consequently the interface has been pinned. Carbides can also pin the interface if it is already present in the austenite. Such interface showed protuberances which were formed as the γ/α interface moved across these carbides. The pinning has a direct effect on the kinetics of the γ/α transformation. It can delay the transformation and hence this approach can be effectively exploited in increasing the hardenability of alloy steels.

Many interesting phenomena were observed when this alloy was isothermally transformed at 850^{0}C for 20 minutes. Figure 4.2 shows that interphase precipitation is not only limited to the low-energy facets but it can also occur on the ledges. It was also observed that the ledges were not of the same height but they varied in height even at the same interface. Figure 4.3 shows another striking phenomenon. Pinning of low energy interface is clearly shown in this micrograph. The fact that cusps are developed where the carbides pin the facets is conclusive and direct evidence that the facets migrate normal to the facet plane without any ledge mechanism. Figure 4.4 shows that facets as well as ledges both move but the rate of migration of the facet is low compared to the ledges. This is also indicated by the fact that separation of the facet increases with distance away from ledges. So the classical view that the facet does not move at all during a diffusional process must be incorrect. Clearly as the temperature drops, the difference in mobility of the low energy and high energy interface must increase. Therefore the ledge mechanism as understood classically becomes well defined for low temperature regions. That is why we observe a very irregular ledge mechanism (Figs. 4.5 and 4.6).

Occasionally the absence of precipitation on mobile ledges was also observed (Fig. 4.7). The interphase precipitation associated with highly facetted idiomorphic ferrite was also noticed (Fig. 4.8). Figure 4.9 shows that the ledges were apparently moving in two opposite directions. It suggests that these ledges might have nucleated on the facet. Figure 10 shows the complex nature of carbide precipitation during the $\gamma \rightarrow \alpha$ transformation. Figure 4.11 illustrates that the interphase precipitation is confined to only one side of the austenite grain boundary. This supports the view proposed by Smith.[19] He proposed that it is energetically more favourable for ferrite to nucleate if it develops a coherent or semi-coherent interface (i.e. one which exhibits interphase precipitation by ledge mechanism) with one abutting austenite grain and a random or incoherent interface with the adjacent

austenite grain. Figure 4.12 shows the highly facetted α-ferrite. (These particular micrographs were taken from the alloy which had slightly different composition than the original one. The chemical composition of this new alloy was Fe-5.9W-1.95Si-0.36C (wt.%). It is believed that this effect is presumably due to the presence of silicon.

The scanning electron micrographs are shown in Figs. 4.13 and 4.14. The interphase precipitation by ledge mechanism does not always result in uniform band spacing, as shown in Fig. 4.13. It further supports the view that the ledges are not uniform in height. Direct evidence to support this view is presented in Fig. 4.2. The SEM taken from the specimen which is slightly different in composition than the original one is shown in Fig. 4.14. This specimen was isothermally transformed at 850°C for 40 minutes. Figures 4.14(a) to (d) show that the carbide precipitation has occurred on the planar facet but apparently there is no evidence of ledges. These micrographs also show that the growth has occurred mainly on one side of the boundary while on the other side its growth is restricted. The carbides present along the boundary might have exerted a pinning action to inhibit the growth on the other side of the boundary. These micrographs also show that the α-ferrite is highly facetted.

The large number of pictures have been included to demonstrate that the features observed are not peculiarities but reflect the general complexity of the carbide precipitation during the transformation.

4.2.2 Isothermal Transformation at 800°C

Isothermal transformation at 800°C for 2.5 minutes showed about 10 volume % transformation. This is the temperature at which minimum incubation period was recorded. It indicates that the nose of TTT diagram is around 800°C. The transformation has occurred predominantly at the austenite grain boundaries (Fig. 4.15). The allotriomorphs appeared as dark etched regions along the grain boundaries. Figure 4.16 needs special attention. This micrograph shows the presence of fibrous carbide associated with the interface which has migrated by ledge mechanism. Evidence of interface pinning was also noticed.

4.2.3 Isothermal Transformation at 750°C

Isothermal transformation at 750°C for 5 minutes showed 10 volume % transformation. Again the reaction has occurred mainly along grain-boundaries as expected. The aspect ratios of these allotriomorphs are quite high compared to the allotriomorphs formed at higher temperatures. A continuous layer of the transformation product was observed in the majority of cases (Fig. 4.17). Pinning of the interface by carbides has also been observed (Fig. 4.18). Fibrous carbide was also recorded (Fig. 4.19).A strong tendency towards facetting was noticed.

4.2.4 Isothermal Transformation at 700°C

The incubation period increased as the transformation temperature was further decreased. Only 6 volume % transformation occurred after holding the specimen at 700°C for 10 minutes. The transformation started at the grain boundaries, forming a continuous layer of the transformation product (Fig. 4.20). In the majority of cases, the interface appeared planar. Figure 4.21 illustrates some important crystallographic aspects of the transformation product on macroscopic scale. This micrograph illustrates the formation of allotriomorphs at the junction where three grain boundaries meet (i.e. formation of allotriomorphs at the triple point). Evidence of interface pinning was noticed, even at this temperature.

At all temperatures, the transformation started at the grain boundaries to form grain-boundary allotriomorphs. At higher temperatures separate nuclei could be seen but as the transformation temperature is lowered a continuous layer of ferrite is formed along the grain boundary. In the majority of cases, the interface appeared planar. Ledges of variable heights were observed at the highest transformation temperature (850°C). Extensive evidence of interphase precipitation was noticed at the highest temperature. Interphase precipitation was not only limited to the low energy facets but it was also extended to the ledges. No evidence of interphase precipitation was obtained optically during the early stage of transformation (10 vol.%) at all temperatures. Ledges appeared more frequently at higher temperatures as compared with lower

temperatures (on a microscopic scale). Direct evidence of the normal migration of facets was recorded at highest temperature of transformation. However, no such evidence was obtained as the transformation was reduced (i.e. 750°C and 700°C). Evidence of interface pinning was also noticed at all temperatures. It was also noticed that the aspect ratio of the allotriomorphs increased with decreasing temperatures. Absence of Widmanstätten ferrite at all transformation temperatures (850°C to 700°C) led to the conclusion that most of the allotriomorphs were bounded by low energy interfaces since Widmanstätten ferrite is believed to grow from incoherent boundaries of the allotriomorphs.[19]

Transmission electron microscopy was used to reveal the details of the microstructural features of the ferrite formed in the temperature range of 850°C to 700°C. Electron micrographs showed extensive evidence of interphase precipitation at 850°C. Figure 4.22 shows that the band spacing is not uniform. It also shows that at some stage of transformation, the ledges have combined together. The point where the two ledges join, the band spacing is doubled in size as shown by arrow in Fig. 4.22. Precipitation on the mobile ledge is shown in Fig. 4.23. With decreasing transformation temperature, it was found that the carbides had a tendency to form from supersaturated ferrite - and not by interphase mechanism (Fig. 4.24). These carbides have been identified as W_2C and M_6C [6-10]

The TTT diagram for 10 volume % transformation is shown in Fig. 4.25. The fastest reaction occurs at 800°C and the transformation starts after an incubation period of approximately 2 minutes at 800°C. The $\gamma \rightarrow \alpha$ transformation can also be described by Avrami-equation, the general form of which is given by

$$f = 1 - \exp(-kt^{\eta})$$

$$\text{where} \quad f = \frac{\text{volume fraction of } \alpha}{\text{equilibrium vol. fraction of } \alpha \text{ at temp. T}}$$

where η is a number whose value can vary from 1 to 4. The value of k depends on nucleation and growth rate and is therefore sensitive to temperature.

Figure 4.26 shows the isothermal section of Fe-Si-C alloy in the temperature range of 1000K to 1373K. Figure 4.27 shows Fe-C equilibrium diagram at constant silicon content. Both these diagrams indicate that silicon has strong tendencies to expand α-field. In addition to this silicon is also believed to decrease the solid solubility of carbides in ferrite. Both these aspects have been exploited to their full extent in the present study of Fe-5.5W-2.03Si-0.37C wt.% alloy.

Wilyman[11] studied the effect of Al and Si on isothermal transformation characteristics of Fe-V-C alloy, and came to the conclusion that these elements accelerate the interphase precipitation which is consistent with our results.

4.2.5 Step Quenching

The specimens were first austenitized at 1200°C for 30 minutes, then isothermally transformed at 850°C for 20 minutes followed by step quenching at 750°C for 10 minutes.

The optical micrographs taken from these specimens (Fig. 4.28(a) to (d)) show the evidence of interphase precipitation surrounded by a thick grey layer. It was expected that the thick grey layer was due to the formation of fibrous carbides at lower transformation temperature. However, contrary to the opinion, the electron micrographs revealed that the thick grey layer consisted of dense carbide precipitates. Absence of fibrous carbides at lower temperature further strengthen the view that most of the interfaces were semi-coherent in nature and hence prevented the formation of fibrous carbides.

Micrographs taken from the double step quenched specimens (i.e. 850°C 20 min → 750°C 20 min → 850°C) were shown in Figs. 4.29 to 4.34. These micrographs show that the carbides have precipitated by interphase mechanism as well as from supersaturated ferrite. Precipitation on the mobile ledges were also observed.

4.3 Discussion

Grain-boundary allotriomorphs were the first transformation product observed over the temperature range (850° to 700°C) of the investigation. A strong tendency towards facetting was observed in this alloy particularly at higher temperatures of transformation. Frequent evidence of ledges implies that these interfaces have been displaced by a ledge mechanism. The aspect ratio of these allotriomorphs increased with decreasing transformation temperatures since the role of grain boundary carbon diffusion in allotriomorphs lengthening then becomes more significant.

Extensive evidence of interphase precipitation was obtained using optical microscopy and SEM. These micrographs also show that the interphase precipitation is not only limited to the broad faces (i.e. low energy facets) but it can also occur on the mobile ledges. The question which immediately arises is how nucleation can occur on the migrating ledges, and once the

nucleation has occurred, how do these ledges migrate instead of being pinned? To understand this unusual behaviour, it is essential to know the migration characteristics of ledges. The migration characteristics of the individual ledge may vary due to the point effect of diffusion acting along its height. It can be anticipated that the higher the ledge height, the slower will be its speed. In the present work, the ledges are unusually very high (μm). The migration velocity of such ledges of exceptional height would be appreciably low. Under such circumstances it is possible for the embryos to develop into successful nuclei before it will be overrun by the ledges. Once an embryo turns into a successful nucleus, it pins the ledges. So a mechanism is needed to explain migration characteristics of such a ledge which has been pinned by carbides. The leading ledges, which are pinned by carbides, are unzipped by trailing ledges which overtake them. This sequence of events is repeated again and again and we get random precipitates along with planar array of interphase precipitation.

It is also possible that some of these ledges lag behind giving an opportunity for nucleation to occur. Another possibility is that during later stages of transformation, some of these ledges are forced to adopt a rational interface orientation and under these circumstances, carbides can easily nucleate on them.

It was also observed that ledges are not of the same height even at the same interface. This variation is about an order of magnitude. The variation in ledge height has also been reported earlier.[11] Variable ledge heights can be explained on the basis of migration characteristic of ledges. Ledges do not migrate with equal velocity due to overlapping diffusion fields of adjacent ledges.[12,13] The velocity of leading ledges is reduced compared to the trailing ledges due to overlapping diffusion fields. As a consequence of which, the trailing ledge catches the leading ledge and merges with it. For the interface containing three ledges, the second ledge can either merge with the first (i.e. leading ledge) or the third ledge (i.e. trailing ledge) depending on its position. If it is nearer to the first ledge, it will merge with the leading ledge. But if it is nearer to the third ledge, it will be caught by the trailing ledge and the first ledge will escape. This explains why we observe trailing ledges of more height than the leading one occasionally. As ledge multiplication occurs during the growth of ledged interfaces and we observe ledges of variable heights, the process of ledge

multiplication continues until the ledges acquire a maximum limited height. Beyond this limited height, the "point effect of diffusion" from the top to the bottom of riser starts acting and hence the ledges become unstable. At this point it is worth mentioning the paper by Bhadeshia.[14] He developed a simple equation to correlate the critical ledge height (h) with interfacial energy (δ)/area and chemical-free energy change per unit volume (ΔF_v^m). This relationship can be written as

$$h^* = \frac{\delta}{\Delta F_v^m}$$

Though the measured ledge height exceeded the predicted minimum value of h*, the calculated and experimental curves showed strikingly similar trends as a function of transformation temperature.

Frequent evidence of cusps on low energy facets was noticed at the highest transformation temperature (Fig. 4.3). Development of cusps on low energy facets led to the view that these interfaces have moved normal to the facet plane without the need of a ledge mechanism. (The cusps are developed as the interface moves across the carbides during the transformation .) So the classical view that the low energy facets do not move at all during diffusional process must be incorrect. Figure 4.4 clearly illustrates the fact that both low energy facets and ledges move during the transformation. But the rate of migration of facets is low compared to the ledges. No such evidence was recorded at lower transformation temperatures. This clearly suggests that as the temperature drops, differences in mobility of the low energy facets and ledges (i.e. high energy facets) must increase. Consequently, the ledge mechanism becomes better defined for low temperature regions.

Occasionally, fibrous tungsten carbides were observed (Fig. 4.16). The interesting point about these carbide fibres is that they appear to grow from the interface that has migrated by ledge mechanism. So far in the literature it is strongly argued that these fibres grow in association with high energy interfaces. This unusual observation needs further investigation before arriving at any conclusion.

At all transformation temperatures, the γ/α interface appeared planar in the majority of cases. A high proportion of the planar γ/α interface observed in this alloy indirectly suggests that silicon has a pronounced effect on modifying the interfacial structure during the early stage of transformation.

Since low energy facets move by a ledge mechanism, it is expected to have extensive interphase precipitation in this alloy.

So far in the literature least attention has been paid to the effect of alloying elements on the morphologies of the α-ferrite. It is usually reported that in the case of many alloy steels the morphology follows the general trends of Dube's morphological classification. The present observation does not fully support this view. It is not clear how the kinetics of the $\gamma \rightarrow \alpha$ transformation can be altered by addition of alloying elements without affecting the nature of the interface which basically controls the transformation during the early stages.[15]

At this stage the argument may appear unsound but it has got some justification and relevance too. Alloying elements may modify the interfacial structure between the parent and the product phase in order to synchronize the transformation kinetics. Those alloying elements which accelerate the transformation kinetics, particularly Al, Co, Si, may tend to develop a nucleus bounded by semi-coherent interface. Formation of semi-coherent nucleus requires considerably less thermodynamic force than those bounded by incoherent ones. The interfacial energy (δ) term is directly related to the minimum energy (ΔG*) required to develop an embryo into successful nucleus within the parent crystal. This relationship may be expressed as follows:

$$\Delta G^* = \frac{16\pi\delta^3}{\Delta G_v^2} + \frac{n^2 E}{1-\nu}(C-C_o)$$

where ΔG_v is volume-free energy term associated with transformation. $n = (1/a)d \ln a/C$, in which a is the lattice parameter, E is Young's modulus, ν Poisson's ratio, C_o is average nucleus composition and C is the change in the nucleus composition as a function of distance.

ΔG* is related to the rate of nucleation (J*) which is a time dependent phenomenon. This relationship is given by:

$$J^* = Z B^* n e^{-\Delta G^*/kT} e^{-\tau/t}$$

where Z is the Zeldovich factor, B* a frequency factor, n the number of nucleation sites and τ the incubation time.

In the above equation the dominating factor is ΔG*.[16] So the rate of nucleation can be accelerated by minimizing the value of ΔG* which is directly

related to the interfacial energy term. The interfacial energy term will be minimized provided the parent and product phases adopt an orientation relationship which allows low energy interfaces to develop between the phases. ΔG^* can be further reduced if the embryo develops on a crystal boundary of the parent phase.[17,18]

Though energetically it is more feasible to form a nucleus bounded by low energy semi-coherent interface, crystallographic restrictions may prevent it doing so and an intermediate situation arises in which a nucleus may develop which is neither fully semi-coherent nor totally incoherent. C.S. Smith[19] long ago proposed that the ferrite nuclei would have one coherent or semi-coherent interface with the austenite and thus normally a random or incoherent interface with the adjacent austenite grain. Recently Howell and Honeycombe (1983)[20] analysed in detail the crystallographic aspects of diffusional transformation in metals and alloys and came to the conclusion that the existence of reproducible orientation relationships implies that partial coherency can exist at the majority of the interface orientations and that a truly incoherent or disordered structure is rare. Further, Ryder et al[21] and King and Bell[22-24] also discovered that the product phase exhibited rational orientations with both abutting parent grains.

The present work supports this view, particularly when the transformation is accelerated by addition of alloying elements such as silicon.

4.4 Experimental Results on Fe-5.8W-0.4C (wt.%) alloy

4.4.1 Isothermal Transformation at 850°C

No evidence of transformation product (ferrite) was obtained at this temperature even after 8 hours at the transformation temperature. Fine precipitates of tungsten carbide within the austenite grain were observed. These carbides are possible of the type M_6C (Fe_4W_2C). In the absence of an appropriate phase diagram, it can be anticipated from microstructural observations that at 850°C, the phase field consists of $\gamma + M_6C$ only.

4.4.2 Isothermal Transformation at 800°C

About 15 volume % transformation was recorded at 800°C after 20 minutes. Nucleation started at the austenite grain-boundaries and growth occurred along these boundaries to form blocky allotriomorphs (Fig. 4.35). The rate of nucleation appeared slow compared with the growth rate. These effects resulted in developing coarse-grained ferrite. The γ/α interfaces appeared curved in most cases. In the majority of cases, the interface appeared serrated as well as ragged (Figs. 4.36 and 4.37). Evidence of carbide precipitation within the ferrite was recorded. The dispersion of these carbides appeared random. With further increase in transformation time (40 minutes), the allotriomorphs grew with a relatively low aspect ratio. Evidence of ledges was also obtained on planar interfaces in some cases. Almost all interfaces appeared either serrated or ragged due to pinning effect. A random distribution of tungsten carbide within the ferrite was noticed.

Evidence of banded structures formed by an interphase mechanism was also noticed in certain cases. The presence of ledges (Figure 4.38) in association with the banded structures indicates that these carbide dispersions have occurred on low energy interfaces which moved by the migration of ledges. This micrograph also shows that the banded structure has developed only on one side of austenite grain, while the other side of the grain shows random distribution of carbide dispersion. Figure 4.39 shows a grain-boundary allotriomorph bounded by planar interface. Cusps were frequently observed on these planar interfaces. Presence of cusps on the planar interfaces is taken as evidence of normal migration of these interfaces without a ledge mechanism. (Cusps are developed as the interface moves across the precipitate particle.)

4.4.3 Isothermal Transformation at 750°C

The minimum incubation period (8-10 minutes) was recorded at this temperature. It suggests that the nose of the TTT diagram is near 750°C. The transformation started mainly at the austenite grain-boundaries leading to the formation of grain-boundary allotriomorphs. The aspect ratios of these

allotriomorphs were high compared to those formed at 800°C. Evidence of interface pinning was also recorded at this temperature.

4.4.4 Transformation at 700°C

The $\gamma \rightarrow \alpha$ transformation started at around 40 minutes at this temperature. Only about 5 volume % transformation was recorded at this temperature (Fig. 4.40). It suggests that the rate of transformation is slowest at this temperature. The transformation started at the grain-boundary and grew rapidly along it to form the allotriomorph (Fig. 4.41). The aspect ratios of these allotriomorphs are quite high compared to those formed at 800°C or 750°C. These ferrites appeared virtually free from carbides. However, precipitation at the γ/α interface was frequently noticed. Figure 4.42 shows clear evidence of pinning of low energy interface. Cusps on these interfaces strongly suggest that these low energy interfaces have moved normal to the facet plane without a ledge mechanism.

No evidence of Widmanstätten ferrite was obtained in the temperature range of 800°C to 700°C.

TEM studies further revealed that there was less evidence of interphase precipitation in this particular alloy. Most of the carbides were formed from supersaturated ferrite. Unlike silicon-containing steels, these carbides appeared in several different morphologies (Fig. 4.43). The volume fraction of these carbides increased with decreasing transformation temperature (Fig. 4.44). The carbides were identified as M_6C (i.e. Fe_2W_4C). Clear evidence of interface pinning by tungsten carbide was recorded (Fig. 4.45).

A TTT diagram is constructed for 10 volume % transformation. This suggests that the transformation is fastest around 750°C and the incubation gradually increases as we move away from this temperature. Figure 4.46 shows a TTT diagram for 10 volume % transformation. The kinetics of $\gamma \rightarrow \alpha$ transformation is compared with the alloy containing the silicon, as shown in Figure 4.47. The figure clearly shows that silicon has a strong tendency to accelerate the transformation kinetics.

4.5 DISCUSSION

This alloy showed a tendency towards contracting the α-phase field. The

rate of transformation appeared slow compared to the alloy containing silicon. These two effects are mainly due to the presence of a higher percentage (0.4 wt.%C) of carbon in the alloy. The Ae_3 temperature for this alloy is around 800°C.

Grain-boundary allotriomorphs were the first transformation product to appear at virtually all austenite grain-boundaries throughout the temperature range of investigation. No evidence of Widmanstätten ferrite was recorded even at temperature as low as 700°C. It indicates that with increasing carbon content, the temperature for formation of Widmanstätten ferrite decreases. The condition required for developing Widmanstätten ferrite depends on two factors, in the case of plain carbon steel.[25] With increasing carbon content, T_w (i.e. temperature for start of Widmanstätten ferrite) also decreases. Further, an appreciable amount of undercooling below Ac_3 curve is a pre-requisite for the formation of Widmanstätten ferrite. In the present case, it appears that none of these conditions are satisfied.

At the highest transformation temperature (800°C), the rate of nucleation appeared slow compared to their growth, which led to coarse-grained ferrite. The aspect ratio of these allotriomorphs appeared low compared to those formed at lower transformation temperature (700°C) as expected for volume diffusion controlled growth of ferrite.

Frequent evidence of curved interfaces was noticed at all temperatures. It appears that in the majority of cases, the ledge mechanism did not play an important role in determining the growth kinetics of the transformation product in this particular alloy in the temperature range of 800°C to 700°C.

Evidence of interface pinning was noticed throughout the temperature range of investigation. Serrated interfaces developed due to pinning action by those carbides which have formed by an interphase mechanism. Ragged protuberances were developed as the interface moved across the carbides which were already present in the austenite. Both these mechanisms of interface pinning can be utilized to delay the transformation kinetics and hence to increase the hardenability of many alloy steels.

Cusps were frequently observed in association with planar interfaces. It is anticipated that those cusps were developed as the planar interfaces moved normal to itself without the ledge mechanism.

Random distribution of alloy carbide (M_6C) within the ferrite was noticed for transformation at 800^0C. These carbides were either formed from supersaturated α-ferrite or by precipitation at the incoherent γ/α interface. However, the ferrites formed at lower temperature (700^oC) were virtually free from carbides. This may be due to high supersaturation of ferrite formed at lower temperature as compared to the ferrite formed at higher temperatures.

It was also observed in limited cases that on one side of the grain, banded carbide dispersion appeared, whereas on the other side random dispersion of alloy carbide was noticed. Ledges were seen in association with the banded structure. This strongly implies that these banded carbides were formed on the low energy interface which moved by ledge mechanism. A random dispersion of alloy carbides was formed possibly by precipitation at incoherent γ/α interfaces.

4.6 Conclusions

1. Silicon has a pronounced effect on enhancing interphase precipitation at high transformation temperatures. It expands the α-phase-field and lowers the solid solubility of the alloy carbides in ferrite. In addition, it has a strong tendency towards developing a high proportion of low energy facets which move by ledge mechanism. It can be anticipated that these factors may combine to enhance interphase precipitation in Fe-5.5W-2.03Si-0.37C (wt%) alloy. It also accelerates the kinetics of the $\gamma \rightarrow \alpha$ transformation.

2. Interphase precipitation is not only limited to the less mobile low energy facets but it can also occur on more mobile high energy facets (i.e. ledges).

3. Ledges may vary in height even at the same temperature and this variation may be on order of magnitude.

4. Near the highest transformation temperature (i.e. just below Ae_3) both low energy facets as well as ledges move. The rate of migration of low energy facets is low compared to the ledges. As the temperature drops,

differences in mobility of the low energy facets and ledges must increase so the ledge mechanism may predominate for low temperature regions.

5. The alloy without silicon showed a tendency to contract the α-phase-field. Random dispersion of tungsten carbides (M_6C) was frequently observed. These carbides have either formed from super-saturated α-ferrite or by interphase precipitation at the incoherent γ/α interface and not at the semi-coherent interface.

6. Pinning of the γ/α interface by tungsten carbide was recorded at all temperatures of transformation in Fe-5.8W-0.4C alloy. Serrated interface indicates that the pinning has occurred due to interphase carbide precipitation at the incoherent γ/α interface. Ragged or protuberance on the interface developed as the γ/α moved across the carbide particles present in the austenite.

7. The γ → α transformation was slower than in the alloy containing the silicon. Slower transformation rate is attributed to the two main factors: (a) high percentage of carbon (i.e. 0.4 wt.%C (b) lower mobility of the γ/α interface due to pinning action.

8. Only in rare cases, the banded carbide dispersions were noticed in Fe-5.8W-0.4C (wt.%) alloy.

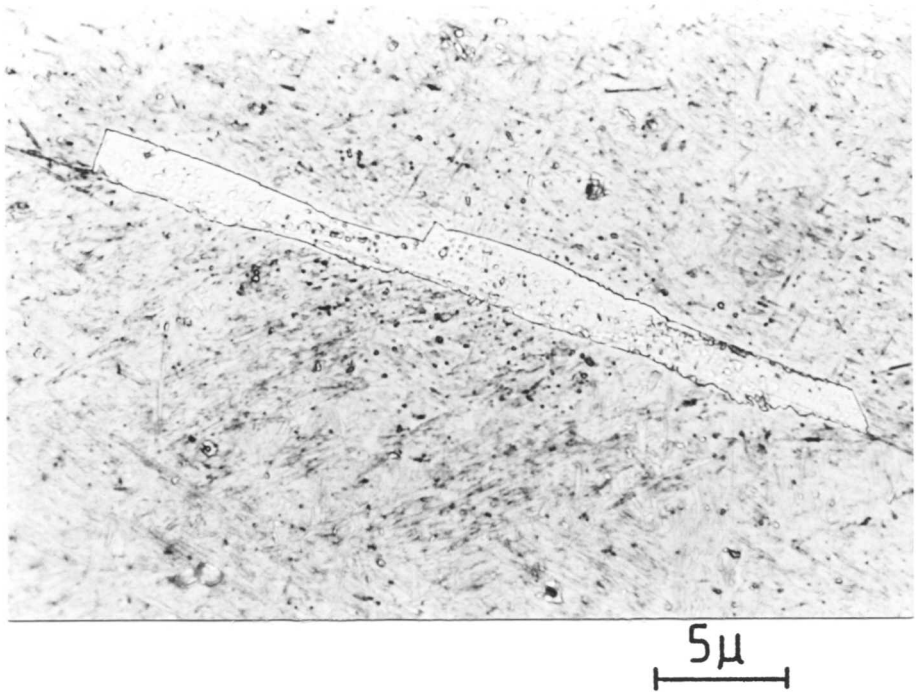

Fig. 4.1(a) Showing grain-boundary allotriomorphic ferrite. (Isothermal transformation at 850°C for 5 minutes.

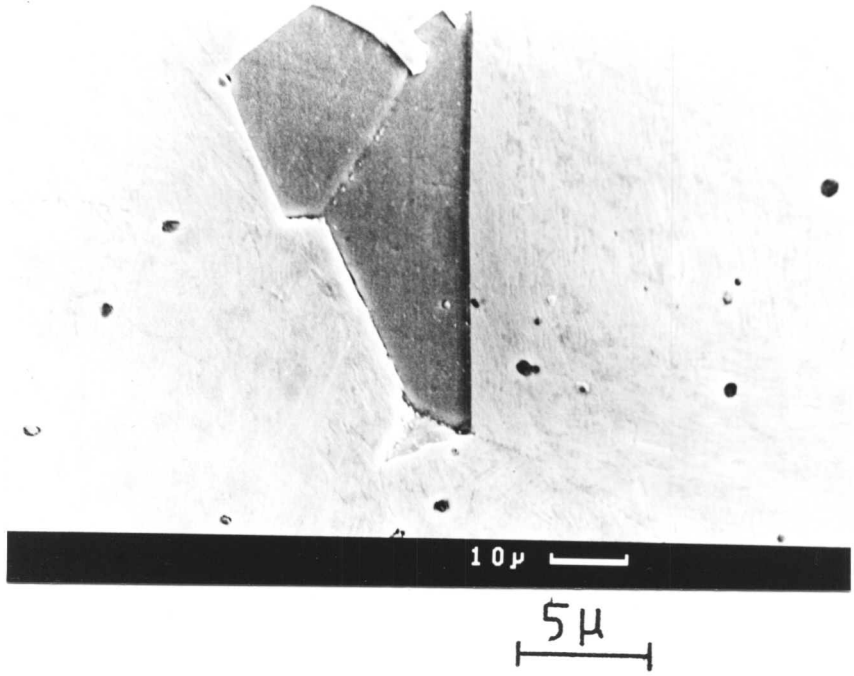

Fig. 4.1 (b) Highly facetted α - ferrite (isothermal transformation at 850°C for 5 minutes).

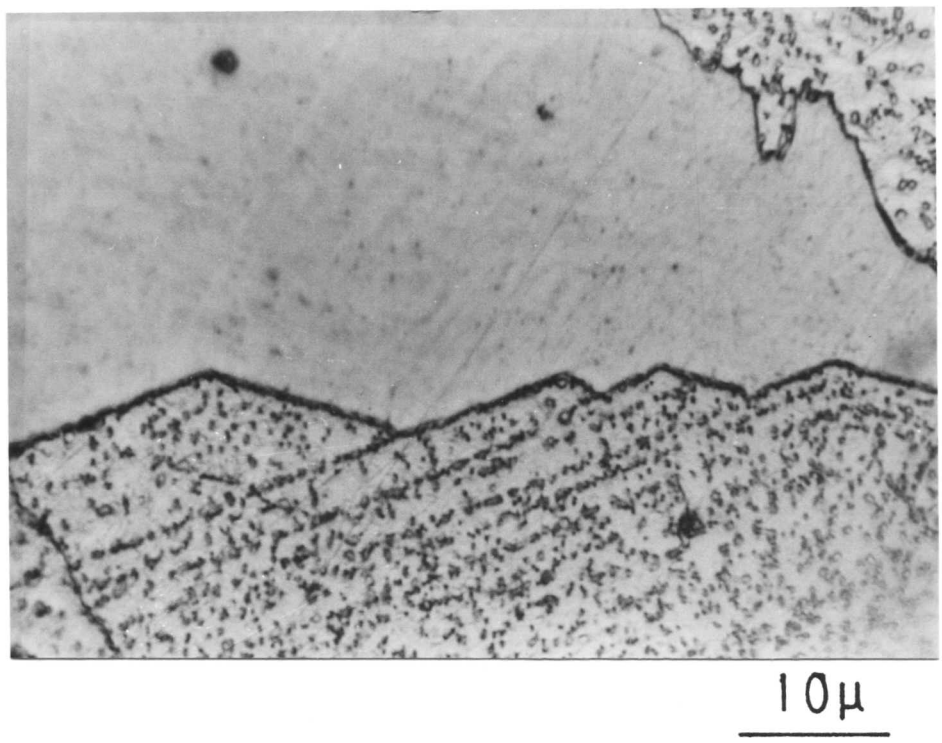

Fig. 4.2 Showing precipitation both at the low energy facets and ledges. Random distribution of alloy carbides are clearly apparent within the banded carbide dispersions. (Isothermal transformation at 850°C for 20 minutes.

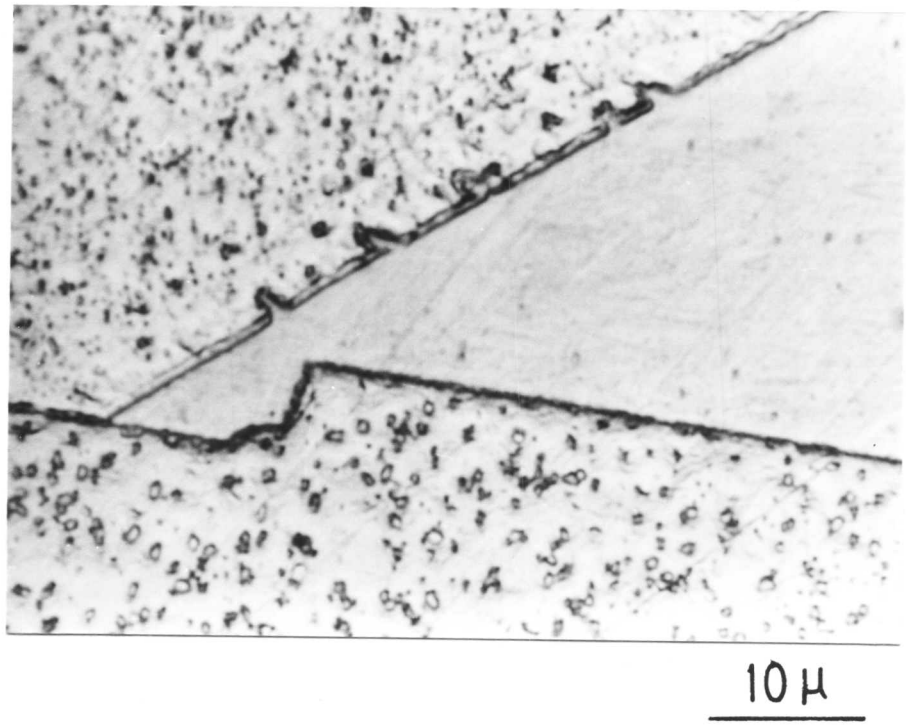

Fig. 4.3 Showing cusps on low energy facets. (Isothermal transforamation at 850°C for 20 minutes.

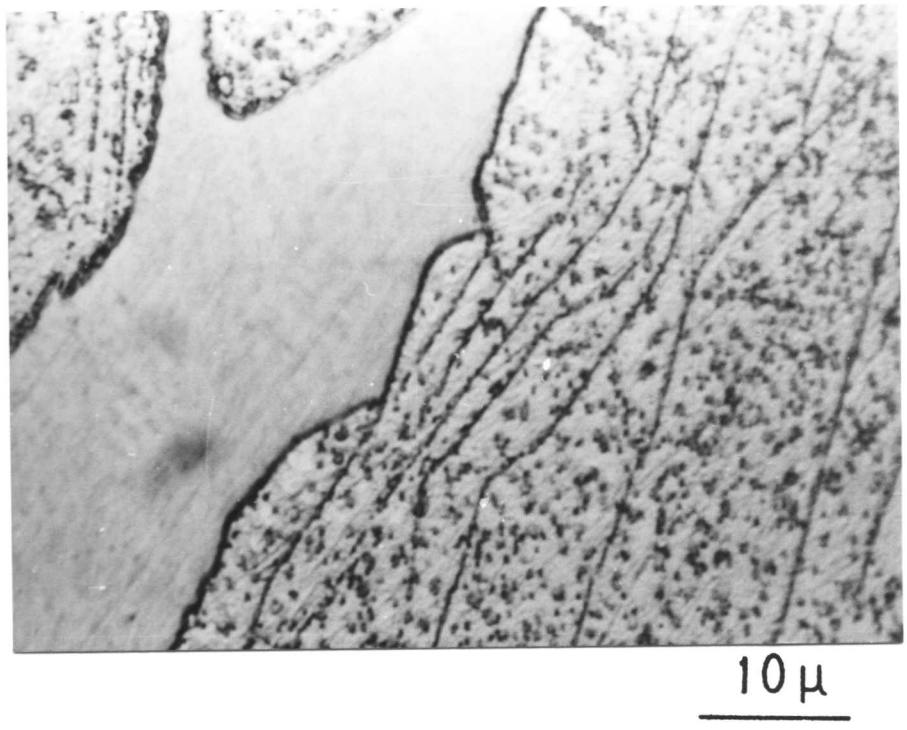

Fig. 4.4 Shows that low energy facets as well as ledges both move. (Isothermal transformation at 850°C for 20 minutes.)

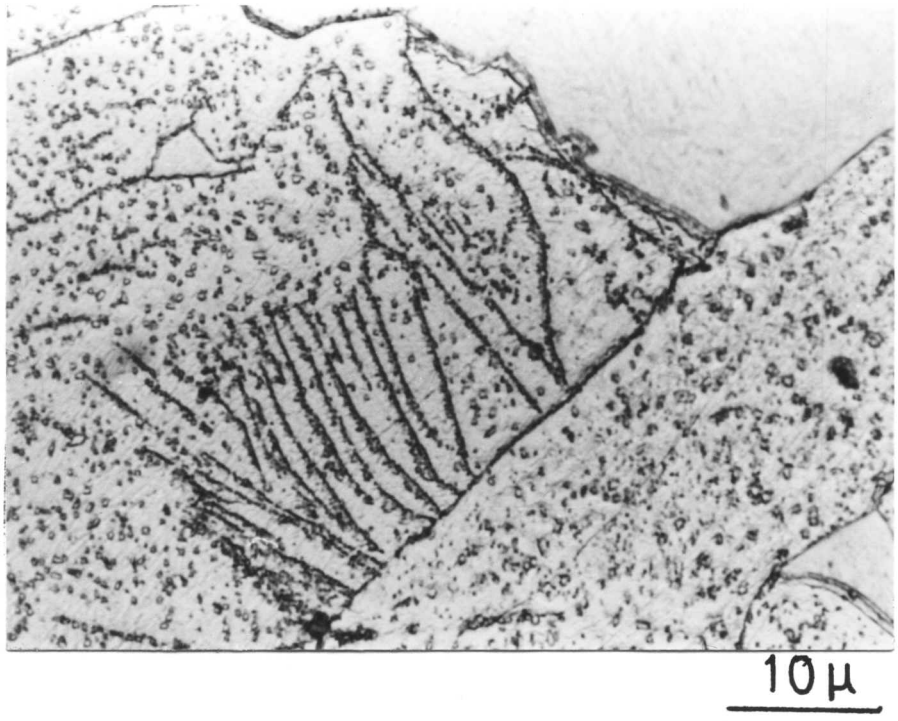

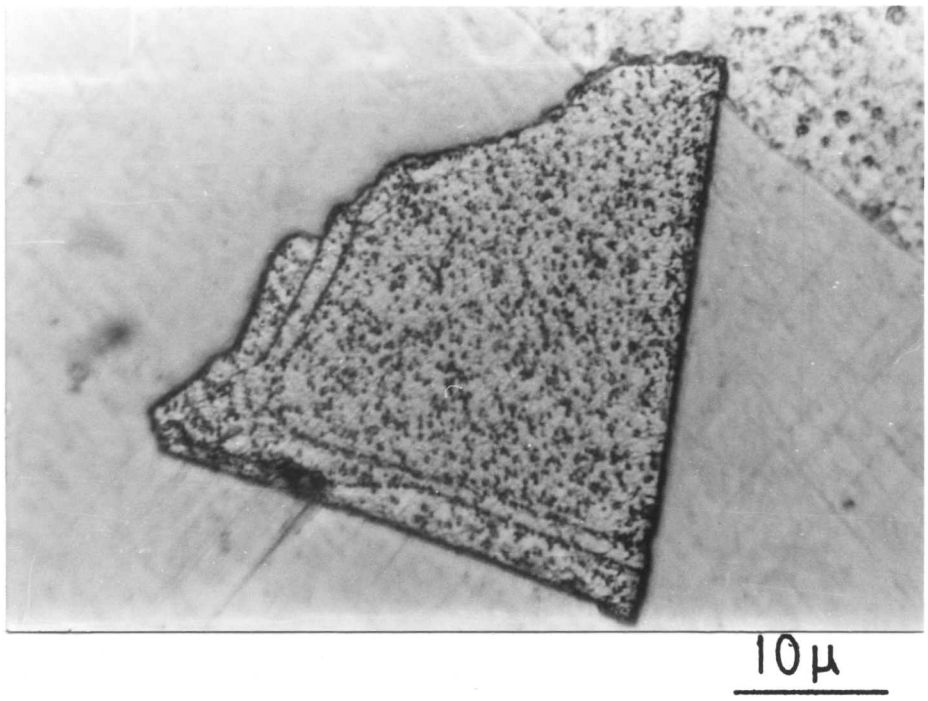

Figs. 4.5 and 4.6 showing an irregular ledge mechanism.
(Isothermal transformation at 850°C for 20 minutes.)

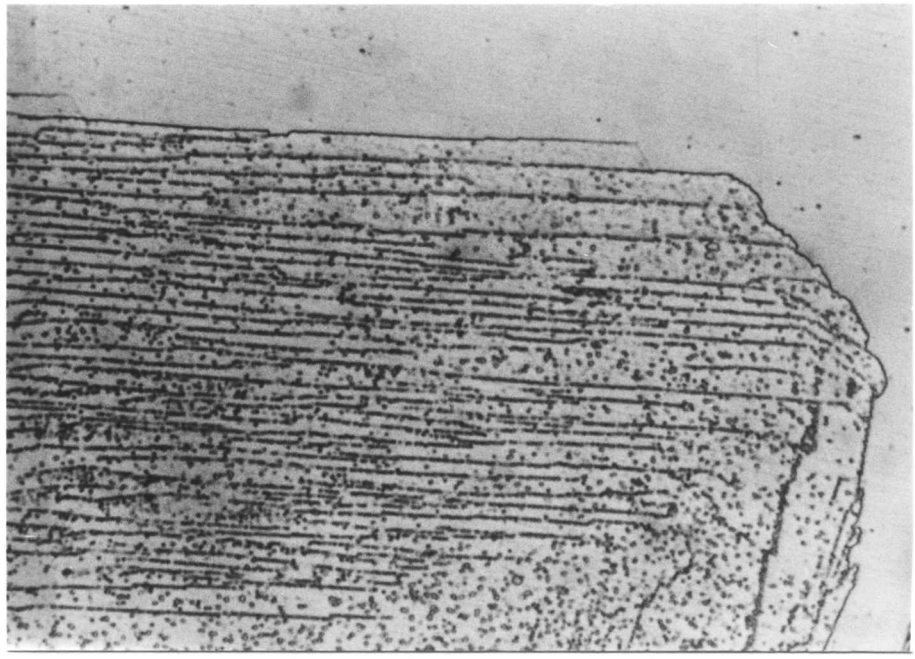

Fig. 4.7 Showing absence of precipitation on mobile ledges.

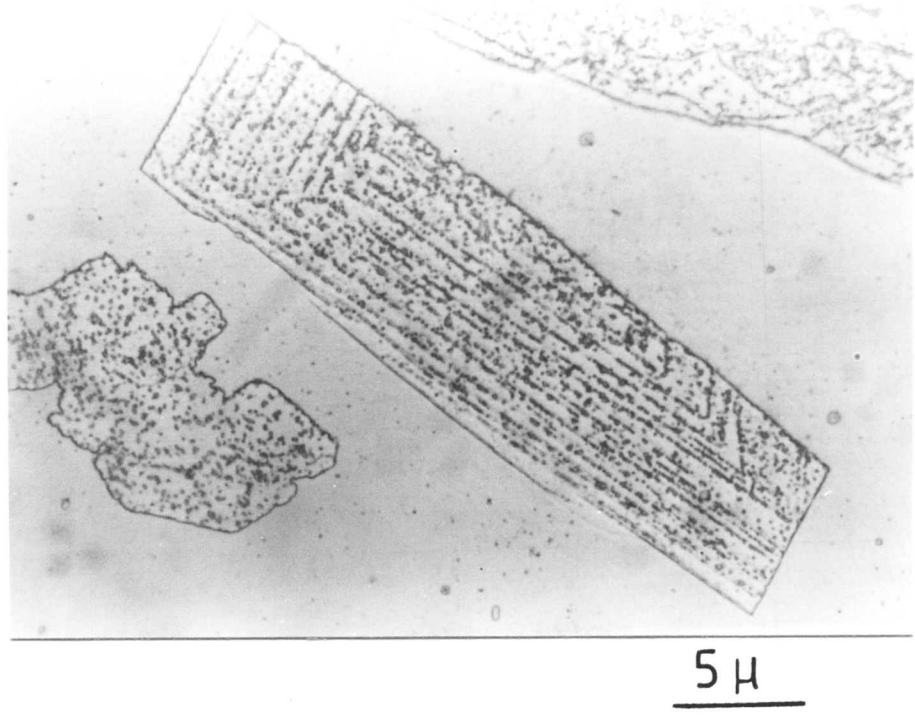

Fig. 4.8(a) The interphase precipitation associated with highly facetted idiomorphic ferrite is evident in this micrograph.

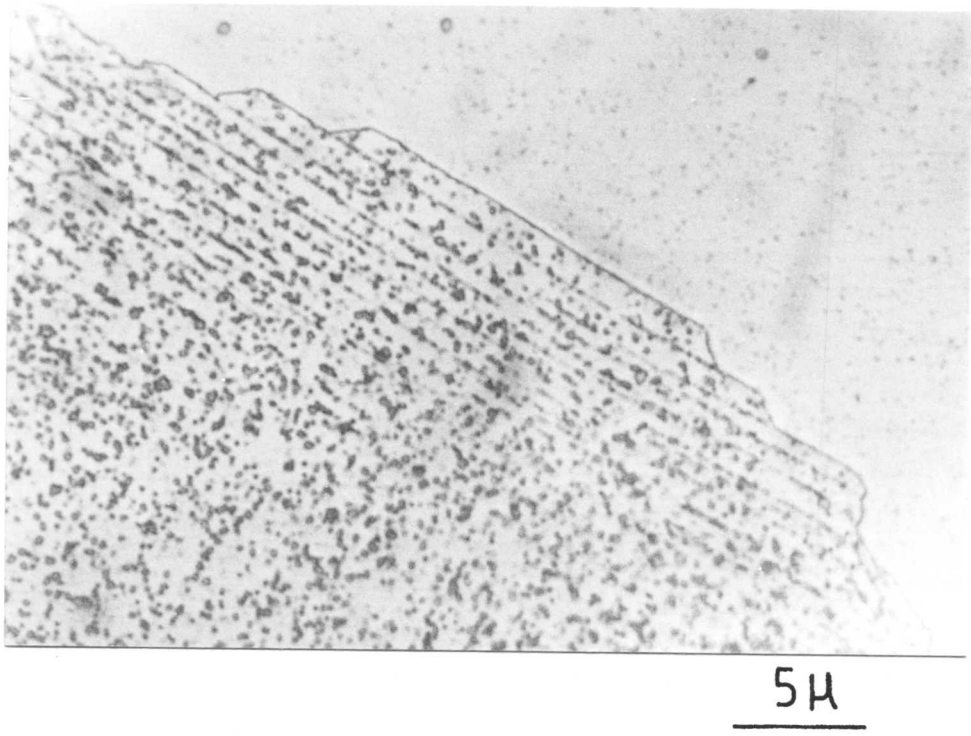

Fig. 4.9 Ledges are moving in two opposite driections on the same interface.

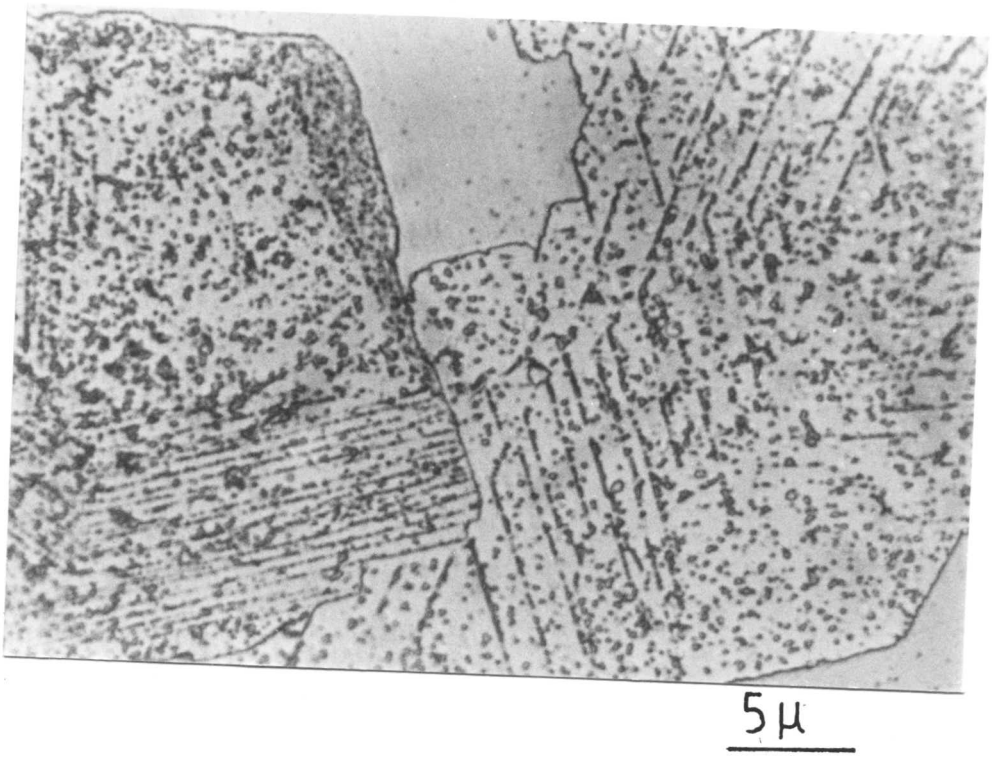

Fig. 4.10(a) Complex nature of carbide precipitation during the $\gamma \rightarrow \alpha$ transformation is apparent in these micrographs.

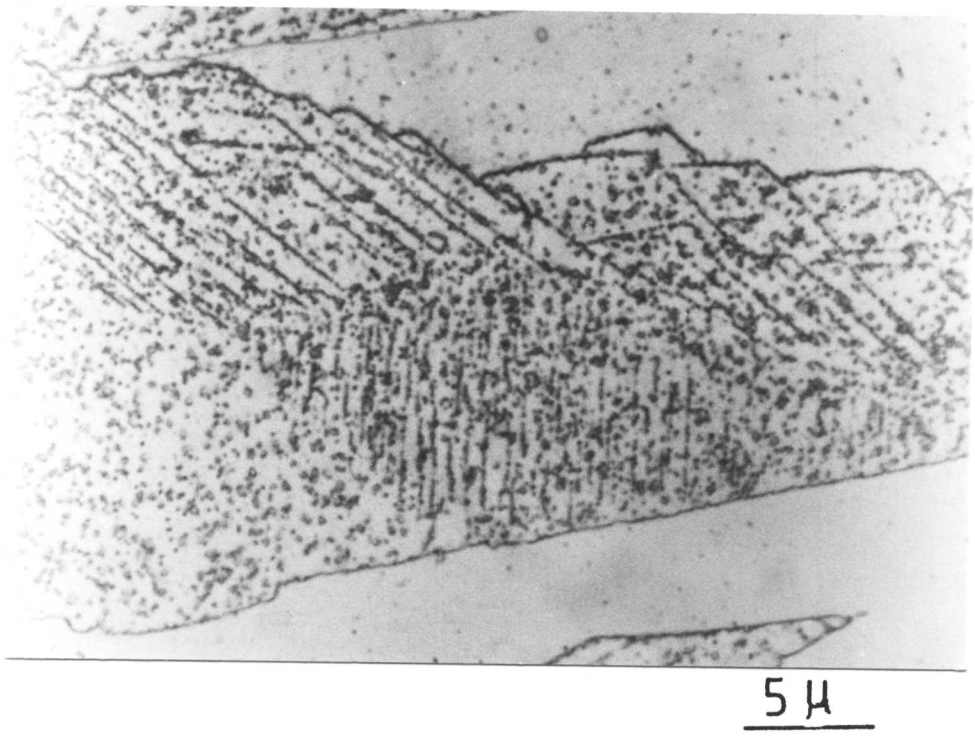

Fig. 4.10 (b)

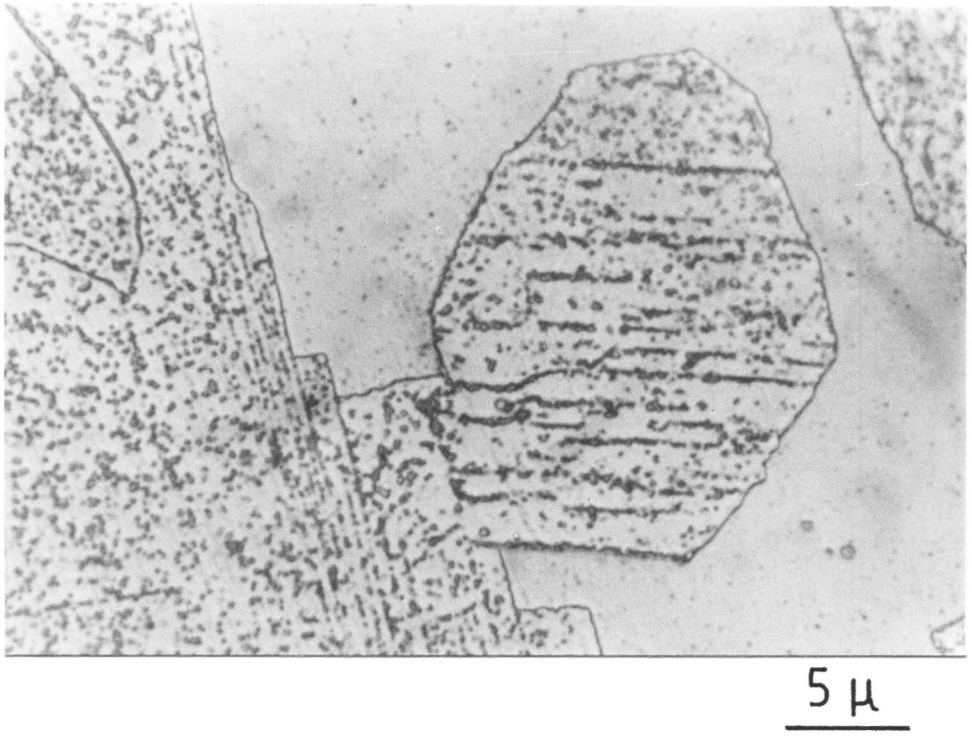

Fig. 4.10 (c)

Fig. 4.10 (b) and (c) Complex nature of carbide precipitation during the $\gamma \rightarrow \alpha$ transformation is apparent in these micrographs.

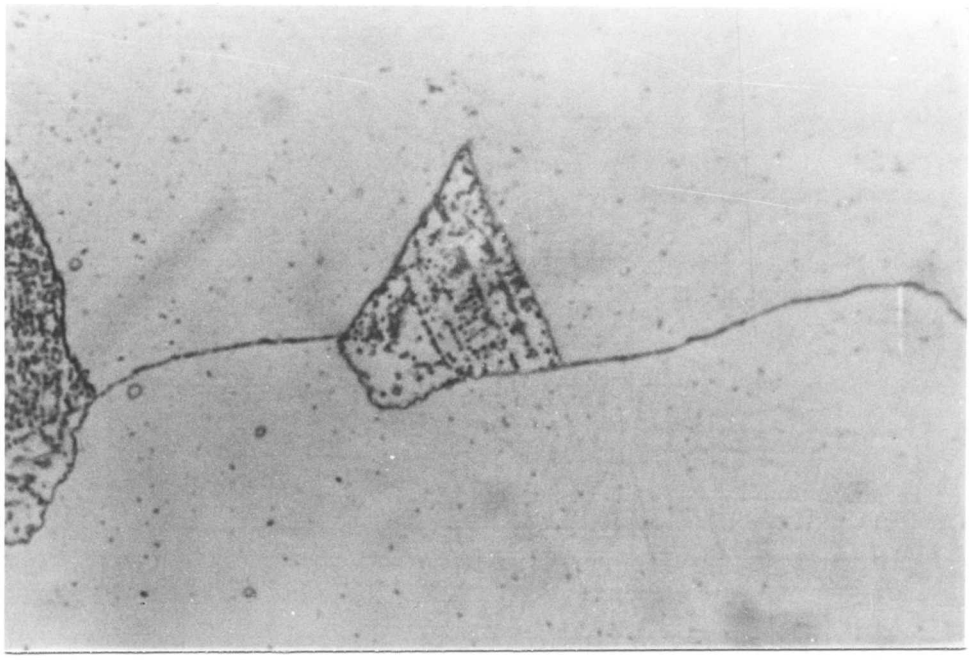

Fig. 4.11 The grain-boundary allotriomorph showing interphase precipitation to only one side of the grain-boundary.

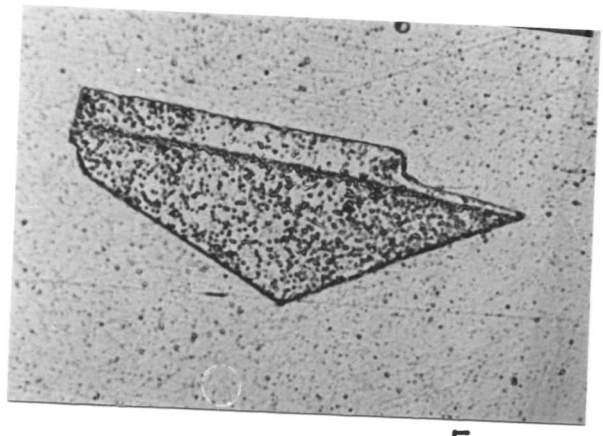

(a)

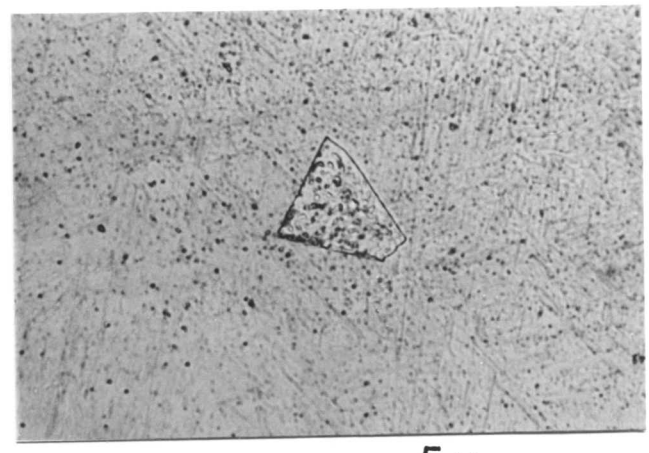

(d)

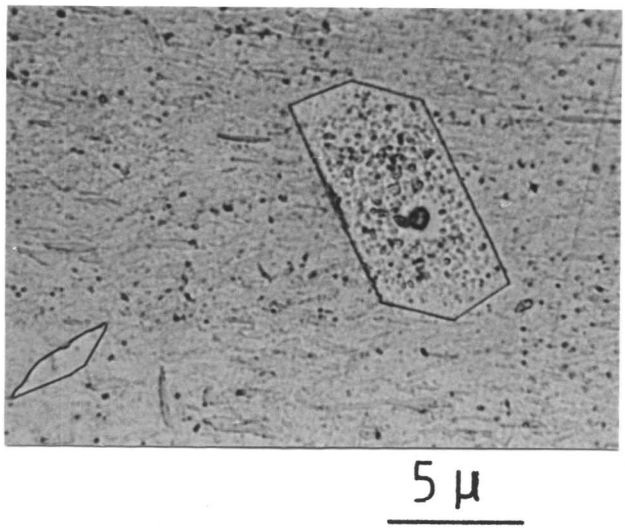

(b)

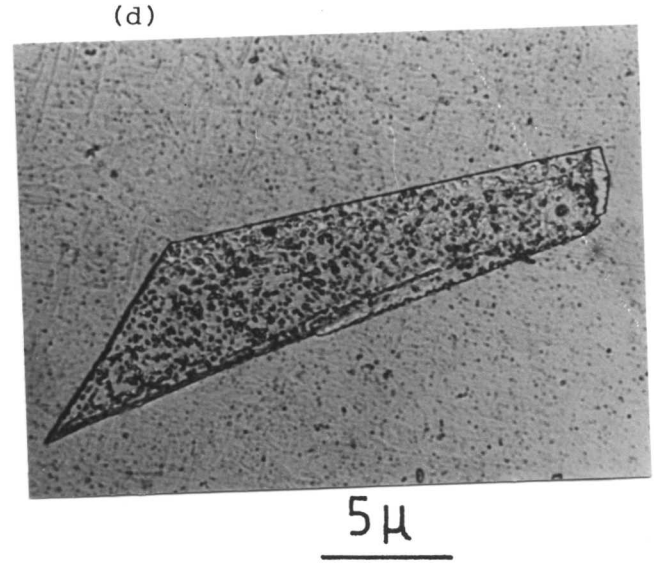

(e)

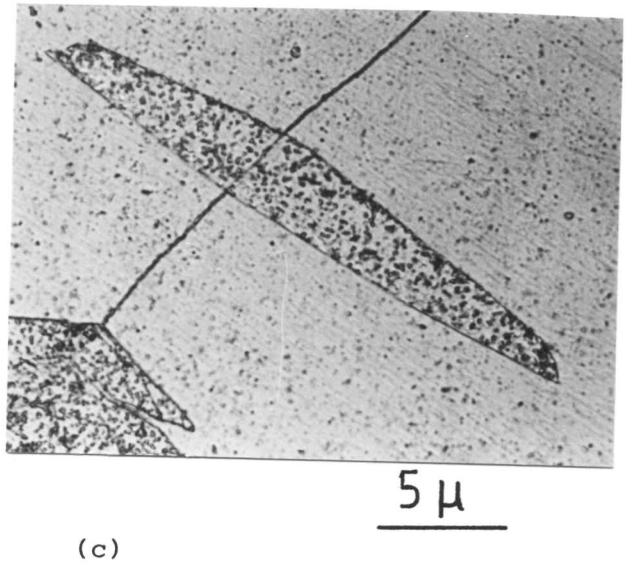

(c)

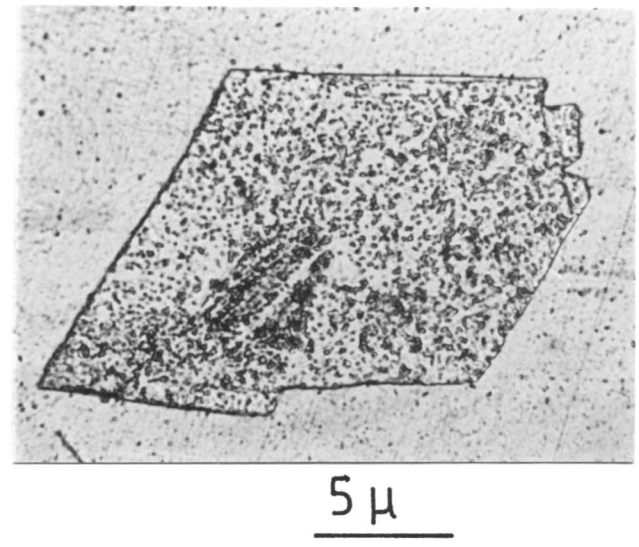

(f)

Fig. 4.12(a) to (f) Showing highly facetted α-ferrite.

(a)

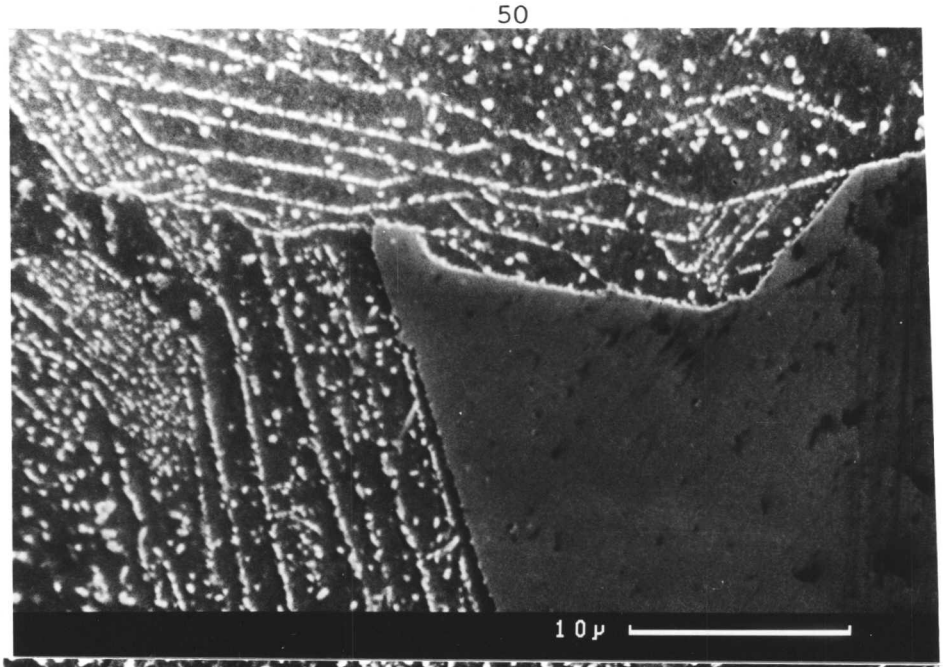

(b)

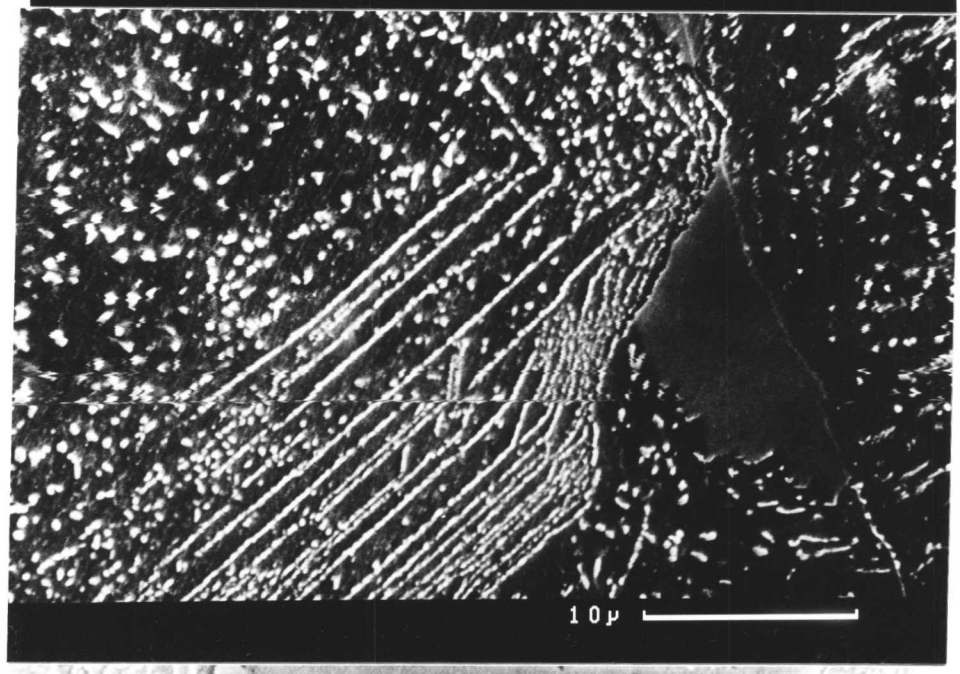

(c)

Fig. 4.13(a) to (c) Showing variation in the band spacing. Random carbide precipitation is also visible.

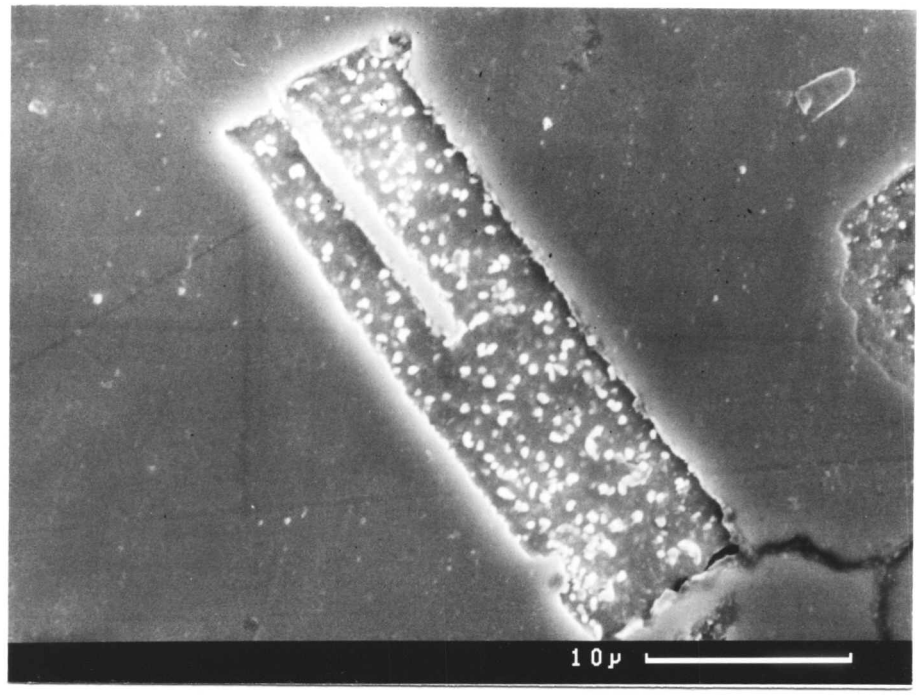

(a)

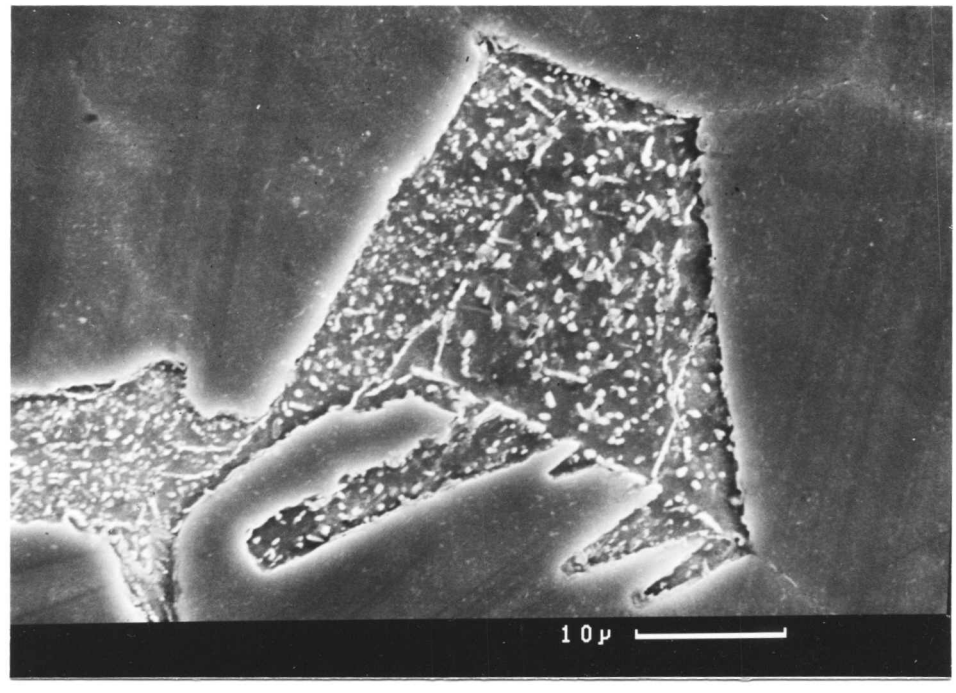

(b)

Fig. 4.14(a) to (b) Showing carbide precipitation along the planar low energy facets. But there is no evidence of ledges on these interfaces.

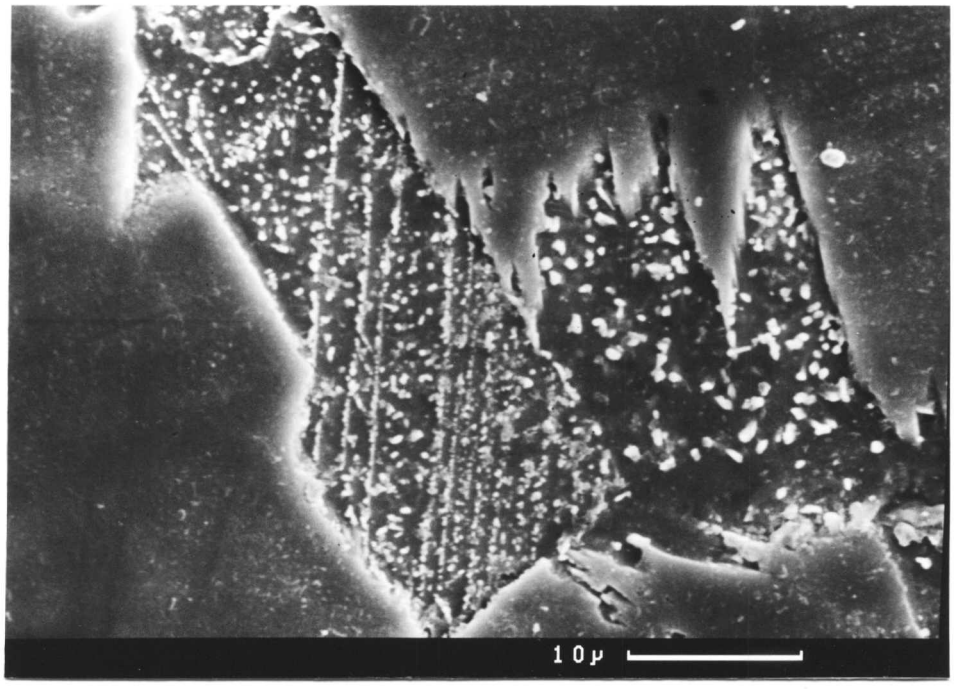

(c)

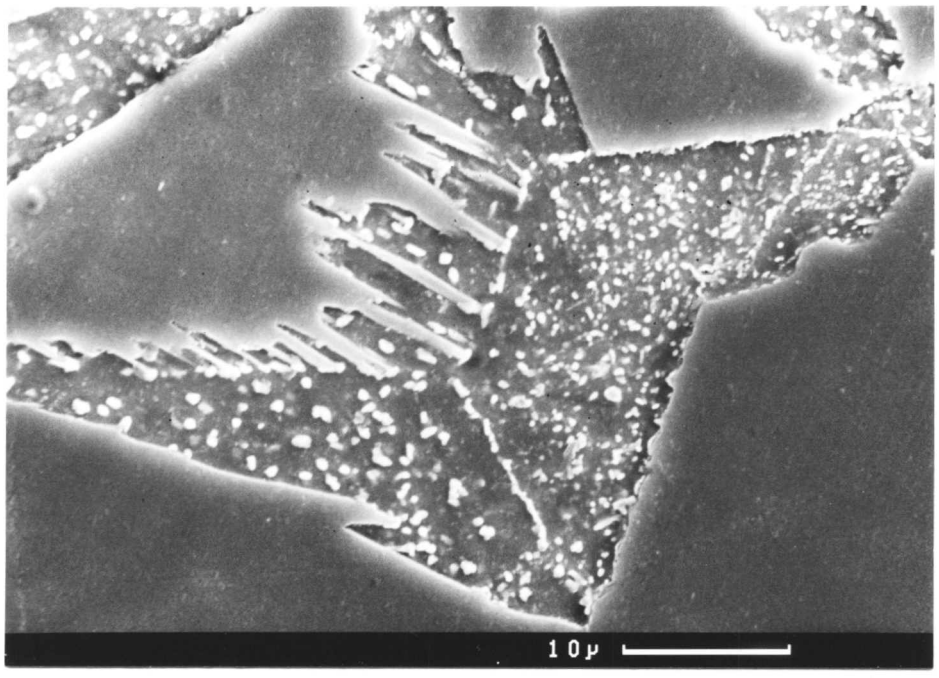

(d)

Fig. 4.14 (c) and (d) Showing carbide precipitation along planar low energy facets. But there is no evidence of ledges on these interfaces.

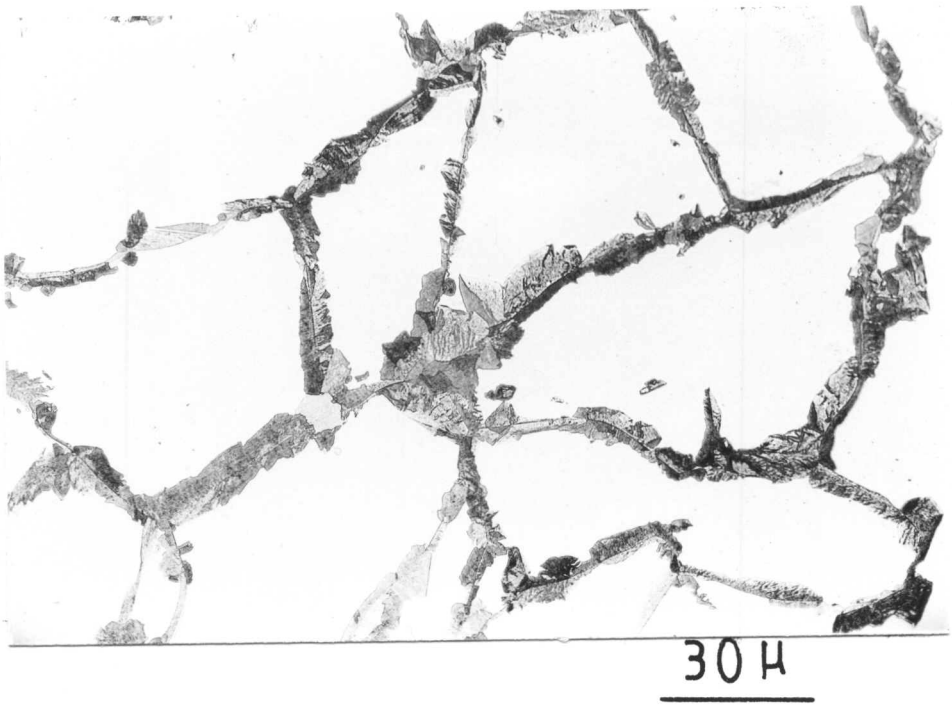

Fig. 4.15 Showing dark etch grain-boundary allotriomorphic ferrite.

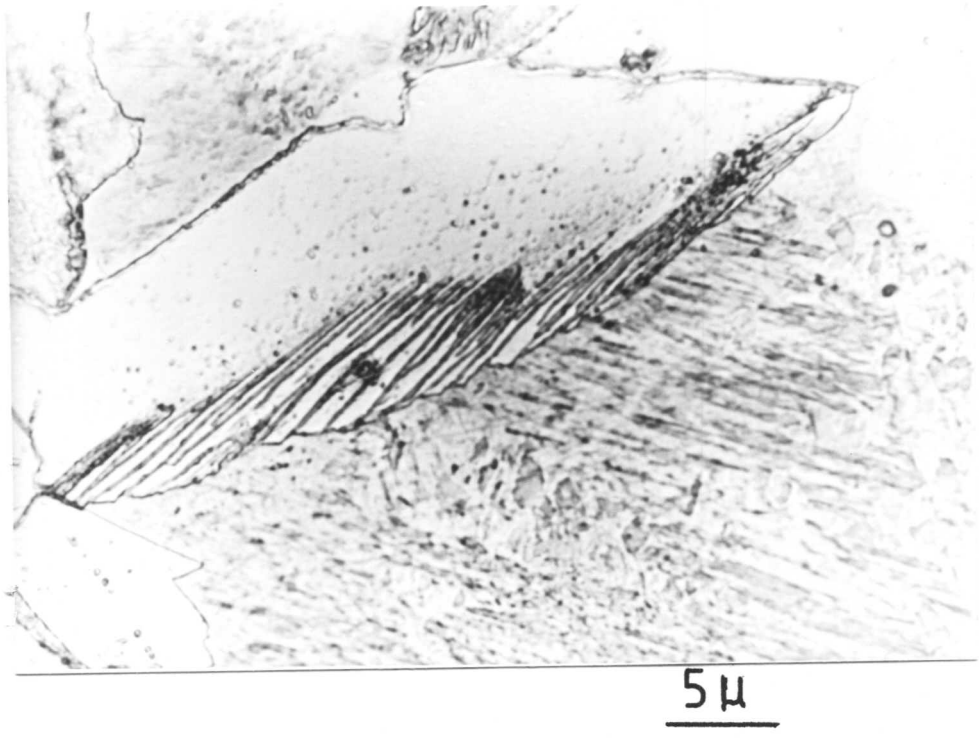

Fig. 4.16 Showing fibrous carbides formed in association with the facet which has been moved by a ledge mechanism.

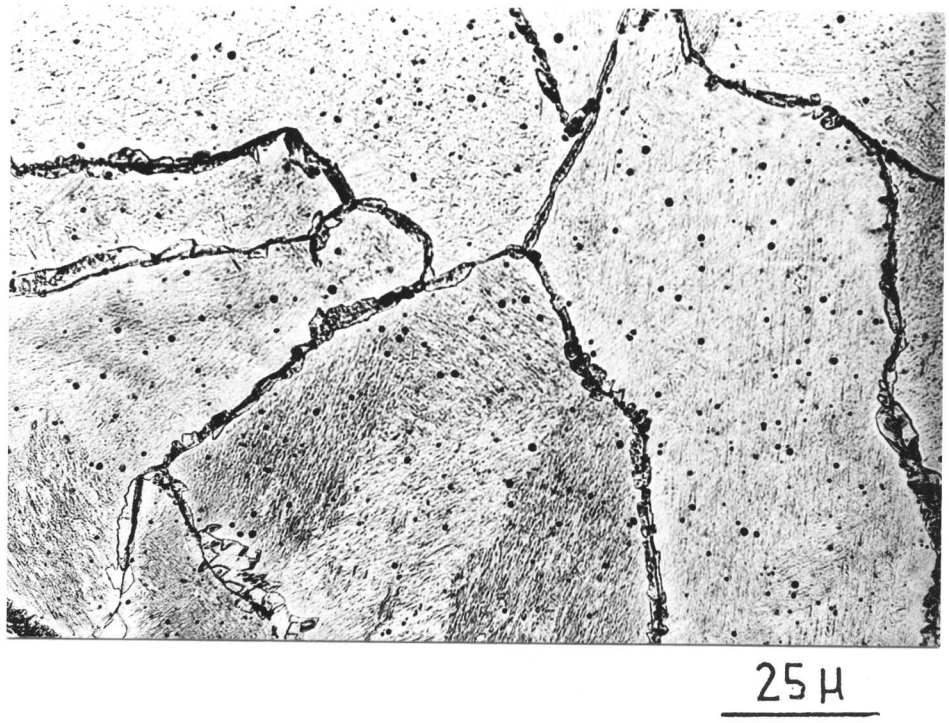

Fig. 4.17 Showing grain-boundary allotriomorphs having high aspect ratio. (Isothermal transformation at 750°C for 5 minutes.)

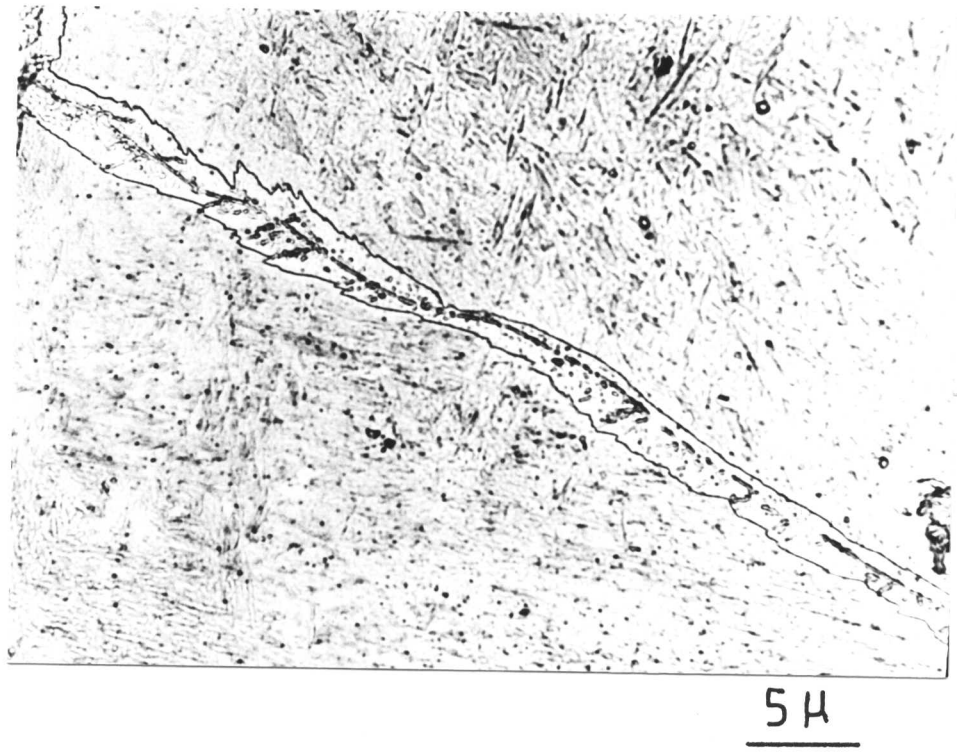

Fig. 4.18 Showing the serrated interface arising as a result of interface pinning by alloy carbides. (Isothermal transformation at 750°C for 5 minutes.)

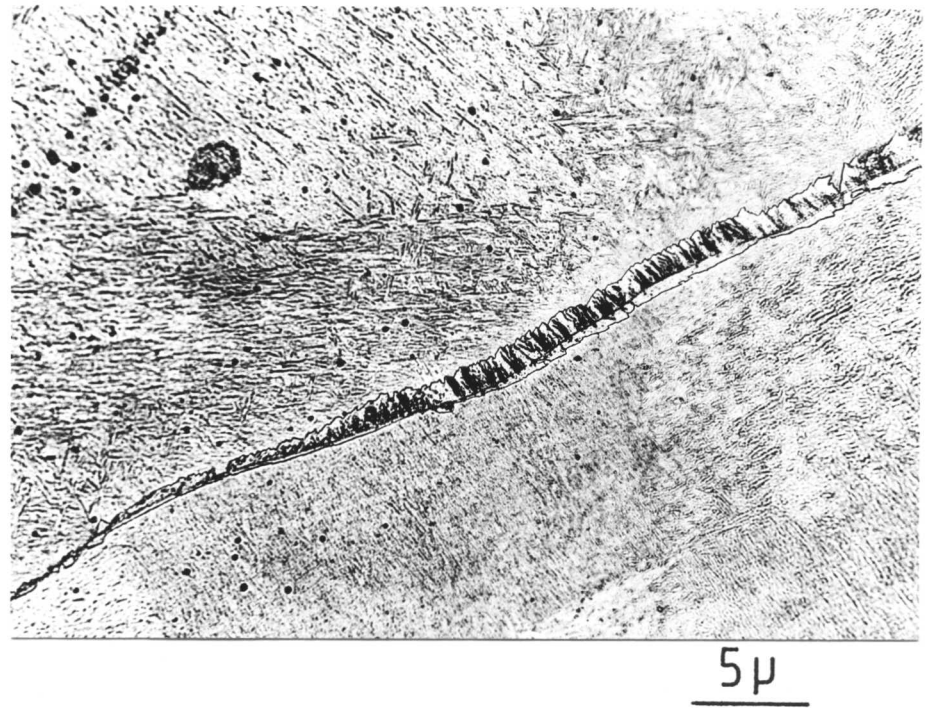

Fig. 4.19 Showing fibrous carbides formed on one side of the boundary. (Isothermal transformation at 750°C for 5 minutes.)

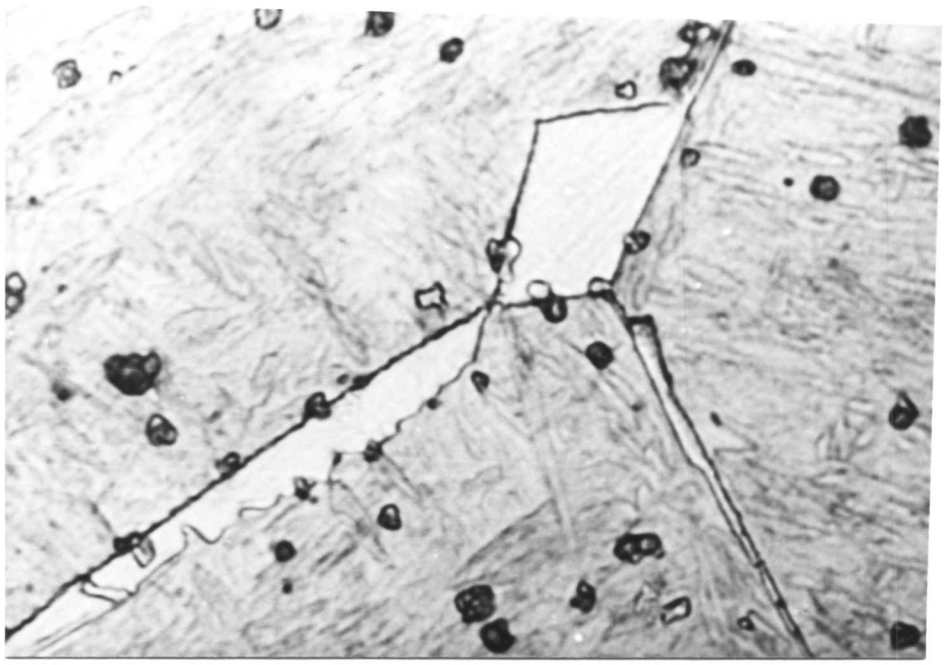

Fig. 4.20 Showing grain-boundary allotriomorphs formed during the early stage of transformation. (Isothermal transformation at 700°C for 10 minutes.)

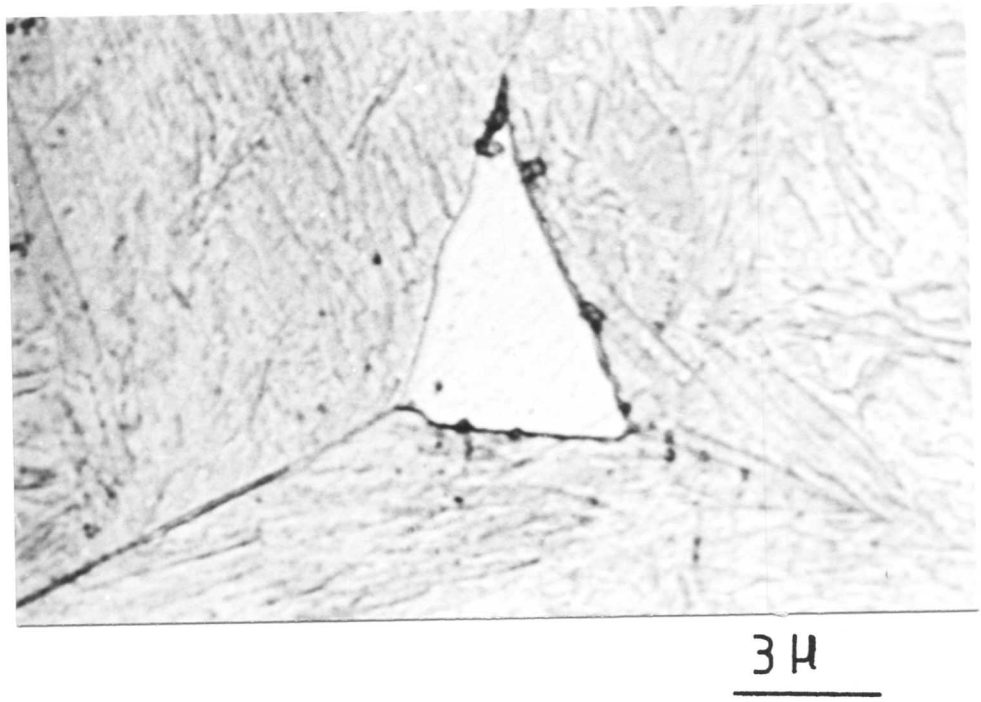

Fig. 4.21 Showing grain-boundary allotriomorphs formed at the junction where three grain-boundaries meet. (Isothermal transformation at 700°C for 10 minutes.)

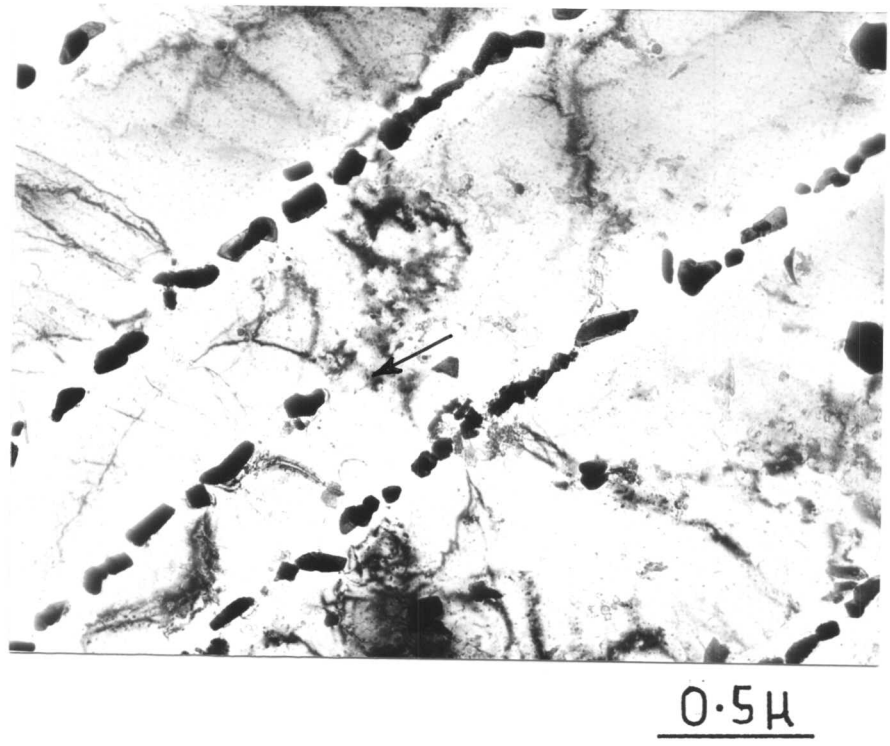

Fig. 4.22 Shows evidence of interphase precipitation. (Isothermal transformation at 850°C for 20 minutes.) Thin foil micrograph.

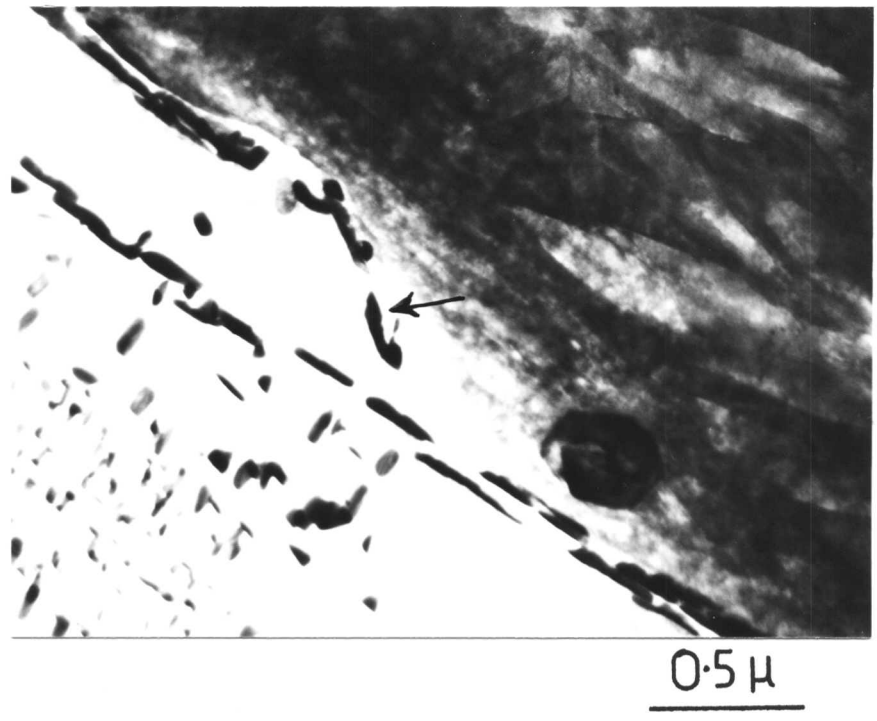

Fig. 4.23 Showing precipitation on the mobile ledge.

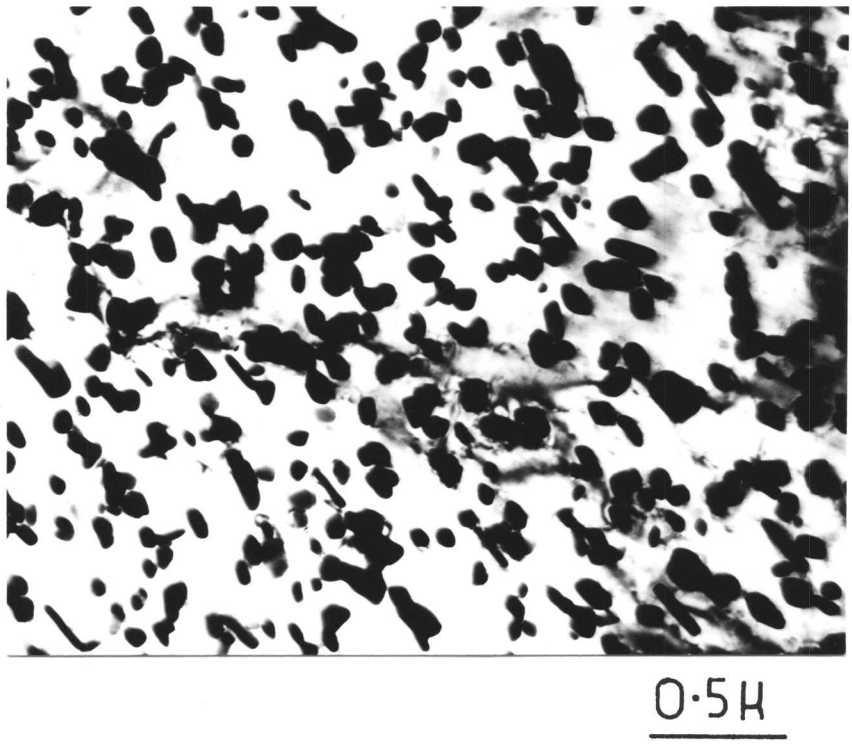

Fig. 4.24 Carbide precipitation from super-saturated ferrite. (Isothermal transformation at 750°C for 5 minutes.)

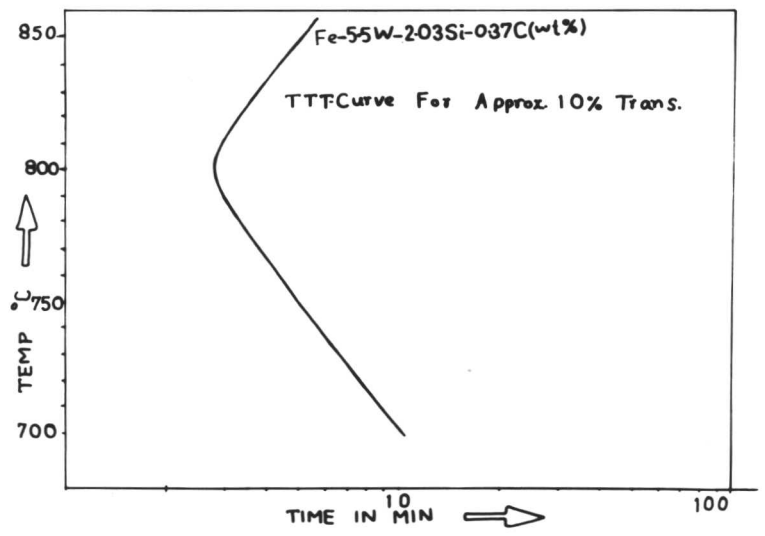

Fig. 4.25 : TTT diagram for 10% transformation in Fe-5.5W-2.03Si-0.37C (wt%) alloy.

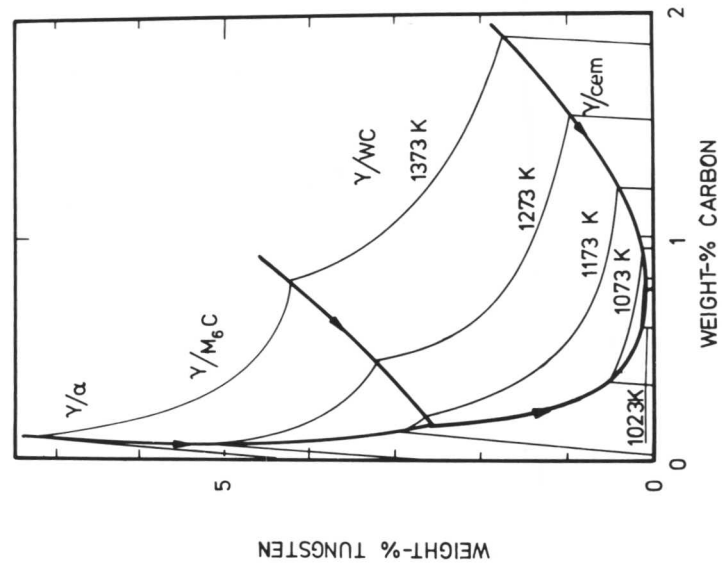

Fig. 4.26 Isothermal section of Fe-Si-C alloy in the temperature range of 1023K to 1373K.

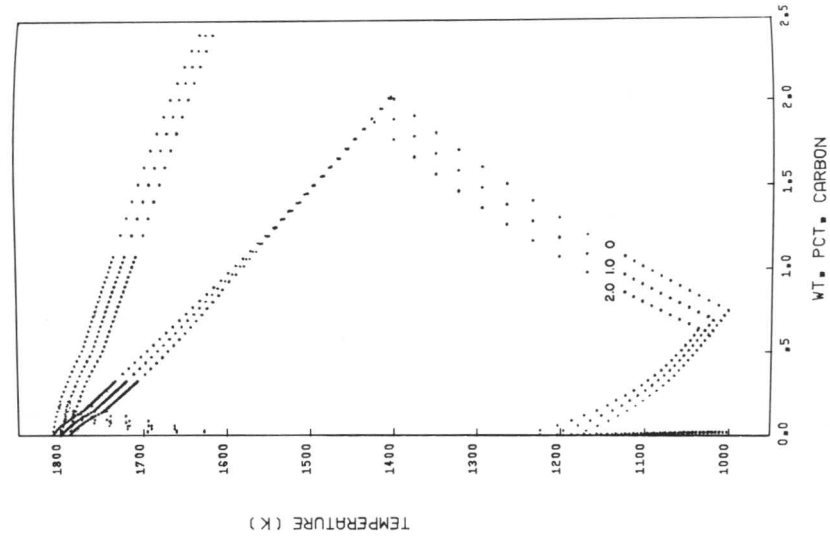

Fig. 4.27 Fe-C equilibrium diagram at constant silicon content.

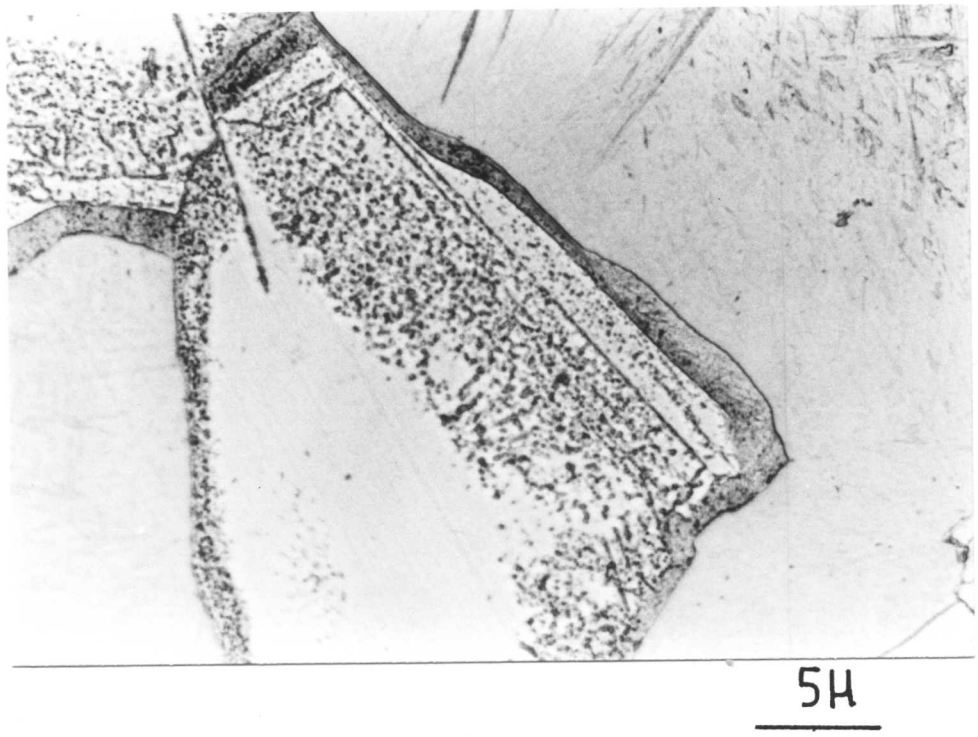

(a)

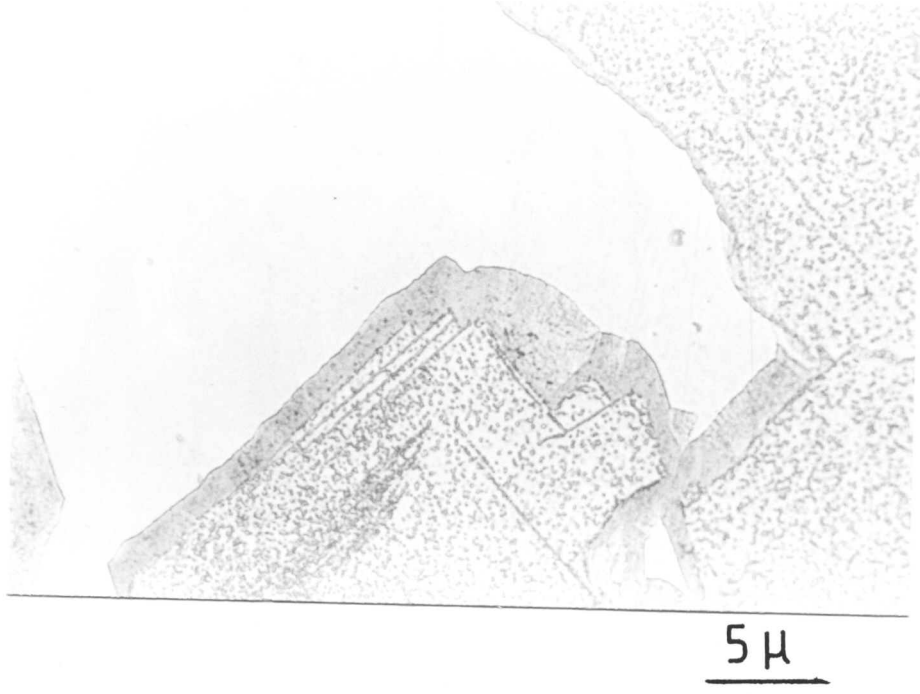

(b)

Fig. 4.28(a) to (b) Interphase precipitation surrounded by a thick grey level. (Isothermal transformation at 850°C, followed by step quenching at 750°C.)

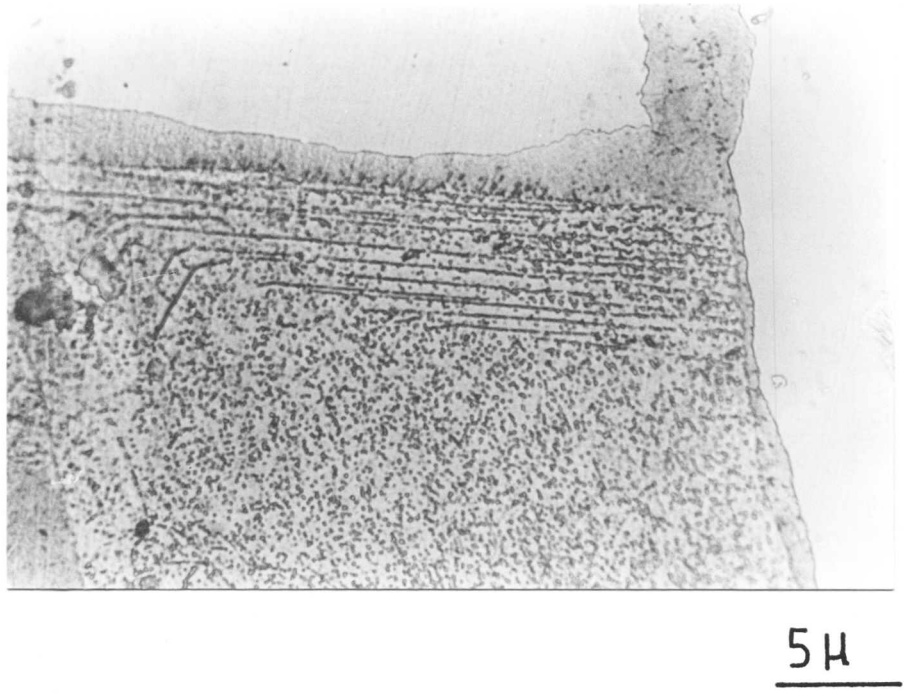

(c)

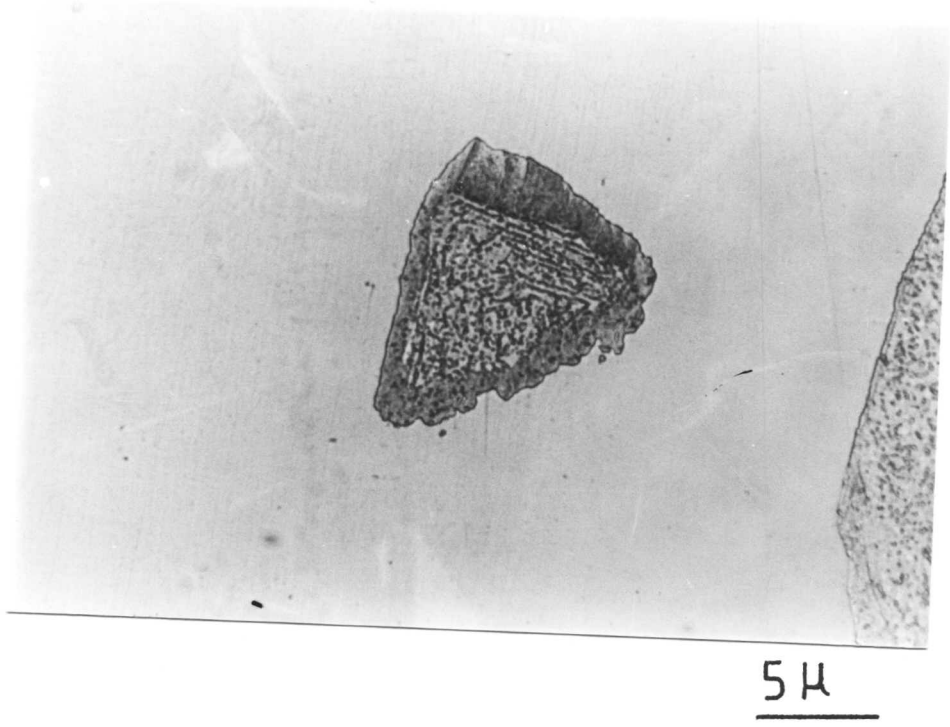

(d)

Fig. 4.28 (c) and (d) Interphase precipitation surrounded by a thick grey level. (Isothermal transformation at 850°C, followed by step quenching at 750°C).

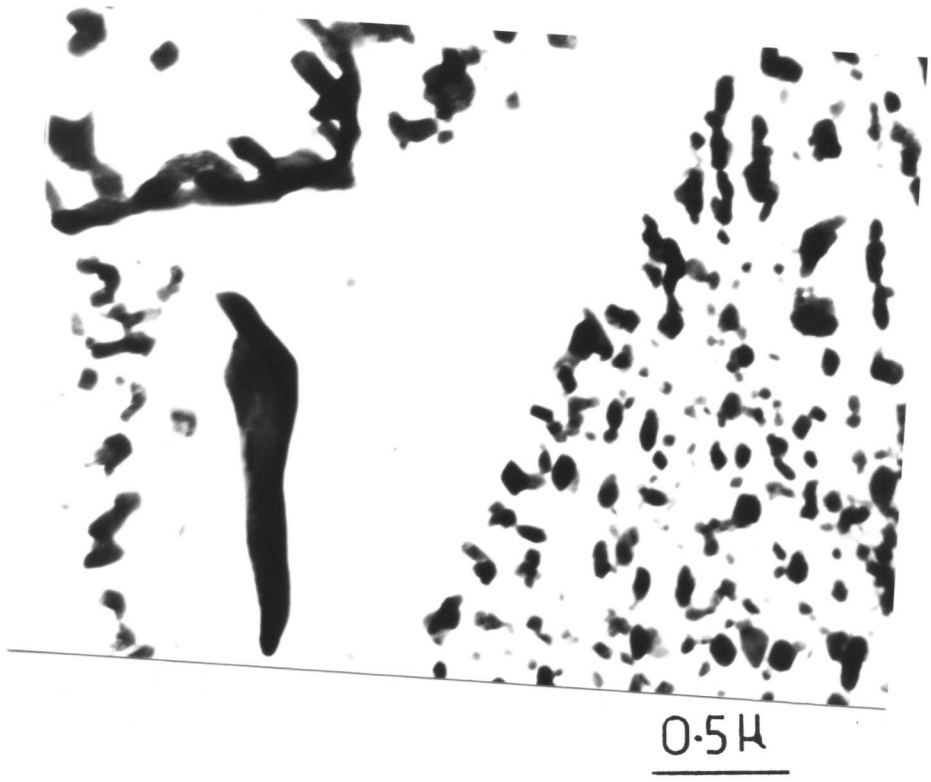

Fig. 4.29 Showing dense carbide precipitation on only side of the micrograph. (Isothermal transformation at 850°C for 20 minutes, followed by step quenching at 750°C.)

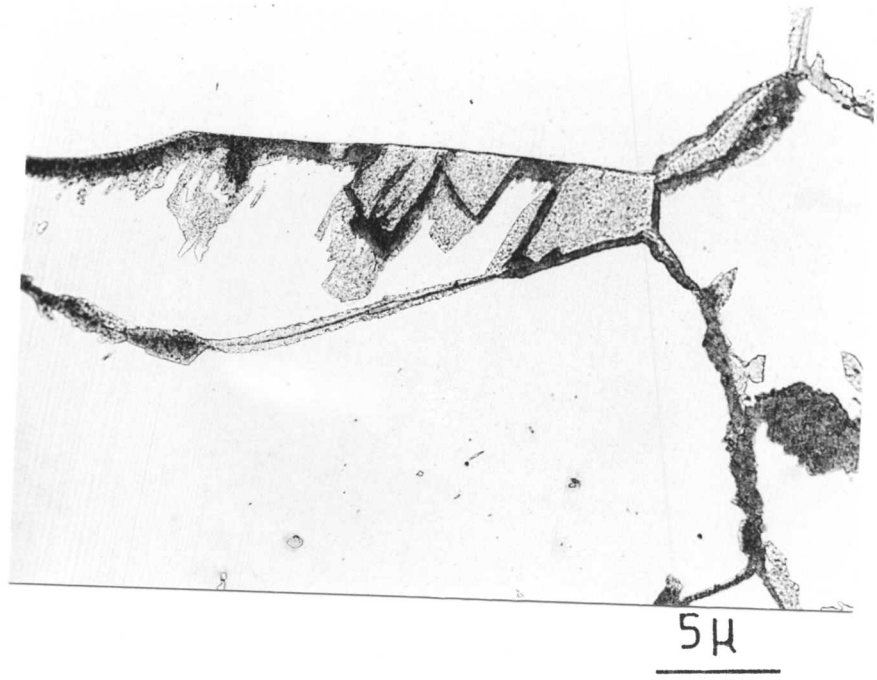

Fig. 4.30

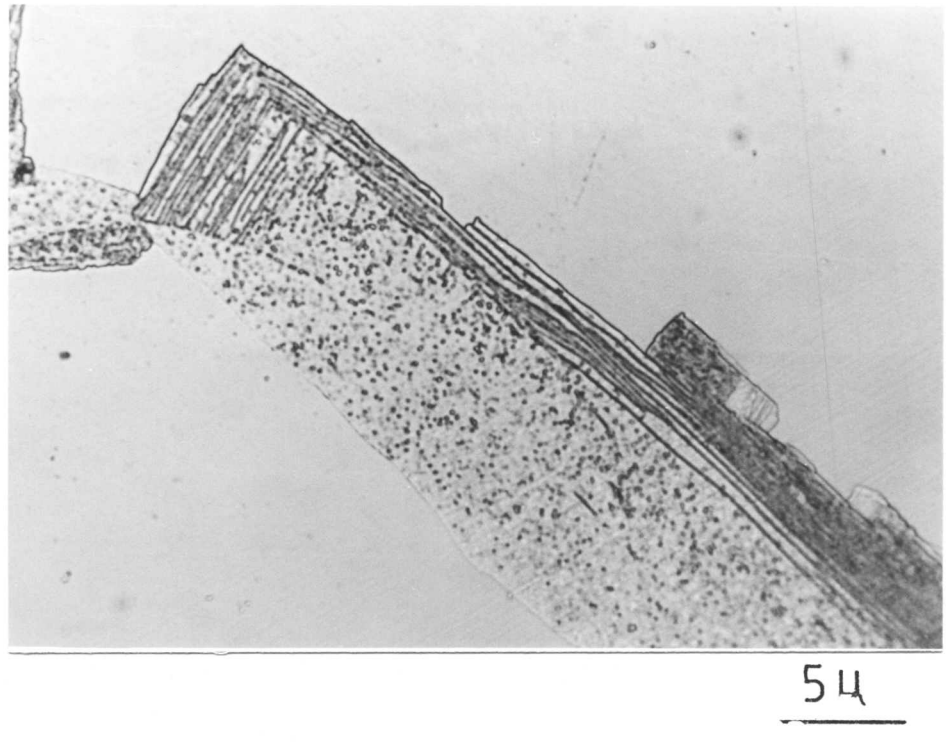

Fig. 4.31

Fig. 4.30 and 4.31 Showing carbide precipitation during double step quenching (i.e. 850°C → 750°C → 850°C). In certain areas there is a dense distribution of carbide whereas in some areas the interphase precipitation is more dominant.

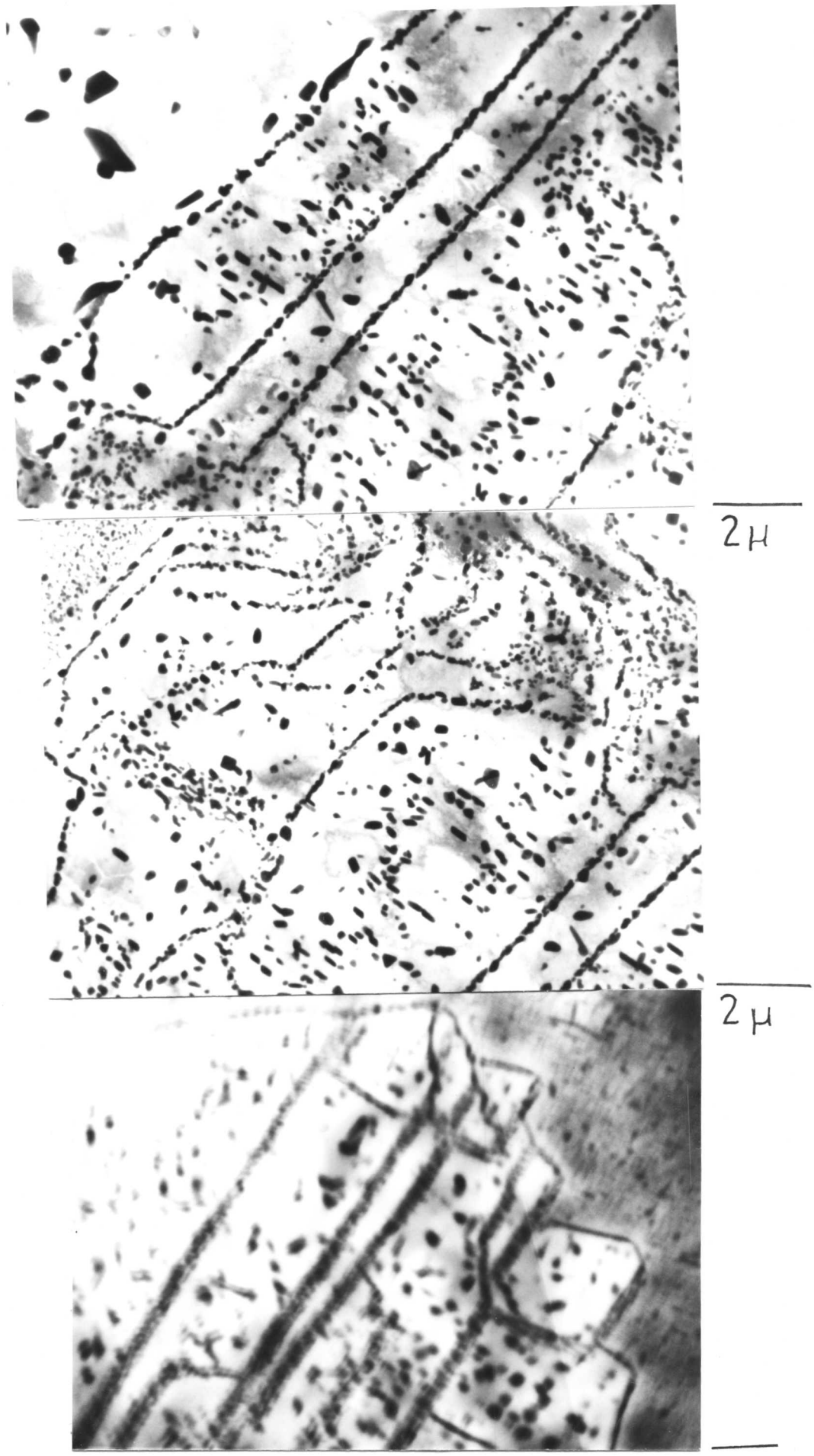

Fig. 4.32 to 4.34: Microstructure developed by double step quenching.

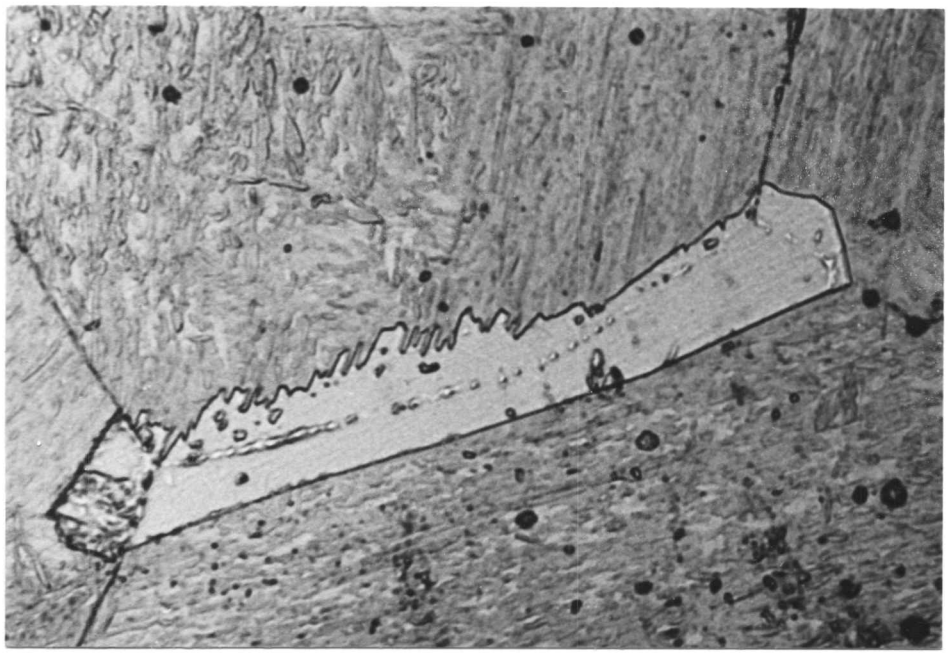

(a)

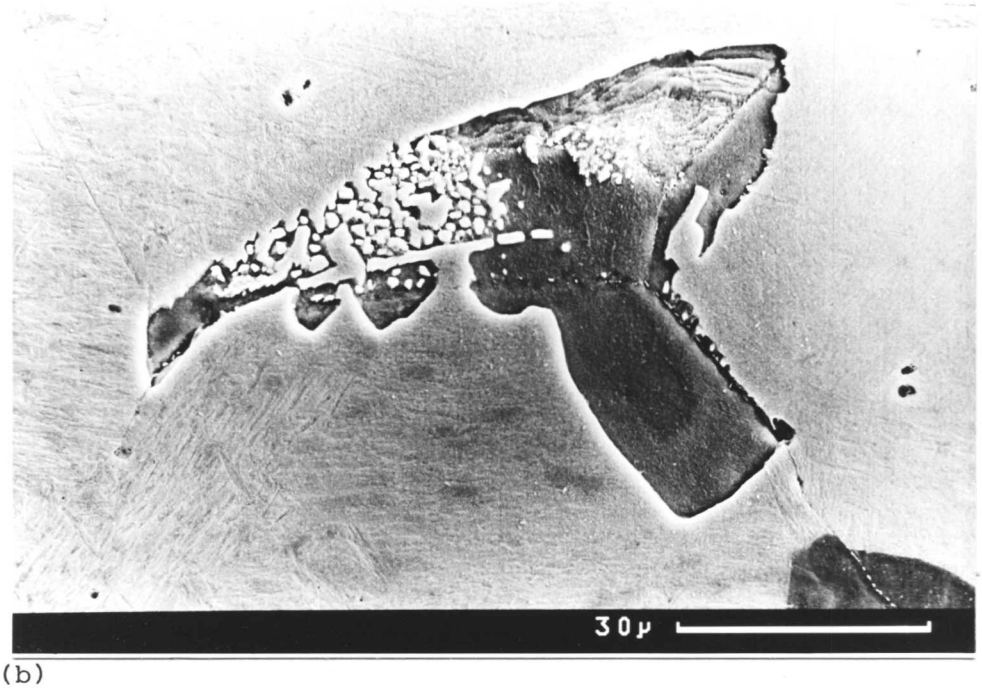

(b)

Fig. 4.35 (a) and (b) Ragged interface formed as a result of pinning by carbides. (Isothermal transformation at 800°C for 20 minutes.)

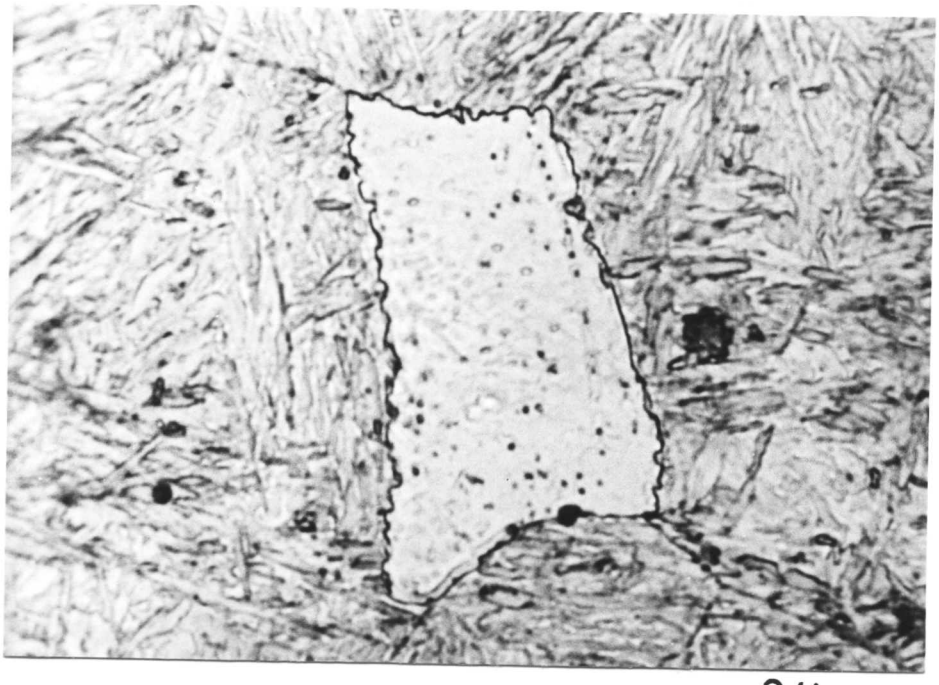

(a)

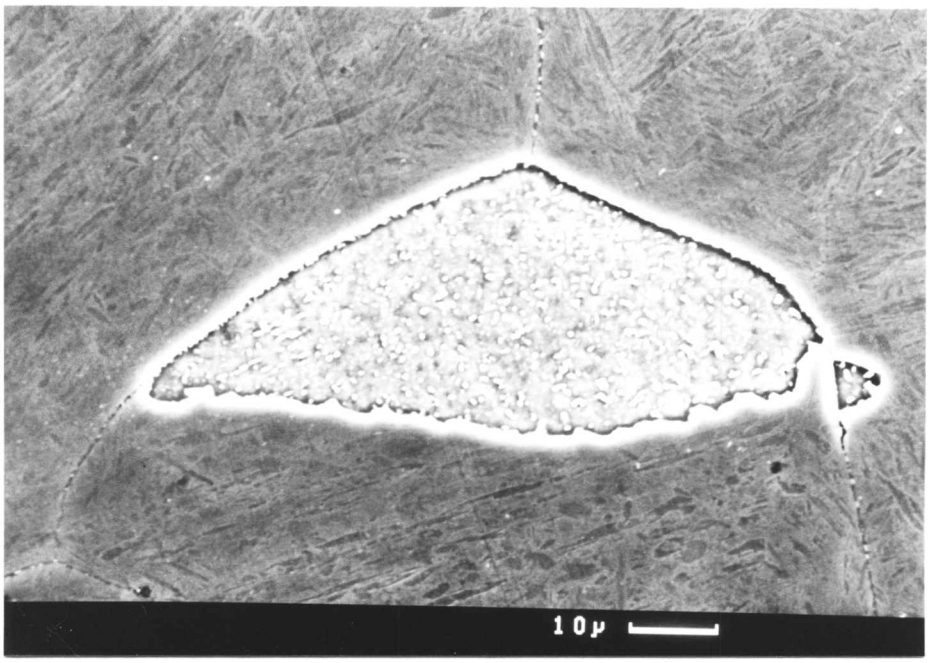

(b)

Fig. 4.36(a) and (b) Showing serrated interface formed as a result of interphase precipitation. (Isothermal transformation at 800°C for 40 minutes.)

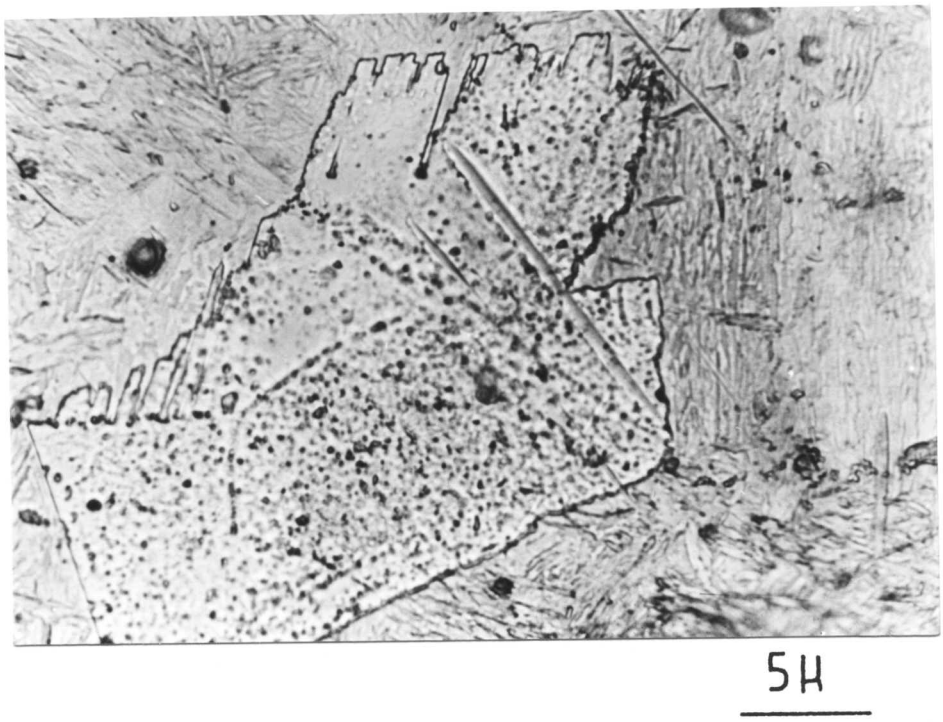

(a)

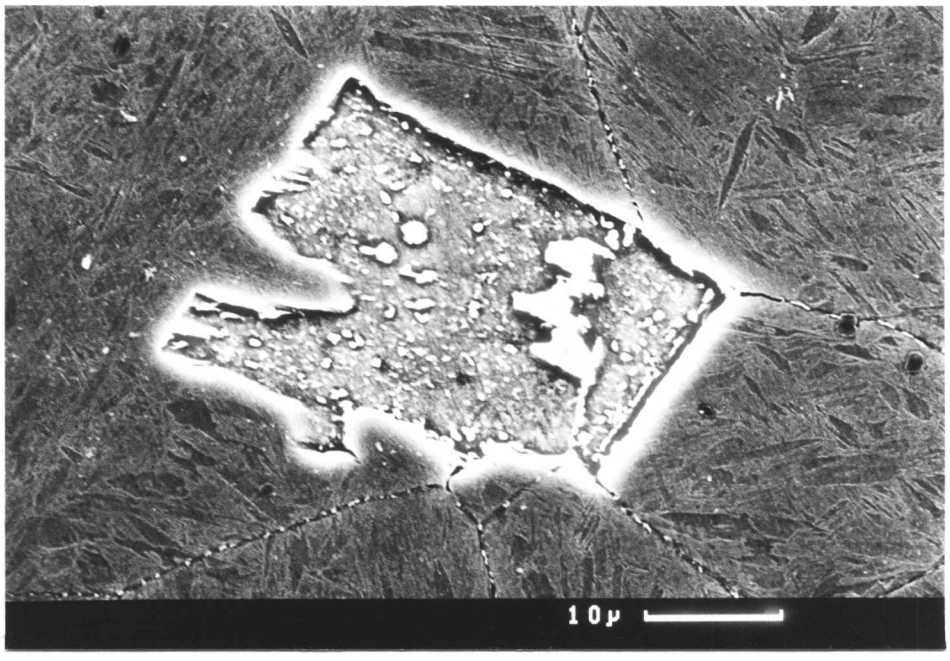

(b)

Figure 4.37(a) and (b) Showing ragged interface formed as a result of pinning by carbides. (Isothermal transformation at 800°C for 40 minutes.)

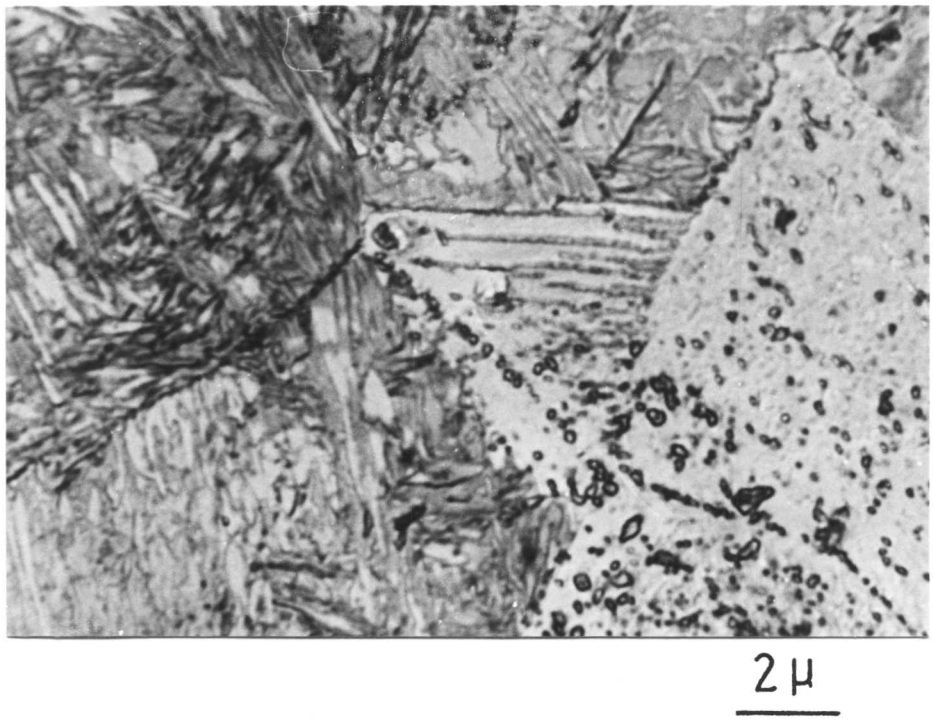

Fig. 4.38 Showing interphase precipitation associated with ledge mechanism. (Isothermal transformation at 800°C for 80 minutes.)

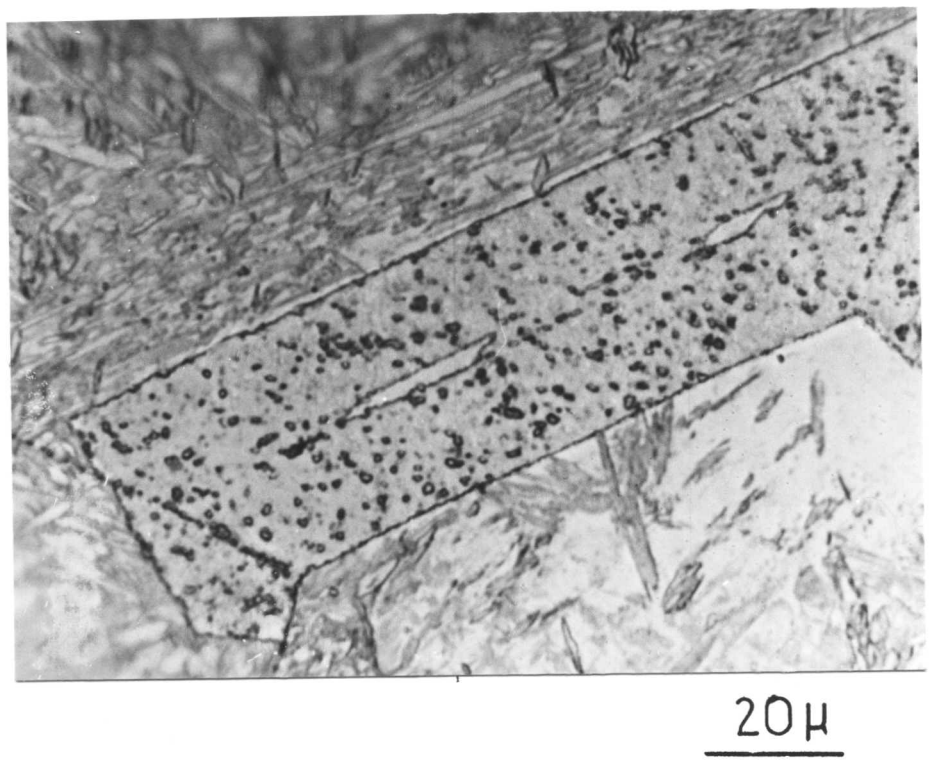

Fig. 4.39 Showing cusps on the low energy facets. (Isothermal transformation at 800°C for 80 minutes.)

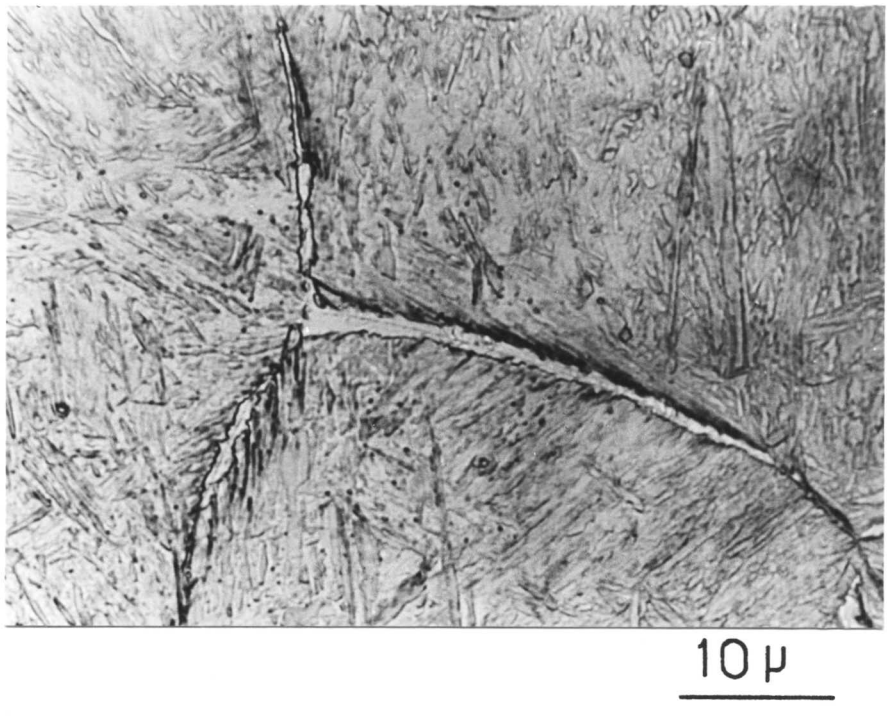

Fig. 4.40 Showing grain-boundary allotriomorphs with high aspect ratio. (Isothermal transformation at 700°C for 40 minutes.)

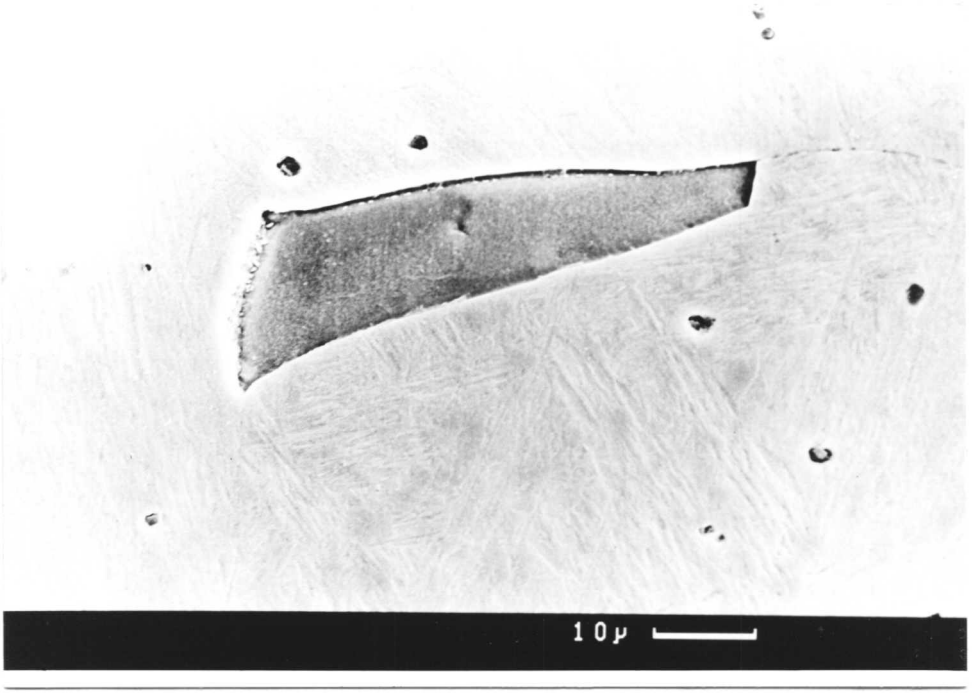

Fig. 4.41 Showing grain-boundary allotriomorphs. (Isothermal transformation at 700°C for 40 minutes.)

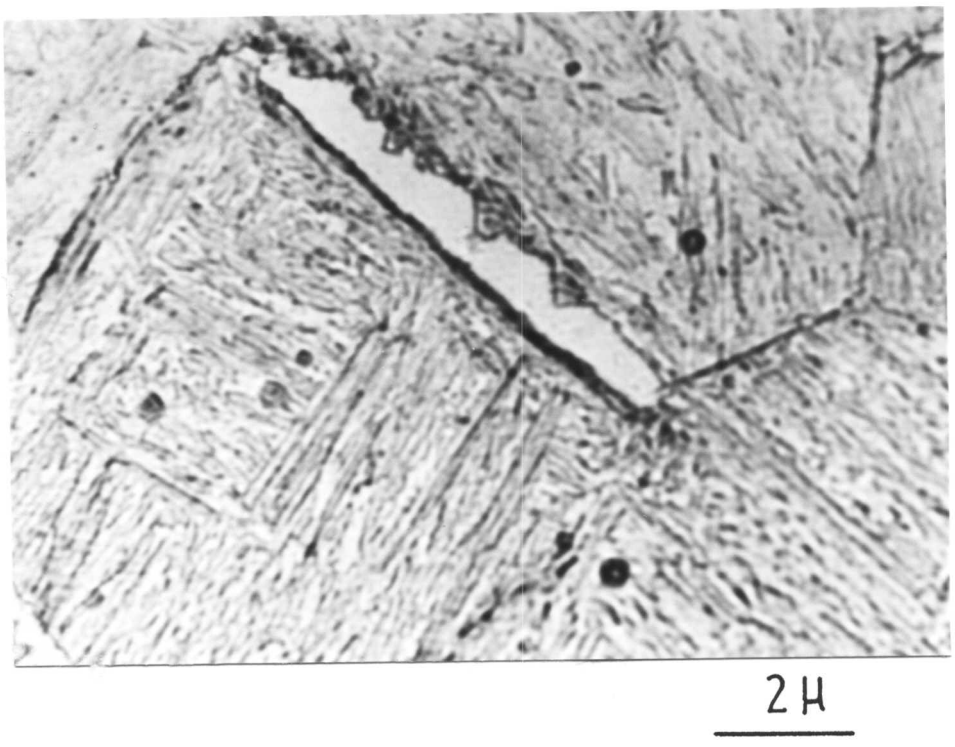

Fig. 4.42 Showing cusps on the low energy facets. (Isothermal transformation at 700°C for 40 minutes.)

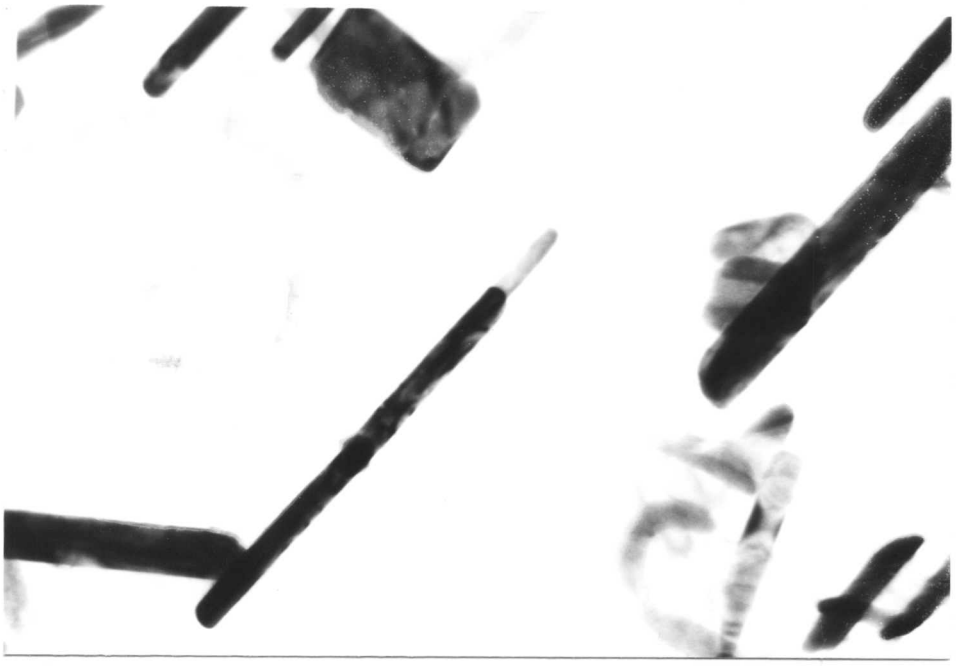

(a)

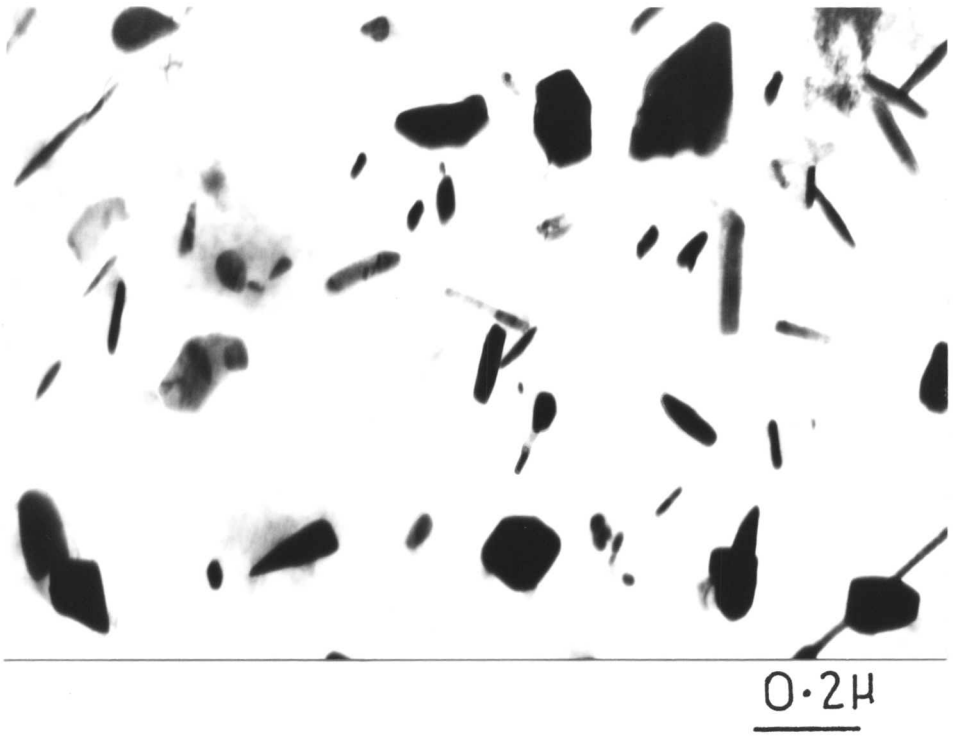

(b)

Fig. 4.43(a) and (b) Showing carbides in several different morphologies. (Isothermal transformation at 800°C for 40 minutes.)

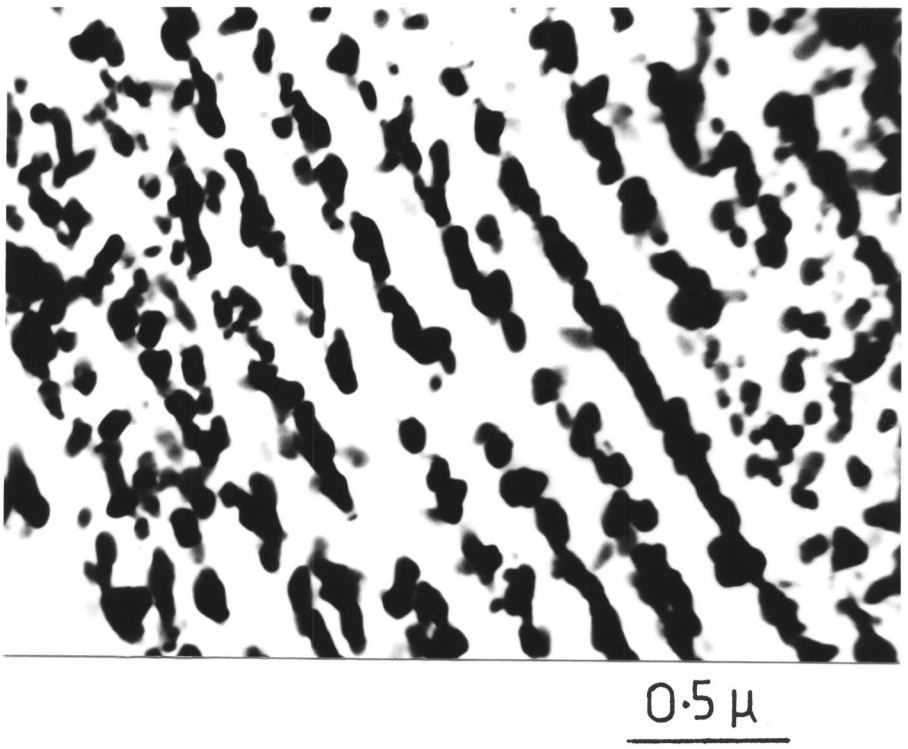

Fig. 4.44: TEM micrograph showing higher volume fraction of tungsten carbide at 750°C compared to that obtained at 800°C

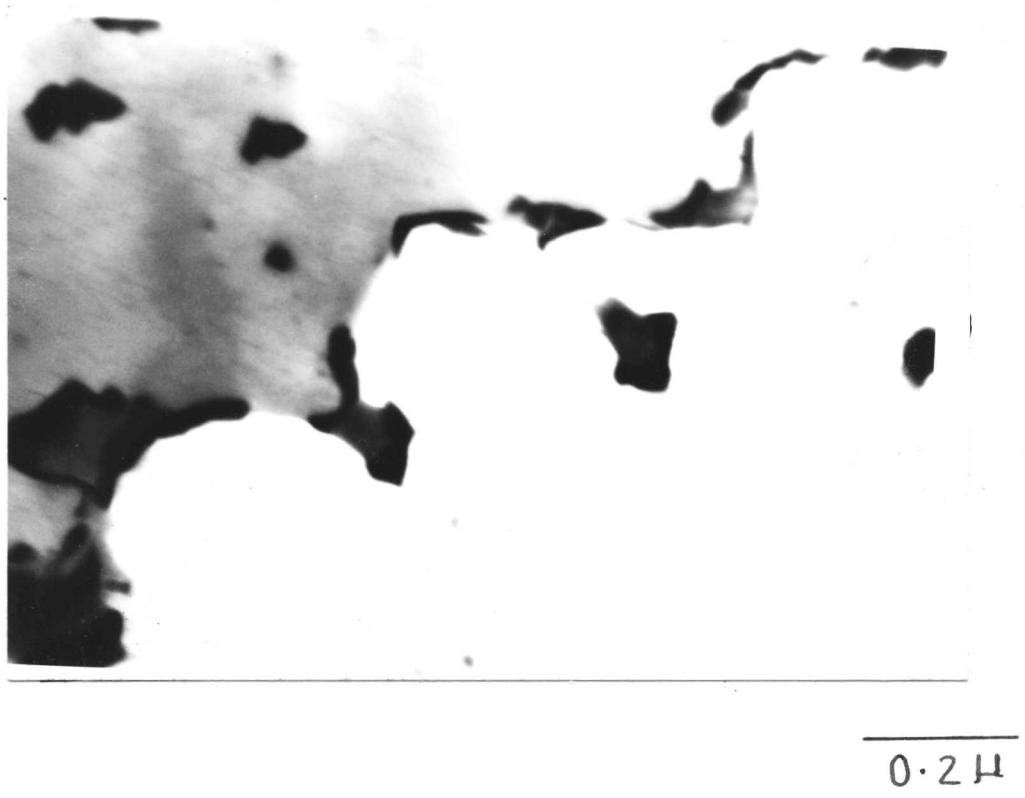

Fig. 4.45 Interface pinning by tungsten carbide.
(Isothermal transformation at 800°C for 40 minutes.)

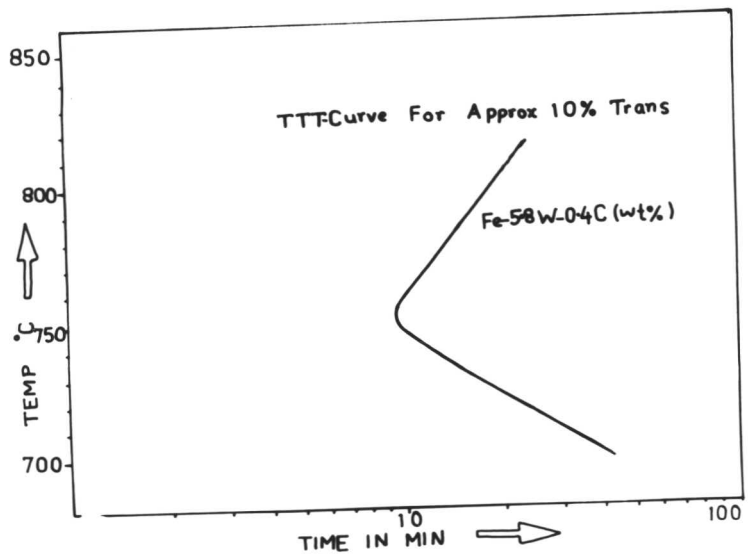

Fig. 4.46: TTT diagram for 10% transformation in Fe-5.8W-0.4C (wt%) alloy.

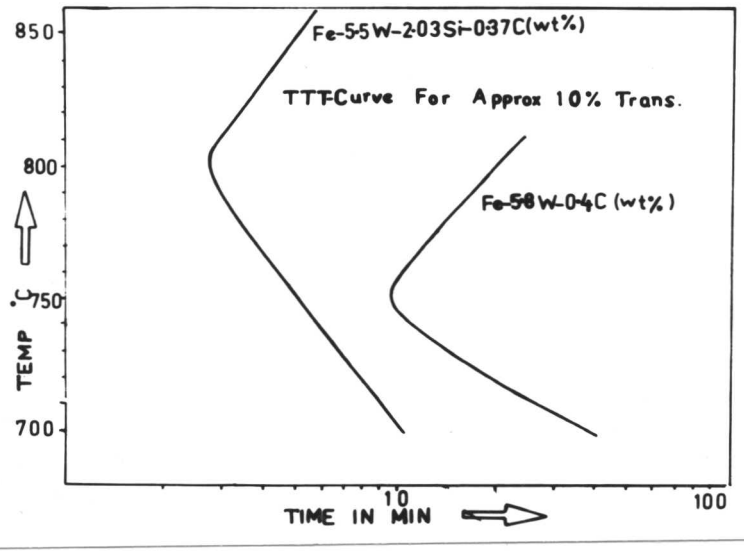

Fig. 4.47: TTT diagram showing effect of Si on the $\gamma \rightarrow \alpha$ transformation in Fe-W-C alloy.

CHAPTER V

The Austenite → Ferrite transformation in Fe-5W-0.23C (wt%)

5.1 INTRODUCTION

The austenite can decompose by several diffusional mechanisms to give rise a variety of microstructures. The resultant microstructure is sensitive to both temperature of transformation and the composition of the alloy. By controlling these two variables, one can control the mechanism through which diffusional transformation can proceed. Several microstructures can develop by variation of temperature and composition, including proeutectoid ferrite proeutectoid cementite, pearlite and bainite. Among these the proeutectoid ferrite reaction has received much attention in the past few decades.

Study of the $\gamma \rightarrow \alpha$ transformation is not only limited to the binary Fe-C system but also extended to the ternary Fe-C-X system where X is a substitutional alloying element such as Cr, Mn, Mo, Ni, Si, Co, Au, Ti, V, etc. This reaction starts predominatly at grain boundaries when the alloy is held below Ae_3 temperature. At low supersaturation (i.e. small undercooling, ΔT), grain boundary allotriomorphs are formed which grow rapidly along the grain boundaries but thicken more slowly. The growth kinetics of grain boundary allotriomorphs have been studied with the help of thermionic electron emission microscopy[1] (1967). The rate of thickening is parabolic in accordance with the relationship

$$S = \alpha_1 t^{1/2}$$

where S = half-thickness, t = growth time, and α_1 is the parabolic rate constant. Hillert[2] developed an expression for the lengthening rate of allotriomorphs with the assumption that the transformation is basically volume diffusion-controlled. The form of the expression is

$$G_L = \frac{D_\gamma (x_\gamma^{\gamma\alpha} - x_\gamma)}{4r^1 (x_\gamma - x_\alpha^{\alpha\gamma}) \sin \phi}$$

where $x_{\gamma}^{\gamma\alpha}$ = equilibrium mole fraction of carbon in austenite at interface

x_{γ} = mole fraction of carbon in alloy

$x_{\alpha}^{\alpha\gamma}$ ≃ equilibrium mole fraction of carbon in ferrite at the $\alpha/\alpha + \gamma$ phase boundary

r^{1} = radius of curvature of the allotriomorphs adjacent to the grain junction

ϕ = equilibrium growth angle determined by the relative energies of the interphase and grain boundaries

However, the recent work[3, 4] has shown that the lengthening is parabolic with respect to time. The rate constant describing the lengthening process is simply α_1 divided by the thickness to length ratio (i.e. aspect ratio) of the allotriomorph. Both the rate of nucleation as well as the rate of growth of these allotrimorphs increases with decreasing temperature due to increasing thermodynamic driving force, however diffusivity decreases. At sufficiently high undercooling, Widmanstätten ferrite develops. The reason for the transformation from grain boundary allotriomorphs to Widmanstätten side plate with increasing undercooling is not well understood. It has been suggested[5] that the relative rates at which semi-coherent and incoherent interfaces can migrate vary with undercooling. At small undercoolings, it is proposed that both semi-coherent and incoherent interfaces can migrate at the same rates, while at large undercoolings only incoherent interfaces can make full use of the increased driving force. However it does not explain the surface relief effect associated with formation of W_s. The other morphologies which develop during the $\gamma \rightarrow \alpha$ transformation are sensitive to temperature and composition and can be described on the basis of morphological classification proposed by Dubé and further extended by Aaronson, the details of which are discussed in Chapter II.

The $\gamma \rightarrow \alpha$ transformation in alloy steels has stimulated much interest in the intervening decades. This transformation provides a direct route of strengthening (in contrast to the use of quenched and tempered steels) by interphase-precipitation of alloy carbides. Alloy carbides are precipitated periodically at the advancing γ/α interface in order to accommodate the solid solubility associated with the decomposition of austenite and hence termed

"interphase precipitation". This form of precipitation appears generally in a banded structure which can be planar, curved or irregular. Planar banded structures are formed when precipitation occurs on low energy semi-coherent interfaces which are displaced by a ledge mechanism. Curved and irregular dispersion of carbides are formed in association with high energy incoherent interfaces. The resultant band spacing can be controlled by either varying the isothermal transformation temperature or by proper choice of alloying elements. At temperatures close to the nose of the T.T.T. diagram, the reaction proceeds rapidly and so the band spacing will be very fine. Similar effect is expected with alloying elements that will accelerate the transformation. However, another kind of carbide formation has also been observed in isothermally transformed steels. These carbides appear fibrous; they grow normal to the incoherent interphase-boundary and are usually observed as the transformation temperature is lowered.

The concept of interphase carbide precipitation has been exploited in the present chapter to investigate the $\gamma \rightarrow \alpha$ transformation in Fe-5W-0.23C (wt%) alloy. Special attention has been given to understand the carbide precipitation at the advancing γ/α interface by partially transforming the specimen at various temperatures. The effects of a small addition of titanium (0.14wt%) on the transformation characteristics of this alloy has been studied briefly.

5.2 Experimental Results on Fe-5W-0.23C (wt%) alloy:

5.2.1 Transformation at 850°C.

Isothermal transformation at 850°C for 2.5 minutes showed approximately 0.2 per cent volume fraction of transformation. Nucleation of proeutectoid ferrite was found to occur primarily at the austenite grain boundaries. The γ/α interface appeared curved as well as planar. Frequent evidence of ledges on the planar interfaces implies that these interfaces have moved by a ledge mechanism (Figure 5.1) although the ledge movement seems irregular. Apparently curved interfaces also showed a tendency towards facetting. This may be as a result of an interface adopting lower energy configurations and it is interesting to speculate whether these facetted interfaces also move by the propagation of ledges[6]. When the time of transformation was increased to 5 minutes at this temperature, the vol. fraction of transformation rapidly increased to 0.6 percent of its equilibrium value. The interfaces in the majority of cases appeared to be planar. Presence of ledges of variable height was noticed. Apparently intragranular ferrite bounded exclusively by planar interfaces was also observed in many cases (Figure 5.2a). Figure 5.2b deserves special attention. It clearly shows the evidence of interface pinning by carbides. Figure 5.2b shows the presence of residual austenite (now martensite) in ferrite. The residual austenite in ferrite has formed as the interface has moved through the carbides. The presence of residual austenite seems to indicate that the precipitate pinned the γ/α interface and then these boundaries were forced to move around the particles by bowing, leaving behind the residual austenite. This is somewhat similar to the Orowan bowing mechanism for looping of dislocations around precipitates. Practically no evidence of precipitation in ferrite was recorded during the early stages. The formation of such a carbide-free ferrite is attributed to the appreciably higher solubility of tungsten carbide in ferrite at this temperature. Carbides free ferrites have also been reported in Fe-Mo-C[7], Fe-V-C(N)[8] and more recently in Fe-Nb-C[9] alloys during this early stages of transformation. Some interesting features were observed when the time of transformation was increased to 20 minutes at 850°C. Carbides were formed at the γ/α interface but appeared to grow in austenite to form a planar array of tungsten carbide (M_6C) (Figure 5.3) in austenite. The reaction can be written as

$$\gamma \rightarrow \alpha + \gamma_1 \rightarrow \alpha + \gamma_2 + M_6C \qquad (1)$$

With increasing time of transformation, all the austenite (γ_1) was replaced by $\gamma_2 + M_6C$. During the later stages of transformation all γ_2 was replaced by ferrite and finally the resultant structure consisted of α-ferrite + M_6C. The whole sequence of reaction can be written as

$$\gamma \rightarrow \gamma_1 + \alpha \rightarrow \gamma_2 + M_6C + \alpha \rightarrow M_6C + \alpha \qquad (2)$$

The microstructural changes which occurred during the isothermal transformation at 850°C are shown in Figures 5.2 to 5.4 and schematically in Figure 5.5.

5.2.2 Transformation at 800°C

Isothermal transformation at 800°C for 1.5 minutes showed about 5 volume % transformation of its equilibrium value. The reaction mainly started at the austenite grain boundries. The grain boundary allotriomorphs showed a tendency towards facetting (Figure 5.6a). Some evidence of Widmanstätten ferrite was also recorded (Figure 5.6b) at this temperature. This Widmanstätten ferrite has grown along martensite trace direction. Figure 5.6c illustrates some important crystallographic aspects of allotriomorphs formed at the junction where three grain boundaries meet. This micrograph indicates that this allotriomorph is crystallographically related only to two abutting grains. (Planar interface is taken here as tentative evidence of a rational orientation relationship between parent and product phase on a macroscopic scale.) With increasing time of transformation (2.5 minutes), the allotriomorphs grew more rapidly along the grain boundaries and thickened slowly. Most of the interfaces appeared planar. Frequent evidence of ledges indicates that these interfaces have moved by ledge mechanism. With further increase in time (5 minutes, 10 minutes) these allotriomorphs developed to form equiaxed ferrite due to impingement effects. The aspect ratio of allotriomorphs increased with decreasing temperature as expected. Ferrites thus formed during early stages were virtually free from carbides. Clear evidence of pinning was recorded (Figure 5.6d-f). This pinning has resulted while the interface has moved across the carbide particles, during transformation. This aspect of interface pinning can be utilized to delay the transformation and hence to increase the hardenability of alloy steels. Some evidence of carbide precipitation was also recorded during the latter stage of transformation (i.e. 40 minutes and 20 minutes) (Figure 5.6g). However, these carbides have precipitated from supersaturated ferrite and not by interphase mechanism. This has been further confirmed by TEM (Figure 5.6h).

5.2.3 Transformation at 750°C

When the transformation temperature was further reduced to 750°C, the reaction started mainly at the austenite grain boundaries to form allotriomorphs, the aspect ratio of these allotriomorphs was further increased. Approximately 15 volume % transformation occurred when the specimen was held at this temperature for five minutes. The interface appeared both planar and curved. However, in the majority of cases, the interface appeared planar. The ferrite grains were again free from carbides during the early stages of transformation.

5.2.4 Transformation at 700°C

With further decrease in temperature (700°C), the incubation period increased. Only 10 volume % transformation was recorded after 10 minutes at this temperature. The transformation mainly started at grain boundaries to form grain boundary allotriomorphs. The aspect ratio of these allotriomorphic ferrite also increased. The amount of transformation increased with increasing time as expected. Again these ferrites were free from carbides. With further increasing time, the amount of transformation increased without any evidence of precipitation.

In the temperature range of 850°C to 700°C the $\gamma \rightarrow \alpha$ transformation exclusively started at austenite grain boundaries to form what are known as grain boundary allotriomorphs. Grain boundary allotriomorphs are defined as crystals which nucleate at the grain boundaries and their morphology does not reflect their crystalline symmetry. A tendency towards facetting was recorded at all temperatures of transformation. Frequent evidence of ledges indicates that the planar interfaces have been displaced by migration of ledges. Evidence of facetting even on the curved interfaces was recorded from time to time. Facetting on these curved interfaces may be due to the interface adopting a low energy configuration. It can be speculated that these interfaces also require a ledge mechanism to operate for their growth. The aspect ratio of these allotriomorphs increased with decreasing transformation temperature as expected. At all temperatures, the transformation proceeded with the formation of carbide free ferrite. During the later stages of transformation at 850°C, carbide precipitation at the interface was noticed. But no such carbide dispersion was observed at lower temperatures. However, some evidence of carbide was observed during the later stages of transformation at 800°C (40 minutes and 80 minutes). But these carbides have precipitated from supersaturated ferrite and not by an interphase mechanism.

TEM investigations were done to study the $\gamma \rightarrow \alpha$ transformations. Figure 5.7 shows rod-shaped tungsten carbide (M_6C) which were formed during the later stages of transformation at 850°C. These tungsten carbide particles have been identified as η-carbide[10, 11, 12]. The η-carbide is represented by M_6C (Fe_4W_2C) and has a complex cubic structure. This structure contains 112 atoms per unit cell viz 96M and 16C[13]. The lattice parameter of η-carbide is 11.04 Å.

A TTT diagram for 10 volume % transformation is shown in Figure 5.8. It indicates that minimum incubation period lies between 800°C and 850°C.

Table V shows the change in microstructure as a function of transformation temperature and time.

5.3 The effects of a small addition of titanium (0.14 wt%) on transformations in Fe5.9W-0.21C (wt%) alloy: Titanium forms a carbide which has a NaCl-type structure, whose composition varies between $TiC_{0.6}$ to TiC due to vacancies in the carbon sublattice[14]. The solubility limit of titanium carbide in austenite can be estimated by using the relationship[15]:

$$\text{Log}_{10}\left[\text{Ti}\right]\gamma\left[\text{C}\right]\gamma = -\frac{7000}{T} + 2.75$$

where $\left[\text{Ti}\right]\gamma$ and $\left[\text{C}\right]\gamma$ are wt% concentrations in austenite.

This expression enables the estimation of the amount of titanium used up in forming titanium - carbide at a particular austenitizing temperature, the remainder being in solid solution.

Titanium carbide (like niobium carbide) forms preferentially along the grain-boundaries and hence inhibits austenite grain-growth.

However its precise role on the kinetics of $\gamma \rightarrow \alpha$ transformation is not established. The present investigation was carried out to study the influence of Ti on the kinetics of the $\gamma \rightarrow \alpha$ transformation. The specimens were isothermally transformed in the range of 900°C to 700°C after austenitizing at 1200°C for 30 minutes. The volume fraction of α in partially transformed specimens was quantified by using the image analyse Quantimet 720. Figs. 5.9 & 5.10 show the microstructures that were developed at a fixed interval of time at each isothermal temperature, both in alloys with and without titanium. Figure 5.11 shows that titanium is effective in retarding the kinetics of the $\gamma \rightarrow \alpha$ transformation.

In order to investigate the details of the microstructure of α, TEM studies were done. At all temperatures, the decomposition of austenite started with nucleation of virtually carbide-free α-ferrite (Fig. 5.12). But during the later stages of transformation, carbides were precipitated either by an

interphase precipitation mechanism or from supersaturated ferrite.

5.4 Discussion: The $\gamma \rightarrow \alpha$ transformation started primarily at the austenite grain-boundaries by nucleation of proeutectoid ferrite. Smith[16] proposed a simplified crystallographic relationship between ferrite nuclei and austenite. According to him, a ferrite nucleus would form with a rational orientation relationship with one abutting grain and an irrational orientation relationship with the other adjacent austenite grain. The usual orientation relationship between austenite and ferrite is approximately represented by the Kurdjumov-Sachs relationship. This allows parallelism of the closest packed planes in the two structures, perhaps giving a degree of atomic misfit. Hillert[17] observed that in the majority of cases, the proeutectoid ferrite allotriomorphs had straight interfaces with both abutting grains, indicating partial coherency with both grains. He proposed that the ferrite nuclei may be closely related to form highly coherent interface with one austenite grain and still related to the other grain, forming an interface with lower coherency. Ryder et al.[18] also observed that during fcc → bcc transformations in Co-20 wt% Fe alloy, the grain-boundary nucleated product phase was crystallographically related to both adjacent parent grains. King and Bell[19,20] reported similar observations while working on 0.41C wt% steel. A recent elegant and extensive review by Howell and Honeycombe[21] strongly suggests the existence of partial coherency at the majority of interfacial orientations and that a truly incoherent structure is rare. The present observation indicates that the grain-boundary allotriomorphs are bounded by planar interfaces in the majority of cases. Frequent evidence of ledges implies that these interfaces have been displaced by a ledge mechanism[22]. Curved interfaces also showed a tendency towards facetting. This may be as a result of the interface adopting a lower energy configuration and it is interesting to speculate whether these facetted interfaces also move by the propagation of small steps[6].

The aspect ratio of the grain-boundary allotriomorphs increased with decreasing transformation temperature. This may be attributed to the diffusivity of C in austenite (D_C^{γ}) as a function of temperature. Thickening of the allotriomorphs is controlled by the volume diffusion of carbon in austenite[22]. As the temperature of transformation is decreased D_C^{γ} also decreases and consequently the rate of thickening is gradually reduced. This results in an increasing aspect ratio of the allotriomorphs with decreasing temperature since the role grain-boundary carbon diffusion in allotriomorph lengthening then becomes more significant.

At all transformation temperatures, the reaction started with the formation of carbide free ferrite. The formation of such a carbide free ferrite is

attributed to the appreciably lower supersaturation of tungsten carbide in ferrite at this temperature. During later stages of transformation at 850°C (20 minutes), evidence of carbide precipitation was noticed, at the γ/α interface. With increasing time of transformation, these carbides grew into the austenite. The sequence of reaction is represented by equations (1) and (2) and schematically shown in Figure 5.5. The reason for the transition from clean ferrite to ferrite + tungsten carbide may be explained on the basis of continued carbon enrichment of austenite during the $\gamma \rightarrow \alpha$ transformation. As the transformation proceeds, C is continuously rejected ahead γ/α interface in the austenite. Ultimately the carbon content of the austenite near the γ/α interface is sufficiently increased to induce $\gamma_1 \rightarrow \gamma_2 + M_6C$ reaction.

Sakuma and Honeycombe[9] while working on Fe-Nb-C alloys tried to analyse the reason for transition from clean ferrite to ferrite + alloy carbide by recording the micro-hardness of isothermally transformed alloys as an index of the 'C' content of austenite. The increase in micro-hardness of martensite with increasing time is attributed to the increase in the carbon content of austenite[22]. Figure 5.13 shows schematically the carbon concentration profile near the moving interface[9] under two different circumstances. Figure 5.13a shows a steady state carbon concentration profile which is achieved under high driving force operating in lower temperature ranges. But at high temperatures, the carbon concentration profile will change with time due to its increased diffusivity (Figure 5.13b). Under this condition, the migration rate of the interface will gradually decrease and thus provide an opportunity for precipitation at the γ/α interface during the latter stage of transformation.

The reason for transition from clean ferrite to ferrite + alloy carbide can be explained on the boundary migration rate and nucleation rate of carbide on the boundary[23]. According to the analysis,[23] favourable conditions for carbide nucleation will be created only when the migration rate is low. The migration rate of an interface continuously changes with time during the isothermal transformation in Fe-X-C[24]. Growth rate of grain-boundary allotriomorphs during the isothermal transformation of austenite in ternary system has been divided into three stages: an initial no-partition stage which includes a parabolic growth rate and subsequent non-parabolic stage and the final stage in which partitioning of substitutional alloying elements occurs[25, 26]. During the first stage, no partitioning occurs due to the greater difference between the diffusivities of C and X. Experimental evidence of no partition growth of ferrite allotriomorphs has been reported in many ternary Fe-C-X alloys[27].

As the transformation proceeds, the supersaturation or the driving force for transformation decreases and eventually reaches a point where appreciable partitioning of substitutional element X between the parent and product phases must occur. Coates[24] used the concept of local equilibrium at the moving interface to explain the above phenomenon. When the degree of undercooling is high, local equilibrium is maintained without partitioning of alloying element. Under this condition (NP-L.E) the rate of reaction is controlled by the fast diffuser 'C' and the ferrite inherits the alloy content of austenite. Local equilibrium with partition (P-L.E) occurs when the transformation rate is slow and the transformation is mainly controlled by the slower diffuser 'X'.

Titanium seems to have a retarding effect on the kinetics of the $\gamma \rightarrow \alpha$ transformation. On austenitizing at 1200°C, titanium carbides are preferentially formed along the austenite grain-bounderies. Some carbides are also precipitated within the grains. The presence of copious precipitation of titanium carbide reduces the number of available sites for the nucleation of α and hence reduces its nucleation efficiency. Once the nucleation has occurred the carbides present within the austenite grain offer resistance to the growing γ/α interface by a pinning action.

5.5 Conclusions:

1. In the present study, the majority of the interfaces appeared planar in partially transformed specimens. More frequently ledges were observed on these planar interfaces. Facetting was also observed on the curved interfaces. It suggests that the ledge mechanism plays a significant role in controlling the mobility of the γ/α interface during the transformation.

The mobility of the such interfaces will depend both on the frequency with which the ledges are nucleated as well as their ability to move during the transformation.

2. The $\gamma \rightarrow \alpha$ + carbide reaction is found to occur in at least two distinguishable stages. The first stage involves the formation of allotriomorphic ferrite, and the carbon partitioning accompanying this reaction induces the precipitation of carbides in the austenite ahead of the γ/α interface. The ferrite subsequently engulfs the carbides as the remaining austenite transforms further to ferrite. This sequence of events has been tentatively interpreted in terms of local equilibrium theory.

3. Ti showed tendency to suppress the kinetics of the $\gamma \rightarrow \alpha$ transformation in the temperature range of 700°C to 900°C.

Showing change in microstructure as a function of isothermal temperature

Change in microstructure as a function of isothermal

Temperature °C	Time in minutes	Vol.%	Nature of Interface	Presence of Ledges	Aspect Ratio	Pr
	2.5	18 - 21%	Both Planar & Curved	Frequently	Low equiaxed	
	5	55 - 67%	"	Less	"	
	10	69 - 72%	"	Less	"	
	20	74 - 78%	"	"	"	
850°C	40	slightly increased	"	"	"	
	80	"	"	"	"	
	320	100%	Curved mostly	No	"	
	500	100%	"	No	"	
	1.5	3 - 5%	Both Planar & Curved	Frequently	Increased	
	2.5	6 - 8%	"	"	Increased	
	5	34 - 37%	"	Less	Equiaxed	
800°C	20	37 - 41%	"	Less	"	
	40	39 - 44%	"	Less	"	
	80	slightly increased	"	Less	"	
750°C	5	12 - 15%	Both Planar & Curved	Frequently	Increased	
700°C	10	8 - 10%	Both Planar & Curved	Frequently	Increased	

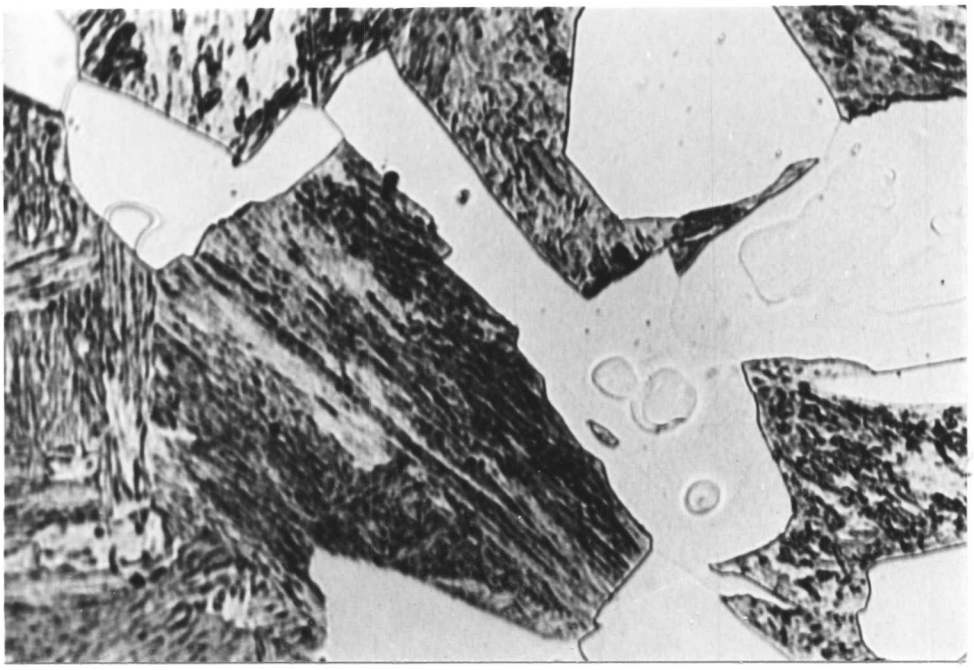

Figure 5.1: High proportion of planar boundary (i.e. semi-coherent γ/α interface) is depicted in this micrograph. Presence of ledges implies that these interfaces have been displaced by ledge mechanism. (850°C/2.5 Min).

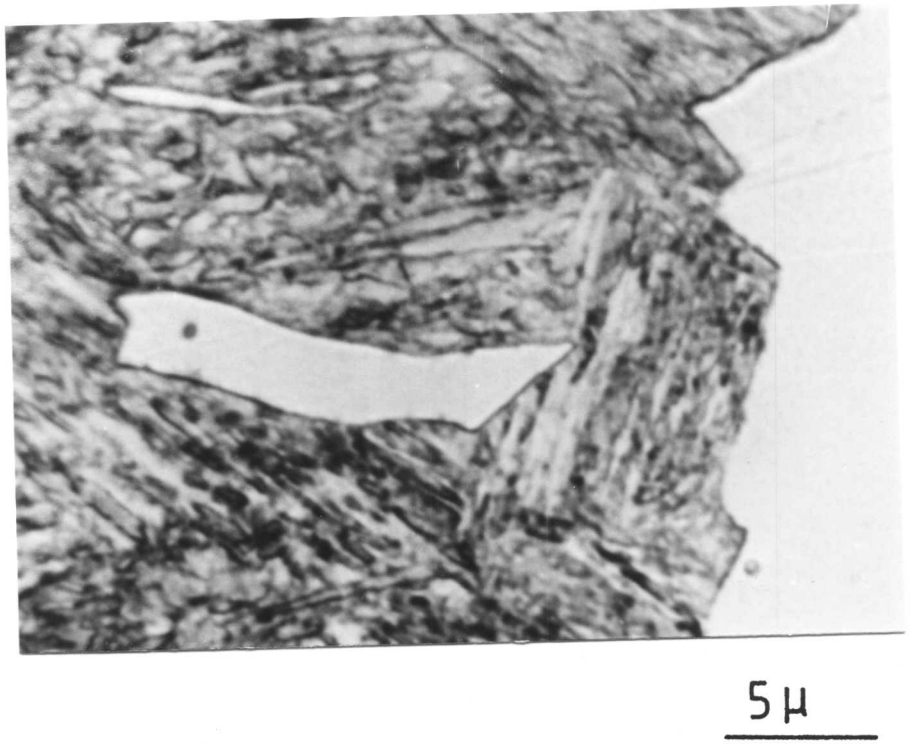

Figure 5.2a: Intragranular ferrite bounded exclusively by planar interfaces. (850°C/5 Min).

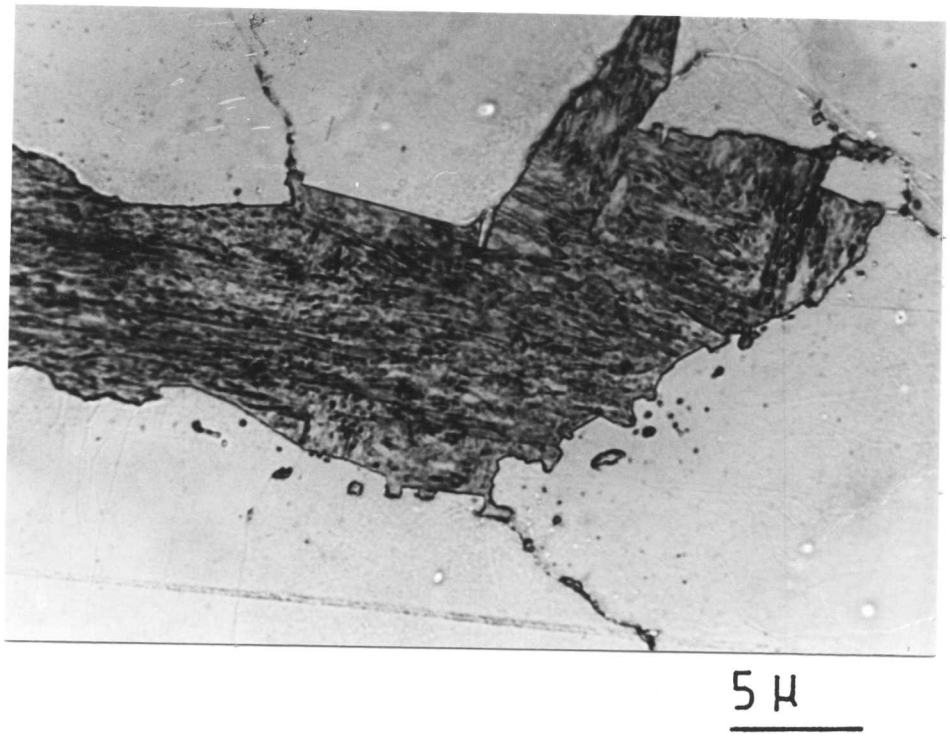

Figure 5.2b: The moving γ/α interfaces have been pinned by tungsten carbide. This results in formation of ragged interface. Some entrapped austenite are also present within the ferrite grain (850°C/5 Min).

Figure 5.3a: Precipitation of tungsten carbide at the γ/α interface. These carbides appear to grow in the austenite. (850°C/20 Min).

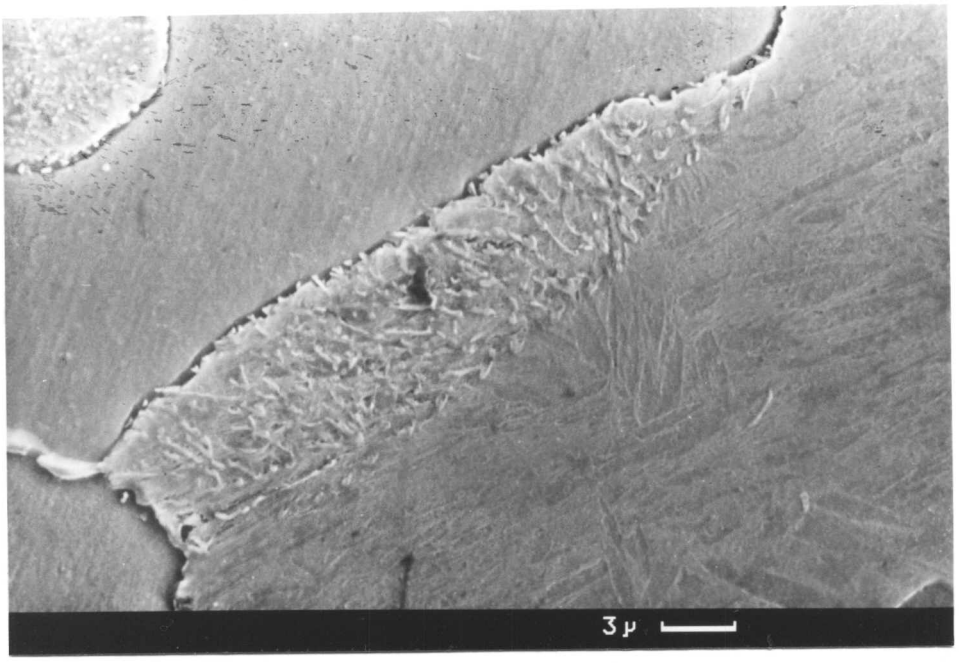

Figure 5.3b: Scanning micrograph showing growth of tungsten carbide away from the γ/α interface but within the austenite grain (850°C/20 Min).

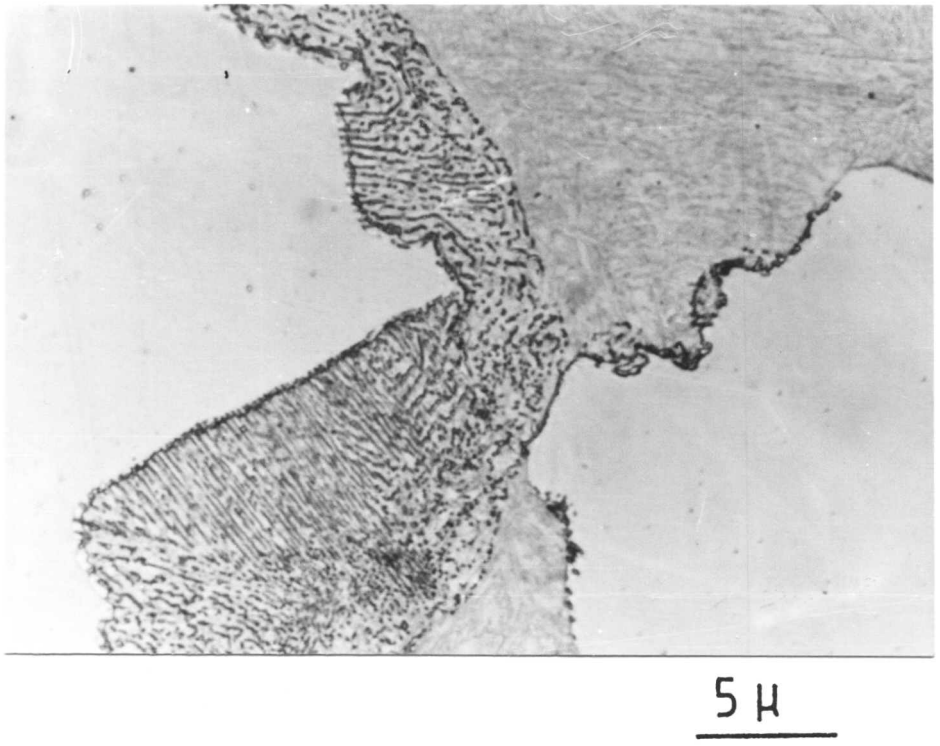

Figure 5.3c: Planar array of tungsten carbide within the austenite grain (850°C/20 Min).

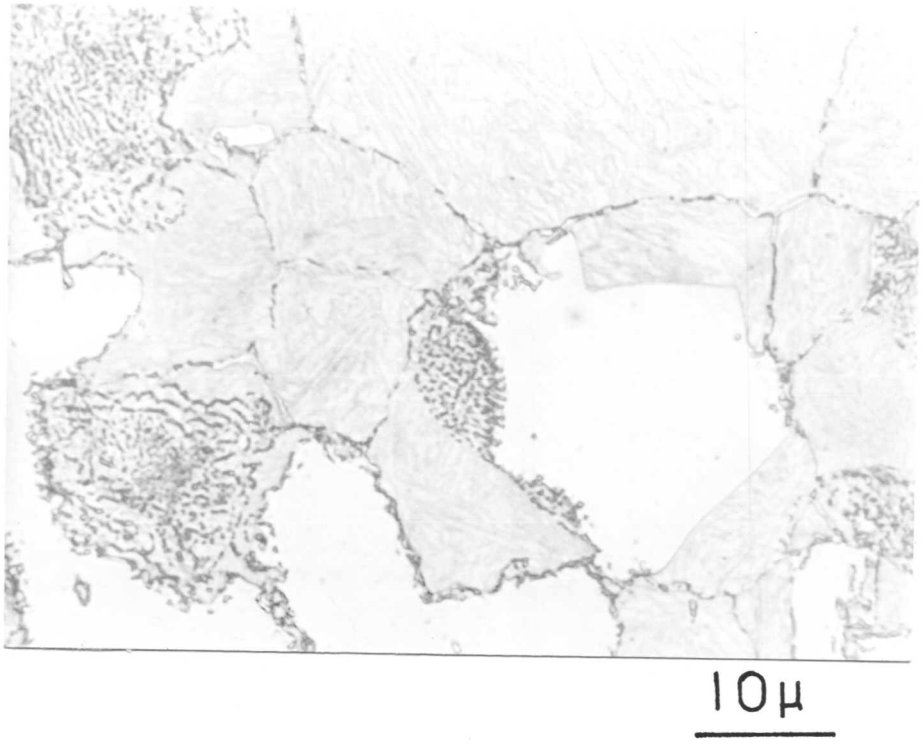

Figure 5.4a: With increasing time of transformation the carbides grew in austenite (850°C/80 Min).

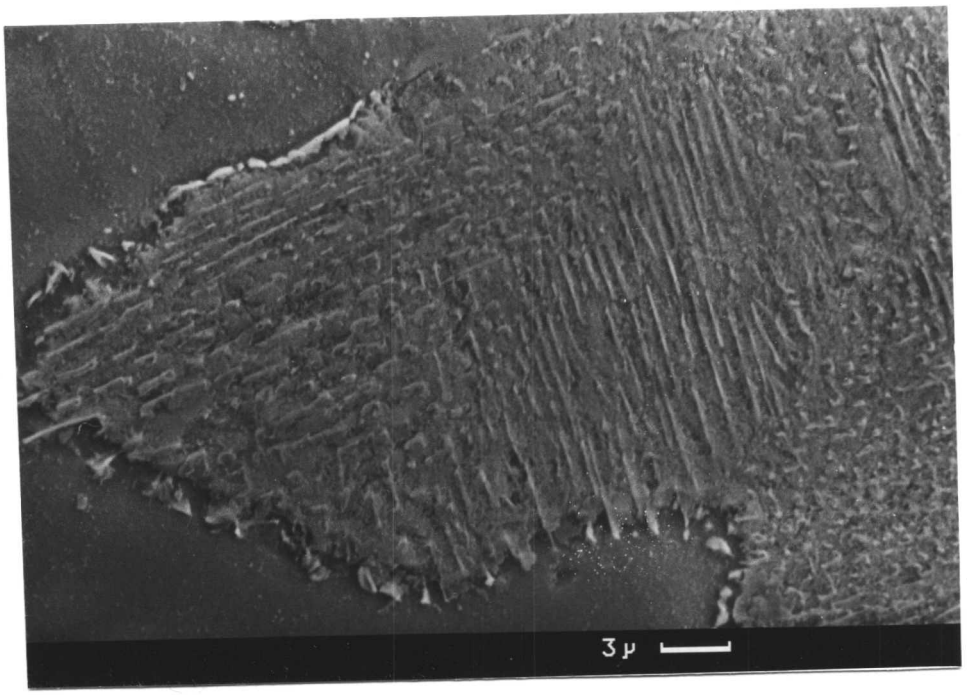

Figure 5.4b: Scanning electron micrograph showing further growth of tungsten carbide within the austenite grain (850°C/160 Min).

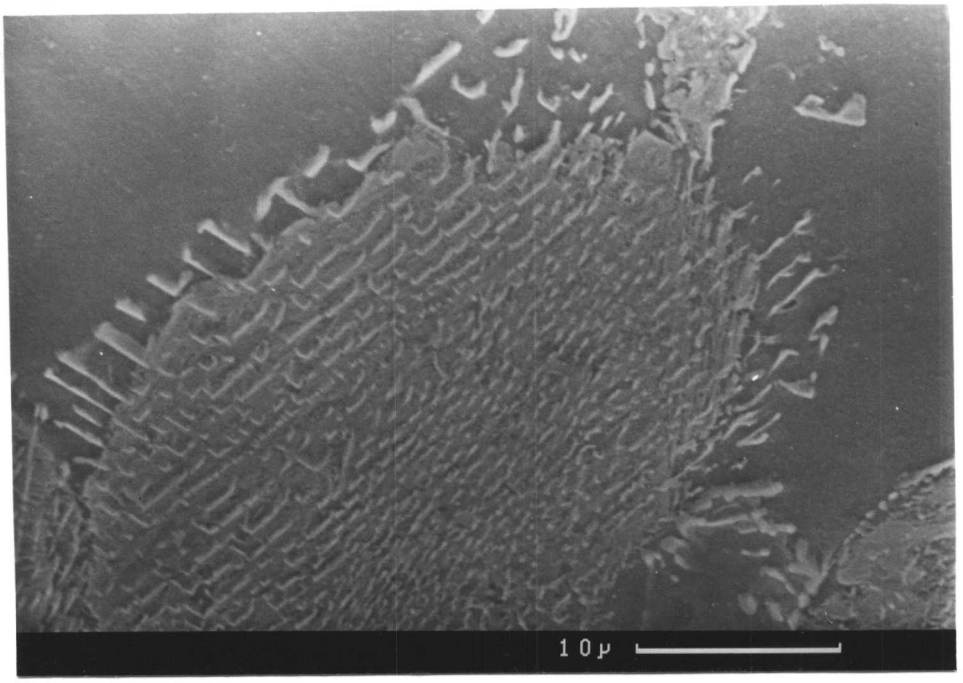

Figure 5.4c: Scanning electron micrograph showing planar array of tungsten carbides within the austenite grain (850°C/160 Min).

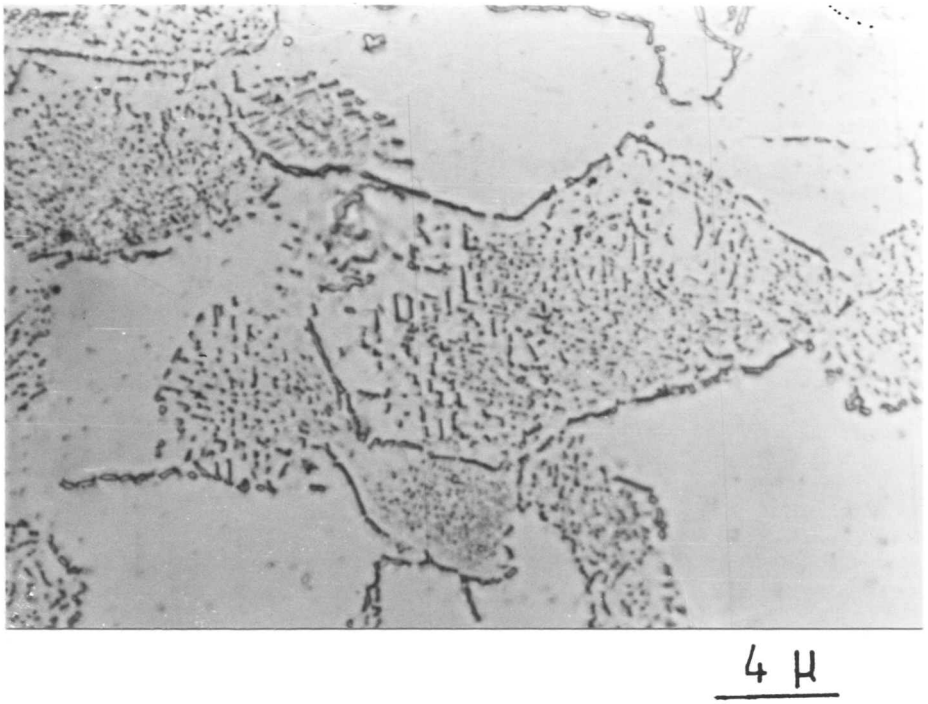

Figure 5.4d: After prolong ageing, the microstructure consisted of $\alpha + M_6C$. (850°C/320 Min).

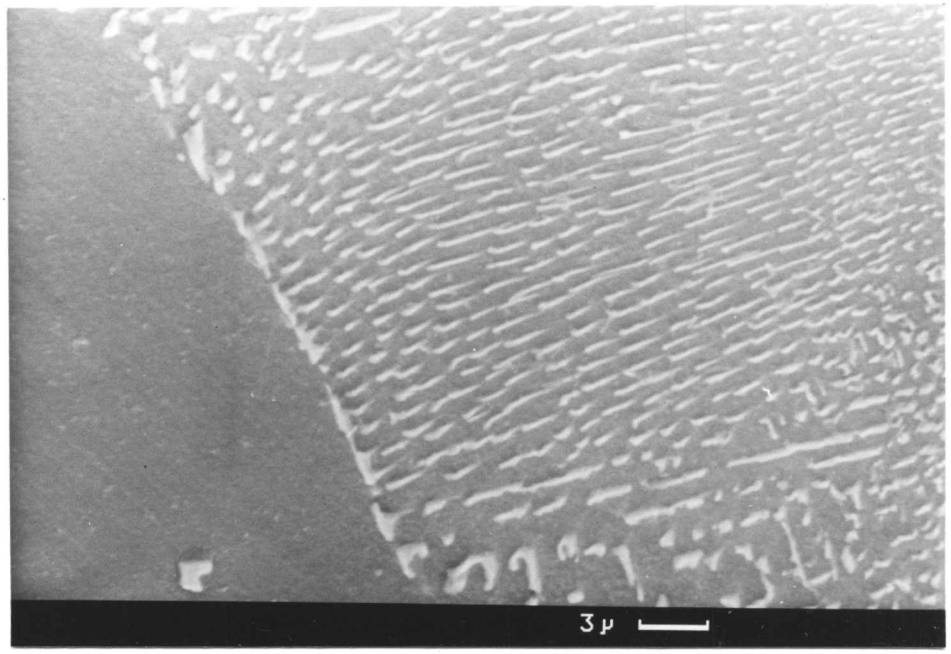

Figure 5.4e: Scanning electron micrograph showing aligned carbide dispersion (850°C/320 Min).

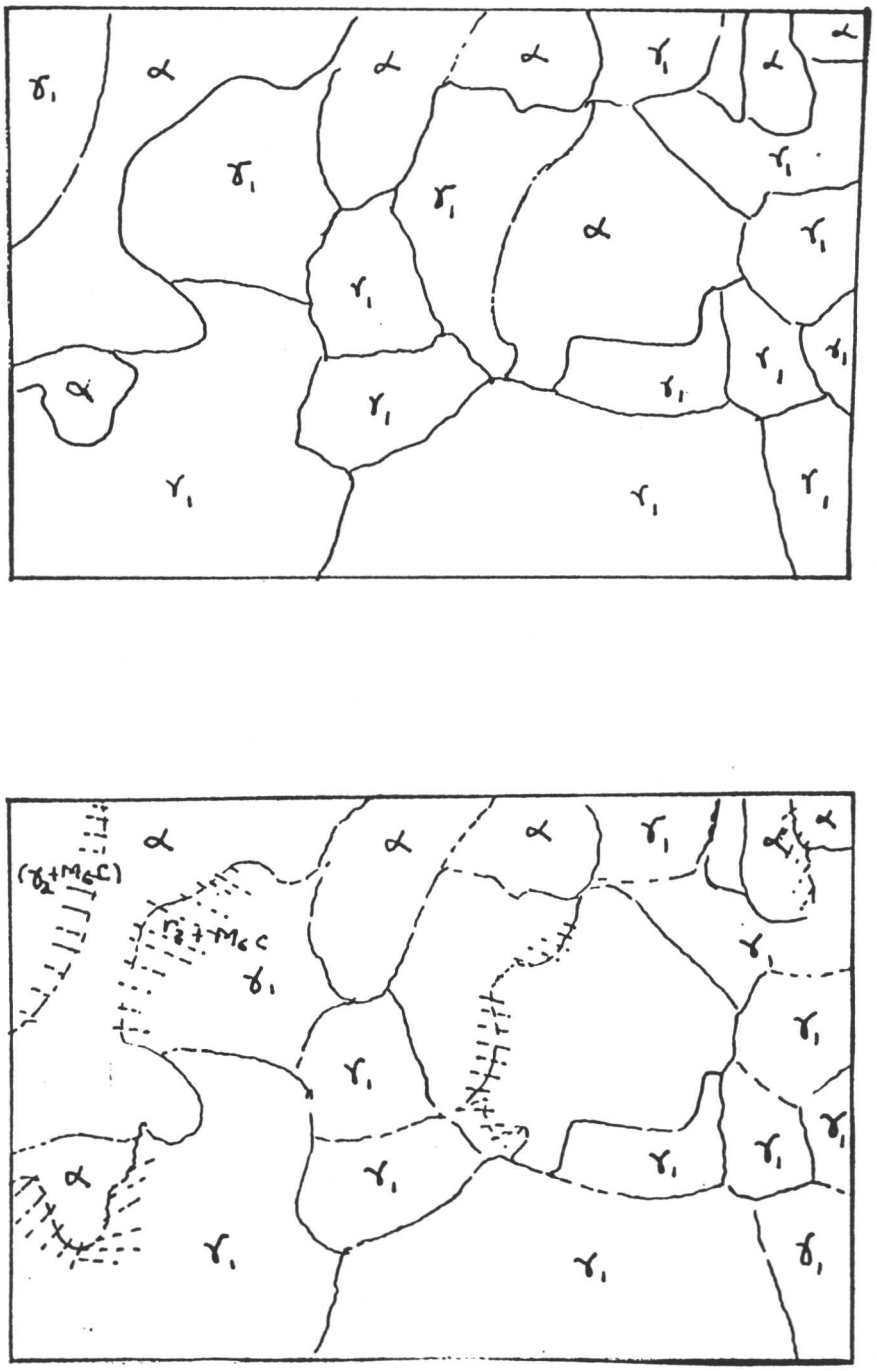

Figure 5.5: Schematic diagram showing the sequence of reaction at 850°C. i.e. $\gamma \rightarrow \alpha + \gamma_1 \rightarrow \alpha + (M_6C + \gamma_2) \rightarrow \alpha + M_6C$.

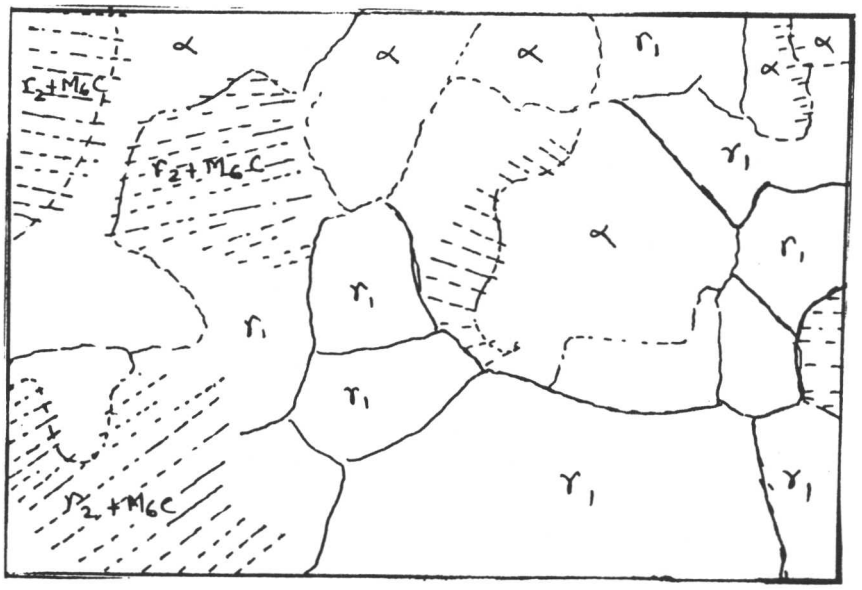

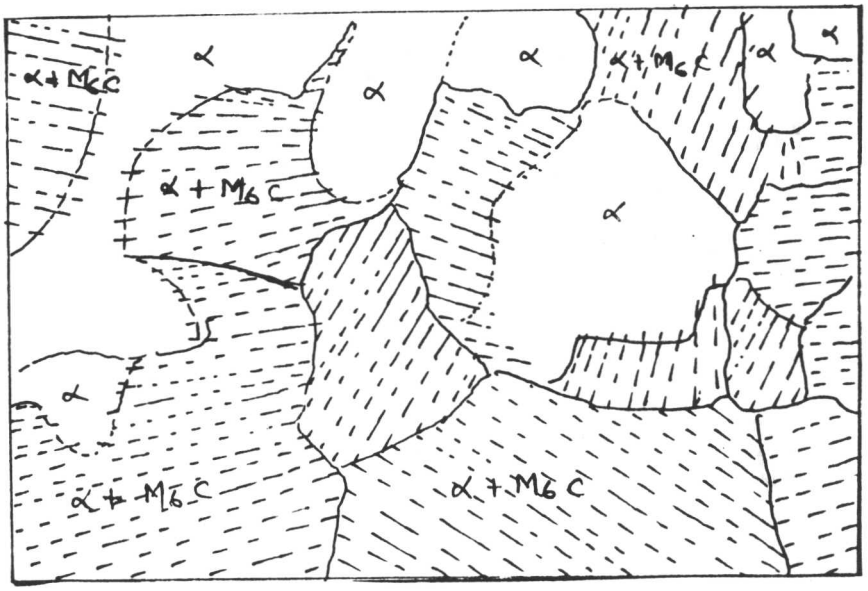

Figure 5.5: Schematic diagram showing the sequence of reaction at 850°C. i.e. $\gamma \rightarrow \alpha + \gamma_1 \rightarrow \alpha + (M_6C + \gamma_2) \rightarrow \alpha + M_6C$.

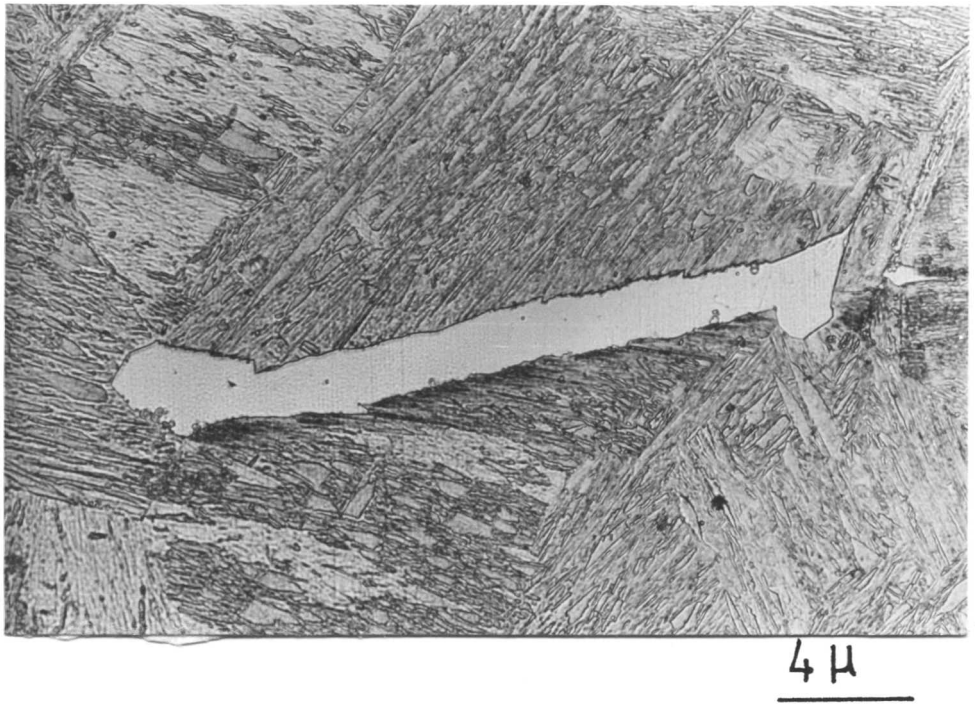

Figure 5.6a: Facetted allotriomorphic ferrite (800°C/1.5 Min).

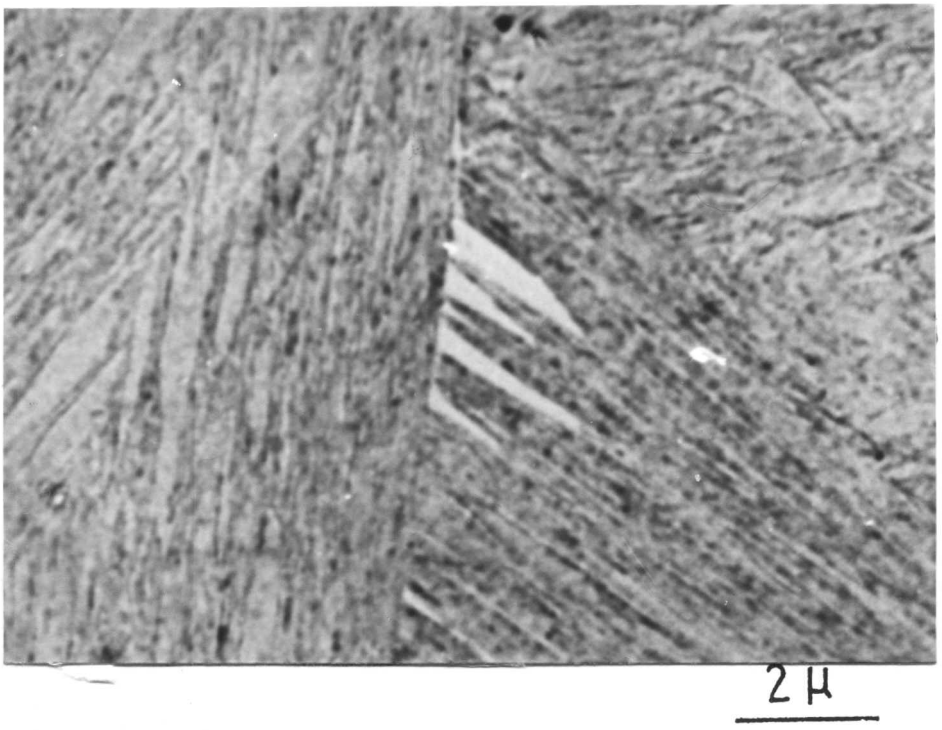

Figure 5.6b: Widmanstätten ferrite growing in the martensite trace direction. (800°C/1.5 Min).

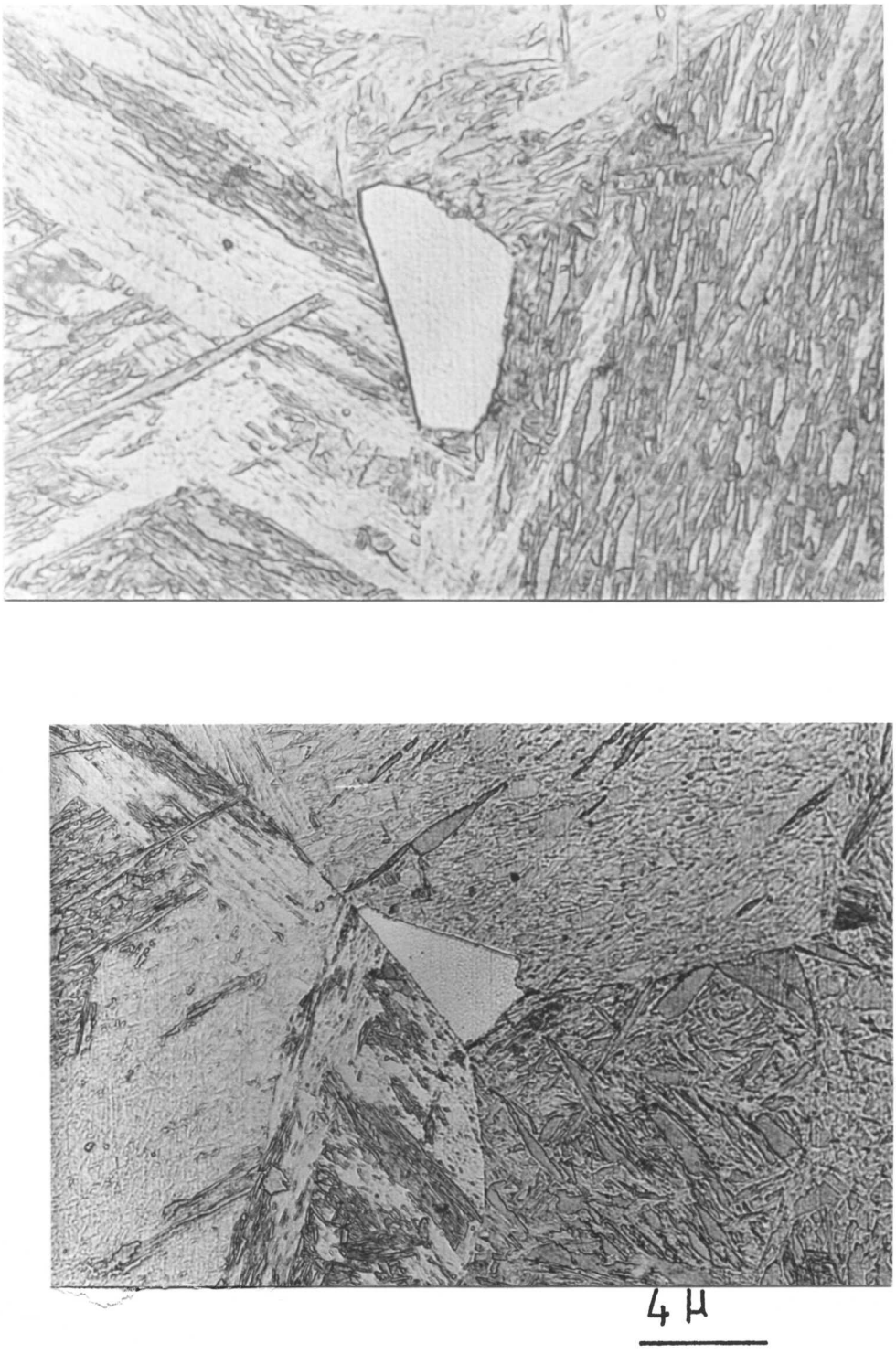

Figure 5.6c: Facetted allotriomorphic ferrite growing at the triple point (800°C/1.5 Min).

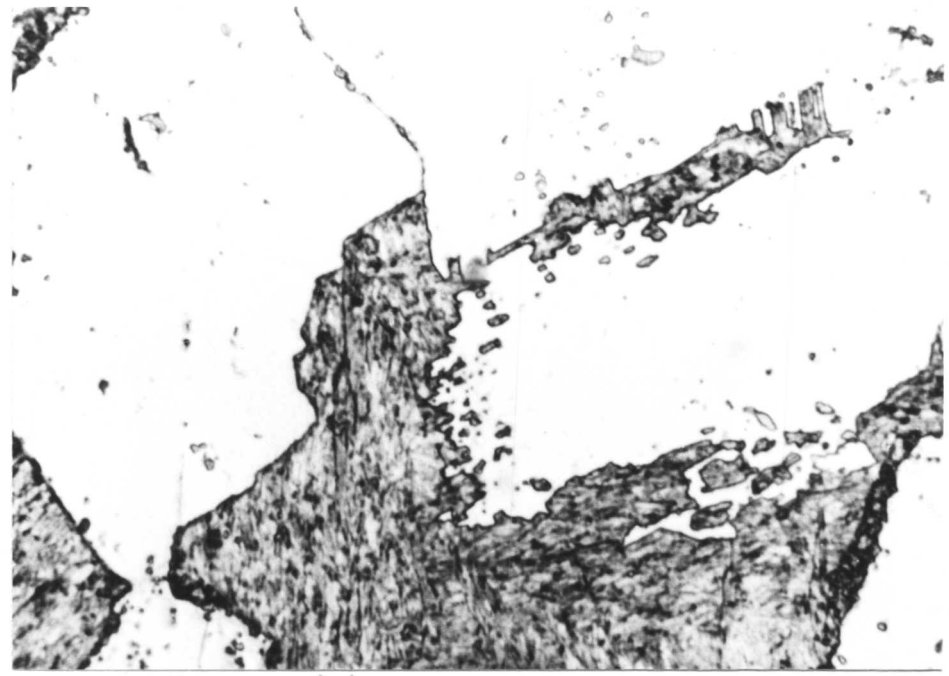

10μ

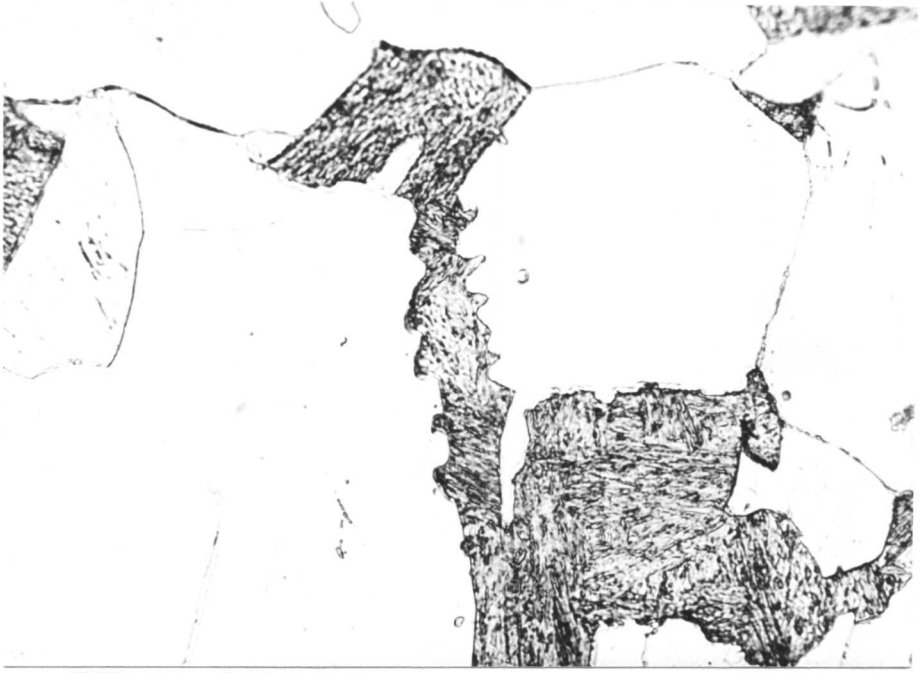

20μ

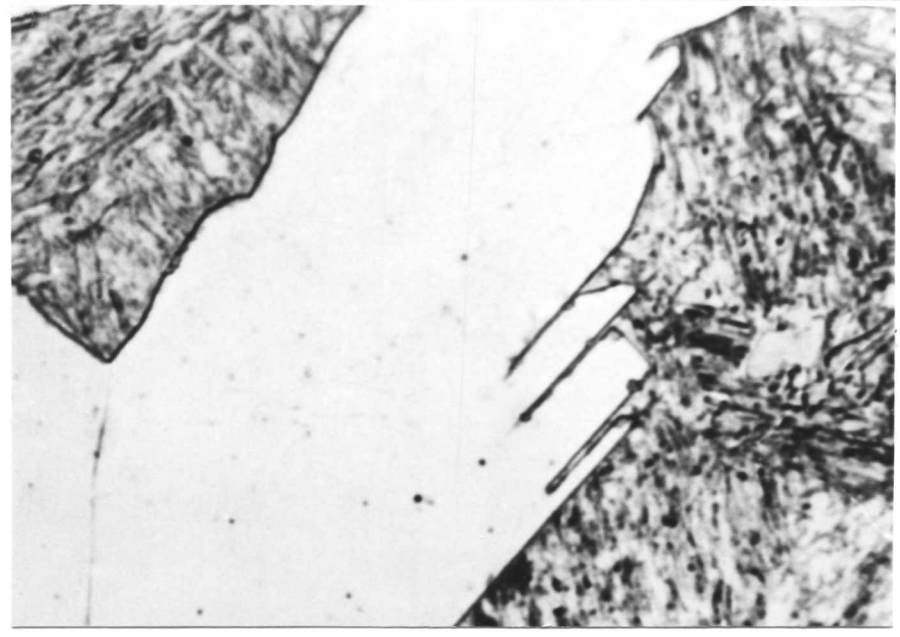

20μ

Figure 5.6d to f: Pinning of the γ/α interface by tungsten carbide.

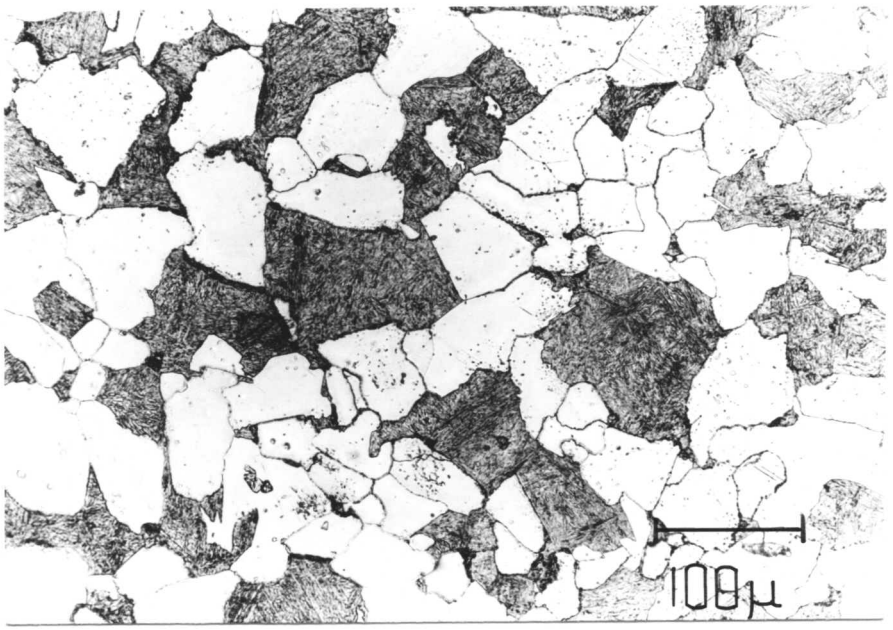

Figure 5.6g: Polygonal ferrite with evidence of carbide precipitation within the ferrite (800°C/40 Min).

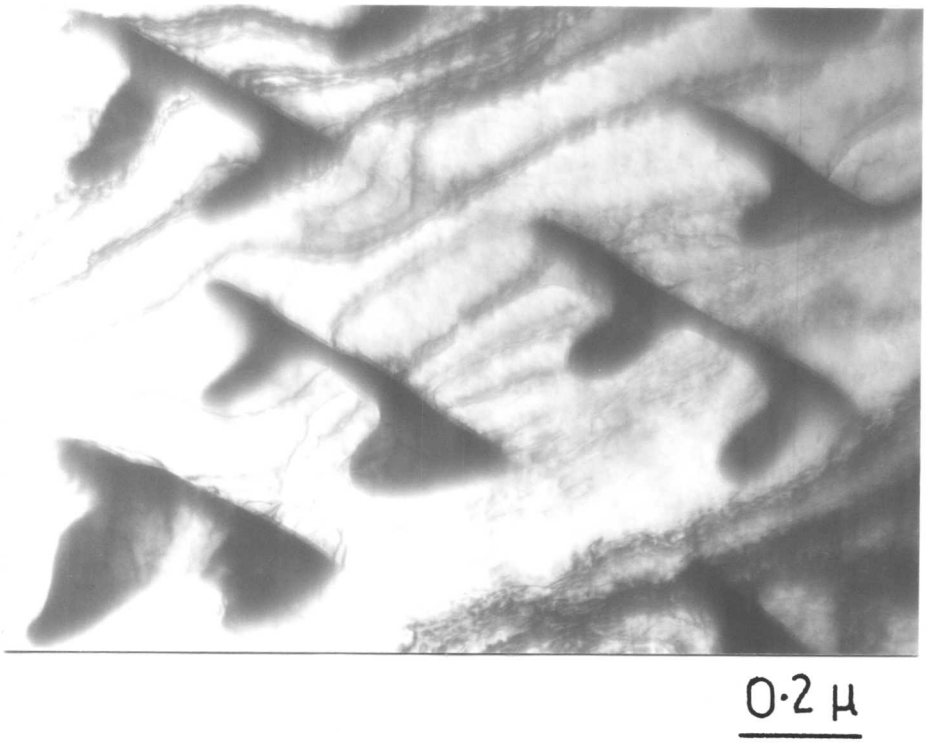

Figure 5.6h: Transmission electron micrograph showing carbide precipitation within ferrite.

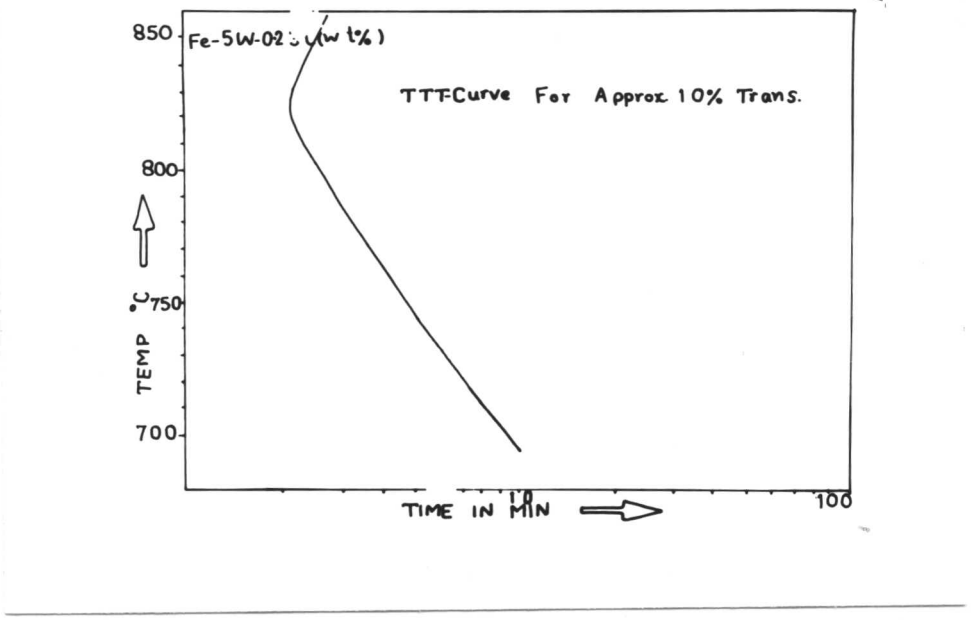

Figure 5.8: TTT diagram constucted to show approximately 10 vol.% transformation.